

From the
Walter-Brendel-Zentrum für Experimentelle Medizin
of the Ludwig-Maximilians-Universität München
Director: Prof. Dr. med. Ulrich Pohl

A circadian zip code guides leukocyte homing

Dissertation
zum Erwerb des Doctor of Philosophy (Ph.D.)
an der Medizinischen Fakultät der
Ludwig-Maximilians-Universität

submitted by

Wenyan He

from
Chongqing, China

On

.....17/01/2018.....



Supervisor: Prof. Dr. Christoph Scheiermann

Second evaluator: Prof. Dr. Barbara Schraml
Prof. Dr. Sabine Steffens
Prof. Dr. Christoph Reichel
PD. Dr. Naoto Kawakami

Dean:
Prof. Dr. Reinhard Hickel

Date of oral defence: 22.05.2018

Acknowledgement

I would like to express my sincere gratitude to my supervisor Prof. Dr. Christoph Scheiermann for giving me this great opportunity to do my Ph.D. in his lab and also the continuous support and excellent guidance during my study.

Besides my supervisor, I would like to thank my thesis advisory committee members Prof. Dr. Schraml and Dr. Moser for their insightful comments and good ideas for my project.

I would also like to thank my lab colleagues, David Druzd, Alba de Juan, Louise Ince, Chien-Sin Chen, Sophia Hergenhan, Stephan Holtkamp, Jasmin Weber and Kerstin Kraus. Without their help, it would not be possible to perform such big experiments.

I benefited a lot from the good scientific environment provided by the SFB914 and also the affiliated IRTG. I would like to thank our coordinator Dr. Verena Kochan for helping me with the arrangement of documents for coming to Germany and also for the continued support during my PhD.

Finally, I would like to thank my family for their tremendous encouragement and support. Their love and faith in me always give me the power to move forward.

Abstract

Circadian rhythms are important for organisms to anticipate predictable environmental changes. Evidence indicates that the oscillation of murine blood numbers is closely related to the lighting schedule. However, the dynamics and the mechanisms of the migration of leukocyte subsets over 24 hours are unknown. Here, we could show that that numbers of circulating leukocyte subsets exhibit circadian rhythms in murine blood, which was regulated by rhythmic homing, with a co-contribution of both microenvironmental and leukocyte-autonomous oscillations. We identified leukocyte and vascular bed specific surface expression oscillations of adhesion molecules and chemokine receptors over 24 hours. To test the relevance of these oscillations, functional blocking experiments using antibodies or functional blockers directed against pro-migratory molecules were performed. Our data indicate the adhesion molecules CD11a, CD49d and L-selectin and the chemokine receptor CXCR4 on the leukocyte side, as well as VCAM-1 and ICAM-1 on the endothelial side to be important in the rhythmic recruitment process of leukocyte subsets. A stronger blocking effect targeting these molecules was found at night for leukocyte subsets. In the homing experiments, we found donor leukocytes preferentially migrated to organs at night, and that the recruitment process of different leukocyte subsets to various organs could be blocked by distinct inhibitors. We exposed the role of circadian genes in the rhythmic recruitment process using B-cell and myeloid-cell-specific knockouts of the circadian gene *Bmal1*, which demonstrated altered expression levels of specific oscillatory molecules and leukocyte numbers in tissues, suggesting that rhythmicity in these factors may be directly regulated by the circadian clock. Furthermore, we detected inverse oscillation patterns of human blood cell numbers compared to murine cells as well as of the expression levels of CXCR4 on leukocyte subsets. Together, our data demonstrate that circadian genes control a rhythmic leukocyte- and tissue-specific molecular signature in the expression of pro-migratory factors, which allows for the recruitment of select leukocyte subsets at distinct times.

Table of contents

Acknowledgement	4
Abstract	5
List of figures	10
List of tables	13
Abbreviations.....	14
1. Introduction.....	15
1.1. The Circadian system.....	15
1.1.1. Circadian rhythms	15
1.1.2. The molecular clock machinery.....	16
1.1.3. The central clock and synchronization of the organism	18
1.1.4. The peripheral clock.....	22
1.2. Leukocyte migration	22
1.2.1. Blood leukocyte numbers oscillate over 24 hours	22
1.2.2. Circulating blood cell numbers	23
1.2.3. Leukocyte adhesion cascade.....	24
1.2.4. Recruitment of leukocytes.....	26
1.3. Homing zip code and circadian rhythmicity	35
2. Materials.....	39
2.1. Animals.....	39
2.2. Genotyping	39
2.3. Antibodies.....	40
2.3.1. Flow cytometry.....	40
2.3.2. Blocking Antibodies.....	43
2.3.3. Antibodies for fluorescence microscopy.....	44
2.4. Blocking chemicals	45
2.5. Primers for qPCR	45

2.6.	Cell and RNA isolation Kits.....	46
2.7.	Buffers	46
2.8.	Software	47
2.9.	Equipment	48
2.10.	Other substances	48
3.	Methods.....	49
3.1.	Flow cytometry	49
3.1.1.	Preparation of samples for flow cytometry	49
3.1.2.	Surface expression analyses of leukocytes	51
3.1.3.	Adoptive transfer and homing assay of leukocytes	53
3.1.4.	Human peripheral blood experiment	62
3.2.	Cell isolation	64
3.3.	qPCR.....	64
3.4.	Immunofluorescence staining and quantitative imaging analyses	65
3.5.	Genotyping	66
3.6.	Statistics	68
4.	Results	69
4.1.	Oscillations in circulating leukocyte subsets are governed by a rhythmic homing process.....	69
4.1.1.	Circulating subsets oscillate during 24 hours	69
4.1.2.	The microenvironment contributes to rhythmic leukocyte homing.....	70
4.1.3.	Leukocytes contribute to rhythmic homing	72
4.1.4.	Both the microenvironment and the leukocyte contribute to rhythmic leukocyte migration.....	73
4.2.	Tissue-specific oscillations in adhesion molecules expressed on endothelial cells contribute to the recruitment process.....	75
4.2.1.	Expression of endothelial adhesion molecules in various organ is oscillatory	75

4.2.2. Blocking endothelial cells adhesion molecules abolishes rhythmic recruitment	76
4.3. Leukocyte subset specific oscillations in adhesion molecules contribute to the recruitment process.....	81
4.3.1. Leukocyte subsets have distinctly rhythmic expression patterns of adhesion molecules and chemokine receptors.....	81
4.3.2. Functional blocking experiments using antibodies or functional inhibitors inhibit the rhythmic recruitment process in a time-dependent manner.....	82
4.4. The homing of leukocyte subsets to specific organs is time-of-day dependent	87
4.5. Time-dependent leukocyte migration of organs is adhesion molecule- and leukocyte subset-specific	89
4.5.1. Migration of donor cells to the lung	91
4.5.2. Migration of donor cells to the liver	93
4.5.3. Migration of donor cells to the lymph node	96
4.5.4. Migration of donor cells to the spleen	99
4.5.5. Migration of donor cells to the bone marrow	102
4.6. Control of rhythmic leukocyte migration by the circadian clock	106
4.6.1. Circadian genes oscillate in leukocyte subsets	106
4.6.2. Leukocyte clocks and rhythmic migration	108
4.6.3. Endothelial cell clocks and rhythmic migration.....	110
4.7. Human blood oscillation	111
5. Discussion	114
5.1. Oscillation and recruitment process of murine blood leukocytes	114
5.2. A zip code for the circadian leukocyte recruitment process.....	115
5.3. Specific migration to organs	117
5.4. Rhythmic homing is under the control of the circadian clock.....	121
5.5. The pathway from SCN to leukocytes	122

5.6. Human blood oscillation	123
5.7. Outlook	123
6. Reference	125
7. Appendix	137
7.1. Curriculum Vitae	137

List of figures

Figure 1.1 The molecular clock.....	17
Figure 1.2 Peripheral clock entrainment pathways	21
Figure 1.3 Adhesion cascade of leukocyte	25
Figure 1.4 Difference in neutrophil migration in pulmonary circulation and in systemic and bronchial circulation	27
Figure 1.5 Leukocyte recruitment in liver in an inflammatory response	29
Figure 1.6 Lymphocytes migration to lymph nodes	31
Figure 1.7 Spleen structure	33
Figure 1.8 Bone marrow blood vessels model.....	35
Figure 3.1 Gating leukocyte subsets	51
Figure 3.2 Gating strategy of adoptive transfer experiment with CFSE donor cells..	55
Figure 3.3 Gating strategy of organs to identify homed myeloid cells : lung	57
Figure 3.4 Gating strategy of organs to identify homed lymphocytes and NK cells: lung	58
Figure 3.5 Gating strategy of homing experiment to organs	60
Figure 3.6 Gating strategy of human blood.....	63
Figure 3.7 Surface expression measurements on liver endothelium	66
Figure 3.8 MFI data results.....	66
Figure 4.1 Oscillations in total white blood cell and leukocyte subset counts	70
Figure 4.2 Adoptive transfer experiment with recipients kept at different phases	71
Figure 4.3 A rhythmic microenvironment contributes to leukocyte number oscillation in peripheral blood.....	71
Figure 4.4 Adoptive transfer experiment with recipients kept in one phase	72
Figure 4.5 Rhythmic recruitment governed by donor cells contributes to the leukocyte number oscillation in peripheral blood	73
Figure 4.6 Reciprocal homing assays.....	74
Figure 4.7 Reciprocal homing assays: leukocyte subsets	74
Figure 4.8 Expression of adhesion molecules in endothelial cells of various organs	76
Figure 4.9 Antibody blocking in combination with adoptive transfer experiments	77
Figure 4.10 Antibody blocking experiment with adoptive transfer experiments	78
Figure 4.11 Adoptive transfer experiment with ICAM-1 knockout mice at ZT1 and ZT13 time points	79
	10

Figure 4.12 Fold change of antibody blocking experiment	80
Figure 4.13 Expression levels of adhesion molecules and chemokine receptors on leukocytes.....	82
Figure 4.14 Antibody blocking with adoptive transfer experiment at one time point .	83
Figure 4.15 Antibody blocking with adoptive transfer experiment.....	84
Figure 4.16 Antibody blocking with adoptive transfer experiment.....	85
Figure 4.17 Antagonist blocking with adoptive transfer experiment.....	86
Figure 4.18 Fold change of CXCR4 antagonist experiments.....	87
Figure 4.19 Homing experiment to organs.....	88
Figure 4.20 Homing experiment to various organs	89
Figure 4.21 Antibody or functional inhibitor blocking experiments	90
Figure 4.22 Flow cytometry of organs in homing experiment after i.v. injection of CD45	91
Figure 4.23 Recruited donor cells in the lung in antibody blocking with homing experiment.....	92
Figure 4.24 Recruited donor cells inside the lung vasculature.....	93
Figure 4.25 Recruited donor cells in the liver in antibody blocking with homing experiment.....	94
Figure 4.26 Recruited donor cells inside the liver vasculature.....	95
Figure 4.27 Recruited donor cells in the lymph nodes in antibody blocking with homing experiment.....	96
Figure 4.28 Recruited donor cells inside or outside the lymph node vasculature	98
Figure 4.29 Recruited donor cells in the spleen in antibody blocking with homing experiment.....	99
Figure 4.30 Recruited donor cells inside or outside the spleen vasculature	101
Figure 4.31 Recruited donor cells in the bone marrow in antibody blocking with homing experiment.....	102
Figure 4.32 Recruited donor cells inside or outside the bone marrow vasculature .	104
Figure 4.33 Matrix of molecular dependency of leukocyte subtype homing to specific organs.....	105
Figure 4.34 Q-PCR analysis of circadian genes in isolated cells.....	107
Figure 4.35 Adoptive transfer with <i>Bmal1</i> KO donor cells	108
Figure 4.36 Donor cells in spleen with <i>Bmal1</i> KO or control mice as donors.....	109

Figure 4.37 Expression levels of adhesion molecules and chemokine receptors on B cells	109
Figure 4.38 Adoptive transfer experiment with <i>Bmal1</i> KO recipients.....	110
Figure 4.39 Adoptive transfer experiment with endothelial cell <i>Bmal1</i> KO	111
Figure 4.40 Human blood flow cytometry	112
Figure 4.41 CXCR4 expression on human leukocytes and murine leukocytes.....	113

List of tables

Table 1.1 Summary of homing zip code for leukocytes	38
Table 2.1 Primer sequence and annealing temperature for genotyping	39
Table 2.2 Reaction mix for genotyping	40
Table 2.3 Antibody list of flow cytometry.....	40
Table 2.4 Blocking antibodies.....	43
Table 2.5 Antibodies for fluorescence microscopy	44
Table 2.6 Blocking chemicals	45
Table 2.7 Primer list for qRCR.....	45
Table 2.8 Cell and RNA isolation kits	46
Table 2.9 RBC lysis buffer	46
Table 2.10 PEB buffer	46
Table 2.11 Tissue digestion buffer.....	46
Table 2.12 Cell incubation buffer	47
Table 2.13 DAPI buffer	47
Table 2.14 Tissue digestion buffer.....	47
Table 2.15 Software used for analyses.....	47
Table 2.16 Equipment used for experiments	48
Table 2.17 Other substances used in experiments.....	48
Table 3.1 Antibodies for surface expression of adhesion molecules and chemokine receptors.....	51
Table 3.2 Flow cytometry panel for blood staining with CFSE donor cells	54
Table 3.3 Flow cytometry panel for blood staining with CFSE and CellTracker Deep Red donor cells.....	56
Table 3.4 Antibody panel for homing experiment to lung and liver group 1	56
Table 3.5 Antibody panel for homing experiment to lung and liver group 2	58
Table 3.6 Flow cytometry panel for homing assay staining	59
Table 3.7 Antibodies and chemicals for function blocking experiments.....	61
Table 3.8 Antibodies for human blood staining.....	62
Table 3.9 Cycling conditions for qPCR	65
Table 3.10 RCR conditions for <i>cre</i>	67
Table 3.11 PCR conditions for <i>Bmal1</i>	67

Abbreviations

ANOVA	Analysis of variance
CD	Cluster of differentiation
cDNA	Complementary deoxyribonucleic acid
cre	Causes recombination
Clock	Circadian locomotor output cycles kaput
CCR	C-C chemokine receptor
CCL	C-C chemokine motif ligand
EDTA	Ethylene diamine tetraacetate
Flox	Flanked by loxP sites
GAPDH	Glyceraldehyde-3-phosphate dehydrogenase
ICAM	Intercellular cell adhesion molecule
LFA-1	Leukocyte function-associated antigen-1
LoxP	Locus of crossing-over Phage 1
Mac-1	Macrophage-1 antigen
MAdCAM-1	Mucosal addressin cell adhesion molecule-1
mRNA	Messenger ribonucleic acid
KO	Knockout
MHC	Major histocompatibility complex
OCT	Optimal cutting temperature compound
PTX	Pertussis toxin
PBS	Phosphate buffered saline
PECAM-1	Platelet endothelial cell adhesion molecule-1
PSGL-1	P-selectin glycoprotein ligand-1
RBC	Red blood cell
VCAM-1	Vascular endothelial cell adhesion molecule
VLA-4	Very late antigen-4
WT	Wild-type
ZT	Zeitgeber time

1. Introduction

1.1. The Circadian system

1.1.1. Circadian rhythms

Circadian rhythms exhibit a period length of about 24 hours. The term *circadian* comes from the Latin *circa*, meaning "around", and *diem* meaning "day". Organisms exposed to daily environmental cycles display rhythms in physiology, metabolism and behavior, which help them anticipate predictable environmental changes.

The simplest organisms known to exhibit circadian rhythms are cyanobacteria (Bhadra et al. 2017). Cyanobacteria can generate nutrients by photosynthesis and nitrogen fixation. Because the by-product of photosynthesis, oxygen, can inhibit the enzymes involved in nitrogen fixation, the two processes need to be separated either spatially or temporally. Since unicellular cyanobacteria do not have means for spatial separation, they therefore temporally separate these two processes, with photosynthesis taking place during the day, while nitrogen fixation occurs during night. Interestingly, when shifted to constant light, this rhythmicity is still maintained (Bhadra et al. 2017; Golden et al. 1997).

This example shows an essential characteristic of a *bona fide* circadian rhythm, namely that these rhythms must oscillate in a constant environment, independent from external factors, such as food intake and light. Moreover, circadian rhythms are driven by endogenous cell-autonomous clocks, but can be entrained to external *Zeitgebers* (time giver, e.g. light and food). Classical factors exhibiting circadian rhythms in mammals are core body temperature oscillations as well as plasma cortisol or melatonin levels.

1.1.2. The molecular clock machinery

The molecular clock consists of autoregulatory transcription-translation feedback loops, which have been largely discovered in studies using drosophila and mice. The core clock genes are *Bmal1* (brain and muscle Arntl-like protein 1) and *Clock* (circadian locomotor output cycles kaput), which are responsible for all circadian output (Hardin and Panda 2013).

The BMAL1 protein heterodimerizes with CLOCK, and together they bind to promoter sequences called Enhancer Boxes (E-Box) to activate transcription of genes (Darlington et al. 1998). This includes their own repressors, which are three PER proteins (period circadian protein 1-3), and two CRY flavoproteins (cryptochrome 1 and 2). These proteins form PER-CRY heterodimer complexes in the cytoplasm and move into the nucleus to interfere with CLOCK-BMAL1 complex activities (Jin et al. 1999; Griffin, Staknis, and Weitz 1999; Gekakis et al. 1998). When enough of the PER/CRY complexes are degraded by the proteasome, BMAL1/CLOCK expression increases and the cycle starts new (Golombek and Rosenstein 2010).

An accessory loop in mammals is generated by the nuclear hormone receptors, RAR-orphan receptor $\alpha/\beta/\gamma$ (Ror $\alpha/\beta/\gamma$), and REV-ERB α /REV-ERB β proteins (encoded by *Nr1d1* and *Nr1d2*), which bind Rev-Erb/ROR response elements (RREs) to active and inhibit *Bmal1* transcription, respectively (Preitner et al. 2002; Sato et al. 2004).

One cycle of the core feedback loop thus includes activator binding to E-boxes, the transcription of clock genes and clock-controlled genes, RNA processing and their cytoplasmic transport, protein synthesis, dimerization and nuclear localization of the repressors, transcriptional repression, and degradation of repressors (Hardin 2011).

A key event regulating circadian period is protein phosphorylation. Protein kinases casein kinase I epsilon (CKI ϵ) and delta (CKI δ) (encoded by *Csnk1d* and *Csnk1e*, respectively) regulate PER1/2/3 and CRY1/2 protein degradation and nuclear localization through phosphorylation (Vielhaber et al. 2000; Maywood et al. 2014; Etchegaray et al. 2009). CKI ϵ or CKI δ can also regulate BMAL1 phosphorylation and thus mediate CLOCK-BMAL1 dependent transcription (Eide et al. 2002). Therefore,

mutations in both *Csnk1d* and *Csnk1e* present profound changes in circadian cycle length.

Moreover, various epigenetic mechanisms that modify the architecture of chromatin have also been implicated in regulating CLOCK-BMAL1 transcriptional output. Circadian transcription of CLOCK-BMAL1 target genes correlates with circadian changes in histone acetylation (Papazyan, Zhang, and Lazar 2016). Four core histones (H2A, H2B, H3, and H4) wrap DNA and form the histone octamer of nucleosome. The histone variant H2A.Z can be deposited at both promoters and intergenic regulatory regions of CLOCK-binding sites to open DNA/nucleosome structure and provide a binding platform for transcription factors to regulate gene expression (Subramanian, Fields, and Boyer 2015). The CLOCK protein has been found to be a histone acetyltransferase (Doi, Hirayama, and Sassone-Corsi 2006), indicating the critical importance of histone acetylation in circadian gene regulation.

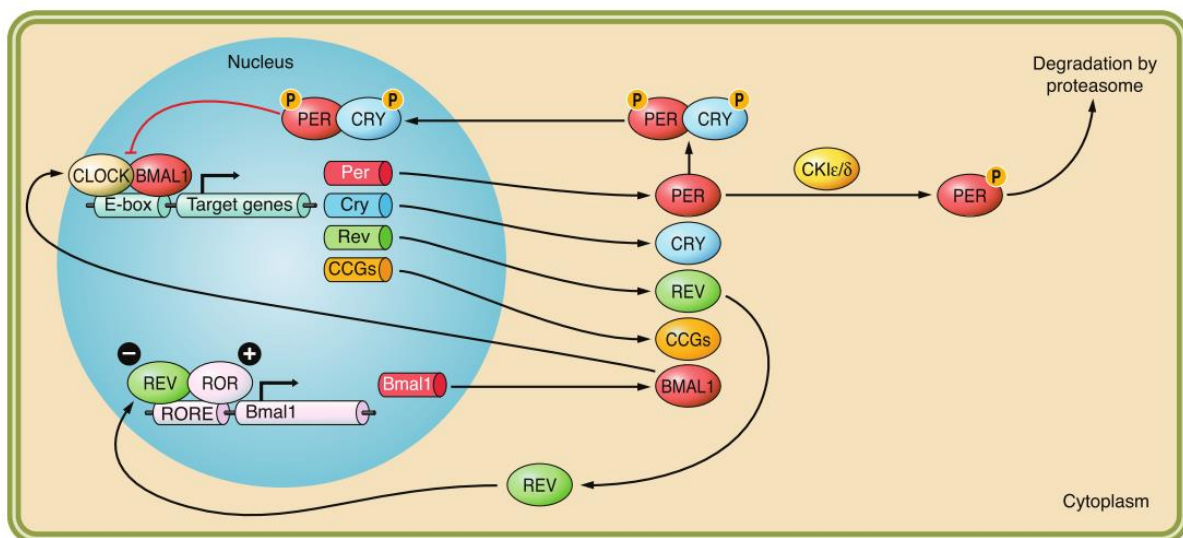


Figure 1.1 The molecular clock

The core component BMAL1 and CLOCK form a heterodimeric transcription factor complex which binds to E-box motifs of clock-controlled genes. This drives the negative feedback loop of PER-CRY heterodimer complexes to inhibit CLOCK/BMAL1-induced gene expression. Phosphorylation of PER by CKIε/δ will cause its degradation by the proteasome. A second feedback loop involves REV-ERBα and REV-ERBβ proteins. They compete with ROR proteins to inhibit *Bmal1* transcription via Rev-Erb/ROR response (RORE) elements (Golombek and Rosenstein 2010).

Also, non-transcriptional/translation events are sufficient to sustain cellular circadian rhythms. In the cyanobacterial clock system, circadian rhythms can be generated without transcription-translation feedback loop (Nakajima et al. 2005). This is also the

case for anuclear red blood cells, where the redox status drives circadian rhythms (O'Neill and Reddy 2011). Therefore, an organism or cell does not necessarily need the above described clock genes to exhibit functional circadian rhythms.

1.1.3. The central clock and synchronization of the organism

Although virtually every cell has its autonomous clock, these clocks need to be synchronized in order to be in phase coherence with the exogenous environment, as well as with tissues and organs within the organism. This is achieved by the central clock, which is located within the suprachiasmatic nuclei (SCN), consisting of about 20000 highly interconnected neurons. The SCN is located above the optic chiasm in the anterior hypothalamus. It links the organism to environmental changes via the eyes. The primary environmental cue of circadian rhythms is therefore light. This timing information is conveyed by non-image forming, photosensitive retinal ganglion cells (Lucas et al. 1999), and transmitted to the central clock via the retinohypothalamic tract. The prominent role of SCN was confirmed due to the loss of activity rhythms after ablation of the SCN and restoration of circadian activity rhythms by SCN tissue transplantation (Lehman et al. 1987)

Output projection from the SCN can target many different brain regions, and these output pathways are responsible for the proper timing of hormone release, behavior states and body temperature fluctuations. For example, the supraventricular zone (sPVz) projections to the medial preoptic region (MPO) are involved in the control of circadian rhythms in body temperature. The dorsomedial nucleus of the hypothalamus (DMH), which receives input from SCN both directly and via the subparaventricular zone (sPVz), controls sleep-wake cycle and daily hormone secretion via the paraventricular nucleus (PVN) of the hypothalamus (Takahashi et al. 2008).

Central clock signals are transmitted to peripheral tissues directly or indirectly via neuronal or humoral pathways. Two hormones that show strong circadian rhythms are

melatonin and glucocorticoids (cortisol in humans and corticosterone in mice). In humans, plasma levels of melatonin start to rise about two hours before the habitual bedtime and remain at a high level during night-time (Benarroch 2008). The primary site of melatonin synthesis is the pineal gland. Increased activity of the SCN during the light phase can reduce sympathetic output to the pineal gland via the SCG (superior cervical ganglion), and inhibit melatonin secretion (Maronde and Stehle 2007). Melatonin has a variety of function, including sleep induction, blood pressure regulation and enhancement of immune responses (Benarroch 2008). However, the most commonly used mouse strain, the C57BL/6 line, is a natural hypomorph for melatonin but still exhibits strong circadian rhythms, indicating a non-critical role for melatonin in mediating rhythmicity in the mouse (Tosini et al. 2014).

Glucocorticoids regulate a broad spectrum of physiologic functions for life. Both in humans and rodents, glucocorticoids peak around the onset of the activity phase, in the early morning in diurnal humans and in the early night in nocturnal animals (Dickmeis 2009). Diurnal glucocorticoid secretion is under control of the SCN, the hypothalamic-pituitary adrenal (HPA) axis as well as an adrenal gland intrinsic oscillator (Chung et al. 2017). Release of adrenocorticotropic hormone (ACTH) is regulated by the SCN and output through the hypothalamus, which causes the production of glucocorticoids in a circadian manner. Rhythmic secretion of glucocorticoids can entrain signals for peripheral oscillators in target tissues, such as lung, liver, heart and skeletal muscles (Almon et al. 2008; Balsalobre et al. 2000; Gibbs et al. 2014).

Another way of transferring a synchronizing signal to peripheral tissues is via cyclical release of norepinephrine locally from nerve varicosities by sympathetic nerves (Scheiermann, Kunisaki, and Frenette 2013). Light exposure can induce changes in the liver mRNA levels of clock genes and output genes. However, this change was abolished by removing liver innervation, indicating autonomic input to be an essential gateway for the transmission of light information from the SCN (Cailotto et al. 2009). Neural inputs mediated by β_2 -adrenergic receptors (β_2 ARs) generate the diurnal variation of lymphocyte egress from lymph node, with less lymphocyte recirculating into blood at night, which contributes to more efficient adaptive immune response this time point (Suzuki et al. 2016). Signals from the sympathetic nervous system delivered

by adrenergic nerves can also regulate rhythmic recruitment of leukocytes to skeletal muscles and bone marrow (Scheiermann et al. 2012). In addition, noradrenaline secreted by the sympathetic nervous system in a circadian manner regulates the rhythmic release of hematopoietic stem cells (HSCs) from the bone marrow and expression of *Cxcl12* in this tissue (Mendez-Ferrer et al. 2008). These examples demonstrate that the sympathetic nervous system serves as an important way to transfer synchronizing information to peripheral tissues.

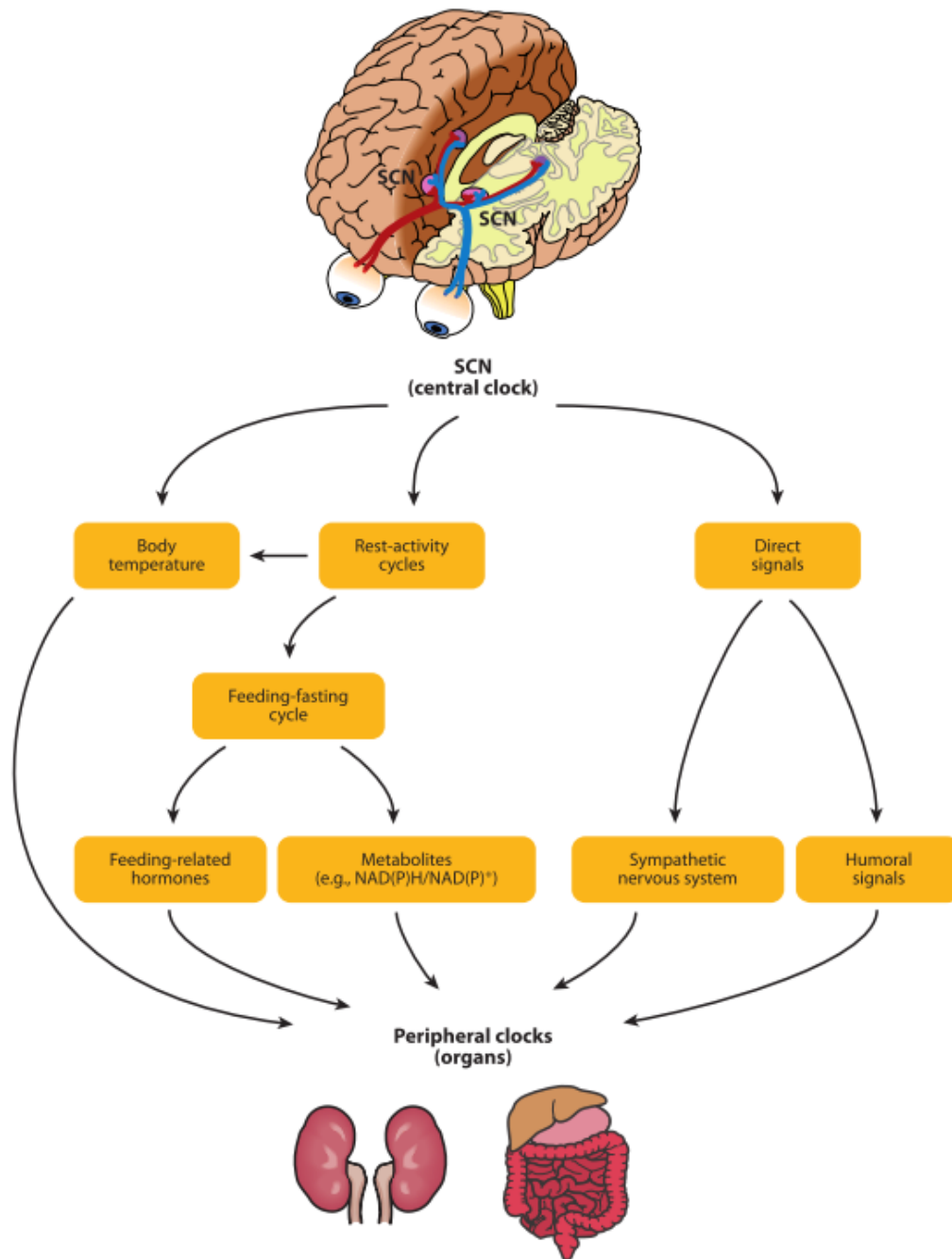


Figure 1.2 Peripheral clock entrainment pathways

The SCN central pacemaker establishes phase coherence in the periphery via multiple routes. Via neural projection into other parts of the brain, the SCN can influence body temperature and rest/behavioral activity. Another way to transmit signals directly to peripheral tissues is via the sympathetic nervous system and humoral signals (Dibner, Schibler, and Albrecht 2010).

1.1.4. The peripheral clock

The circadian clock is ticking not only in central neurons but also in virtually all peripheral tissues (Maury, Ramsey, and Bass 2010). Peripheral clocks are cell autonomous oscillators that can operate independently from the SCN. *In vitro* cultured tissues from liver, lung, kidney and spleen still exhibit strong circadian oscillations in gene expression, demonstrating that non-SCN peripheral cells also contain their own endogenous circadian oscillators (Keller et al. 2009; Sumova et al. 2006). In addition, a liver-specific *Bmal1* deficient mouse strain was shown to lose rhythmic expression of hepatic glucose regulatory genes and exhibits hypoglycemia (Lamia, Storch, and Weitz 2008).

Although the peripheral clock is self-sustained, it still needs the synchronizing information from the SCN. In SCN-lesioned mice, the peripheral tissues continue to oscillate, but their phases are no longer coordinated so that the result is behaviorally arrhythmic animals (Tahara et al. 2012). Furthermore, in 'jet lag' experiments, where light cycles were advanced or delayed by 6 hours, the resynchronization of peripheral oscillators needs over a week, while the SCN can reset rapidly to a time shift (Yamazaki et al. 2000). Taken together, the peripheral clock is synchronized by the SCN, but can oscillate in a self-sustained manner.

1.2. Leukocyte migration

1.2.1. Blood leukocyte numbers oscillate over 24 hours

Blood flow helps distribute leukocytes to where and when they are needed in the body to drive immune responses and facilitate tissue repair. A circadian variation in total leukocyte counts has been known in various species including humans and mice. In murine blood, total leukocyte numbers fluctuate during 24 hours with a peak during the

rest phase and a trough during the active phase (Ohkura et al. 2007). Daily oscillations in peripheral blood have also been described in leukocyte subsets, such as total lymphocytes, neutrophils (Oishi et al. 2006), Ly6G^{hi} monocytes (Nguyen et al. 2013) and T cells (Druzd et al. 2017). In humans, blood cells oscillate in a similar way but at inverse times, since humans are not nocturnal (Born et al. 1997). However, using a humanized mouse model, in which both human and mouse leukocytes circulate in a murine host, it was shown that they exhibit opposite oscillations. Leukocytes exhibited opposite number oscillations due to differential cellular levels of reactive oxygen species in mouse and human cells regulated through p38 mitogen-activated protein kinase pathway (Zhao et al. 2017). This indicates that – at least in this model – leukocytes are responsible for the oscillations in a cell-autonomous manner.

1.2.2. Circulating blood cell numbers

The underlying mechanisms of circadian changes in circulating blood cells are composed of multiple factors, such as distribution of cells between the circulation and a marginal cell compartment in tissues, influx of leukocytes from storage sites, and efflux of blood cells into lymphoid, hematopoietic or other tissues (Scheiermann, Frenette, and Hidalgo 2015; Ohkura et al. 2007).

The efflux of blood leukocyte into tissues could be one of the major reasons of the dramatic leukocyte numbers drop at the onset of activity phase. Leukocytes recruited from blood to tissues in steady-state conditions serve four main purposes, definitive elimination, recirculation, tissue repair and replenishment (Scheiermann, Frenette, and Hidalgo 2015). Regardless of the purpose of the recruited cell, the basic mechanisms that lead leukocytes to migrate into tissues are a series of interactions with the endothelium, which was summarized as the leukocyte adhesion cascade as discussed below.

1.2.3. Leukocyte adhesion cascade

1.2.3.1. Leukocyte migration in venules

Most of the leukocyte migration process to tissues occurs at the sites of postcapillary venules. This process is organized into well recognized steps, including rolling, adhesion, crawling and transmigration. Studies have expanded on this process to include more features such as intraluminal crawling, paracellular and transcellular migration, as well as migration through the basement membrane (Ley et al. 2007; Kolaczkowska and Kubes 2013).

Leukocyte emigration from the blood stream is initiated by the interaction of leukocytes with endothelial cells that coat the vessels and thus provide first interactions points. The cell-surface proteins selectins can interact with glycoproteins and other glycosylated ligands to produce weak binding between leukocytes and endothelial cells. Selectins include L-selectin, P-selectin and E-selectin. Most leukocytes express L-selectin, whereas E-selectin and P-selectin are mostly expressed on endothelial cells, particularly after being induced by inflammatory cytokines (Ley et al. 2007; Hidalgo et al. 2007). All three selectins can interact with P-selectin glycoprotein ligand 1 (PSGL1), which is expressed on almost all leukocytes and also certain endothelial cells, such as venules of murine mesenteric lymph node and small intestine (Rivera-Nieves et al. 2006). In addition to PSGL-1, E-selectin also binds to glycosylated CD44 (Dimitroff et al. 2001) and E-selectin ligand 1 (ESL1) to promote rolling (Hidalgo et al. 2007).

Through the process of rolling, leukocytes slow down and come in close contact with endothelial cells and thus are exposed to chemokines immobilized on the endothelial cell surface. Chemokine binding to G-protein coupled receptors expressed by migrating leukocytes induce conformational changes of leukocyte integrins, from a low-affinity 'bent' structure to an intermediate and 'upright' high affinity conformation, which in turn mediates firm adhesion to the endothelium (Campbell and Humphries 2011). The most important integrins are the two β_2 integrins, leukocyte function-associated antigen-1 (LFA-1, $\alpha_L\beta_2$, CD11a/CD18), which is expressed by all leukocytes, and

Macrophage-1 antigen (Mac-1, $\alpha_M\beta_2$, CD11b/CD18), which is expressed predominantly by myeloid cells, and the two α_4 integrins, very late antigen 4 (VLA-4, $\alpha_4\beta_1$, CD49d/CD29), which is expressed by all leukocytes, and $\alpha_4\beta_7$, which is mainly expressed on T cells for gut-specific homing (Marelli-Berg et al. 2008; Vestweber 2015; Kim 2005; Henderson et al. 2001; Fleming et al. 2003; Gan et al. 2012; Lim et al. 2000). The activated integrins bind to members of the endothelial immunoglobulin superfamily. $\alpha_4\beta_7$ binds to mucosal adhesion-cell adhesion molecule 1 (MAdCAM-1). VLA-4 binds to vascular-cell adhesion molecule 1 (VCAM-1), and β_2 integrins bind intracellular adhesion molecule 1 (ICAM-1), and intracellular adhesion molecule 2 (ICAM-2) (Vestweber 2015).

The final stage in the process of leukocyte emigration into extravascular tissue involves crossing the vascular wall and its associated perivascular basement membrane. Most leukocytes cross the endothelial barrier through endothelial cell junctions, which is called the paracellular route. A minor pathway where leukocytes migrate through the body of endothelial cells is called the transendothelial pathway, which still often occurs close to the cell junction (Vestweber 2015). A lot of molecules are involved in leukocyte diapedesis, such as ICAM-1, ICAM-2; junctional adhesion molecule (JAM) A, B and C; platelet endothelial cell adhesion molecule 1 (PECAM-1); CD99; and endothelial cell-selective adhesion molecule (ESAM) (Marelli-Berg et al. 2008).

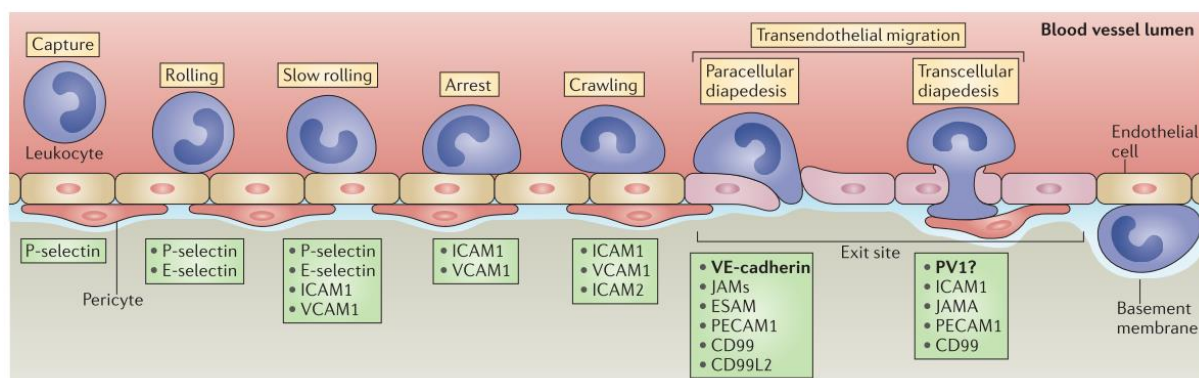


Figure 1.3 Adhesion cascade of leukocyte

Leukocyte migration from blood into tissues through selectin-mediated rolling, chemokine-triggered activation and integrin-dependent arrest, and transendothelial migration (Vestweber 2015).

1.2.4. Recruitment of leukocytes

With the discovery of the adhesion cascade, more and more evidence suggests that a specific expression pattern of pro-migratory molecules in tissues and leukocytes is of key importance for specific leukocyte subsets migrating into distinct tissues.

1.2.4.1. Leukocyte migration to the lung

The lung vasculature is composed of extremely thin capillaries which have a continuous and non-fenestrated endothelium to facilitate gas exchange. The capillaries form a complex interconnecting network of short vessels to build the alveolar-capillary membrane and perform barrier function (Leick et al. 2014; Lahm et al. 2007). Previous studies found leukocyte recruitment to occur predominantly at the level of capillaries, rather than postcapillary venules, which is in stark contrast to other tissues (Looney and Bhattacharya 2014; Wang, Doerschuk, and Mizgerd 2004).

The structural features of the lung capillaries (2-15 μm in diameter) make it difficult for neutrophils (6-8 μm in diameter) and even red blood cells (5-6 μm in diameter) to pass through. Neutrophils (and other cell types) are retained intravascularly in the lung and are temporarily sequestered from the circulation blood. Therefore, the lung serves as a reservoir of leukocytes, which is referred to as marginated pool. The marginated pool helps keep a dynamic equilibrium with the circulating pools of leukocytes (Looney and Bhattacharya 2014; Kuebler and Goetz 2002). In order to pass through the lung capillary network, leukocytes have to perform a morphology change from spherical shapes in arterioles to elongated shapes in the capillary.

Spatial constraints of the lung capillary rather than selectin-mediated rolling seems to dominate neutrophil retention in lung capillaries. Neither P-selectin nor E-selectin is constitutively expressed by the pulmonary capillary endothelium, and L-selectin played no role in neutrophil accumulation and margination in normal lungs (Doyle et al. 1997). However, blocking CD11b/CD18 and ICAM-1 interactions with antibodies largely prevented neutrophil sequestration and emigration into the alveolar space induced by

inflammatory stimuli (Moreland et al. 2002). In addition, CD11b/CD18-independent adhesion was shown not to be mediated by members of the selectin family, VLA-4, or PECAM-1 (Wang, Doerschuk, and Mizgerd 2004).

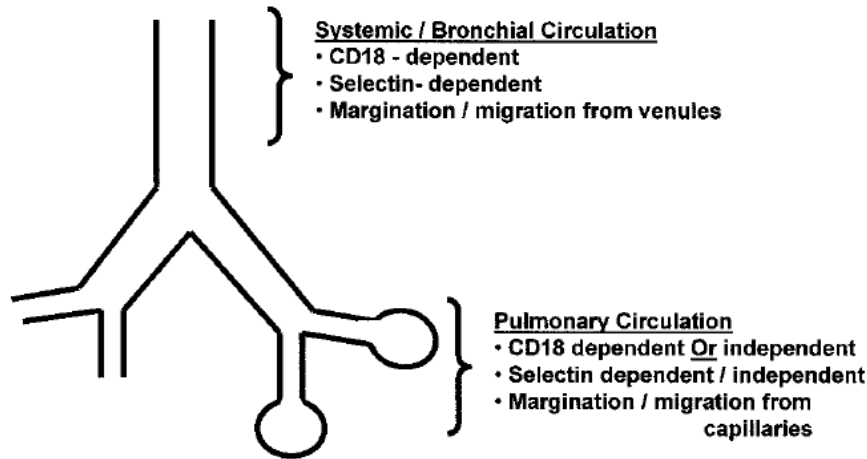


Figure 1.4 Difference in neutrophil migration in pulmonary circulation and in systemic and bronchial circulation

Neutrophils migration in systemic and bronchial circulation is selectin and CD18-dependent, while pulmonary circulation in steady state is selectin and CD18 independent unless induced by inflammatory stimuli (Wagner and Roth 2000).

By in vivo imaging with LysM-GFP transgenic mice, monocytes were found moving in a jerky intermittent pattern in alveolar capillaries and rarely arrested inside vessels or entering the tissue in the absence of inflammation. But monocytes were found rolling and occasionally entering the tissues under inflammatory conditions (Kreisel et al. 2010). In vivo homing assays also found circulating lymphocytes to be retarded for a certain time within the lung. Deficiency in the ICAM-1 pathway resulted in a decreased trapping of lymphocytes in the lung. However, blocking of ICAM-2 did not result in reduced lymphocyte numbers (Lehmann et al. 2003).

To conclude, neutrophils remain in the lung mostly as a marginated pool due to the unique morphology of lung capillaries, while in some inflammatory conditions, adhesion molecules were shown to be involved in neutrophil sequestration in the lung. Monocytes are rarely found in the lung without inflammatory stimuli. Lymphocyte migration into the lung is ICAM-1 dependent.

1.2.4.2. Leukocyte migration in liver

The liver has a dual blood supply due to its unique vascular architecture, consisting of the portal vein and the hepatic artery. Therefore, the microvasculature receives both arterial and venous blood that drains into post sinusoidal central veins. The hepatic capillaries are morphologically unique. They are lined with fenestrated endothelium and are separated from hepatocytes by a discontinuous basement membrane and a perisinusoidal space called 'Space of Disse'. Microvilli of the hepatocytes can extend into this space, and Kupffer cells, which are also known as stellate macrophages in the liver, are located in the space (Leick et al. 2014).

The majority of leukocyte adhesion in the liver occurs within sinusoids (80%), while only 20% of adhesion occurs in post-sinusoidal venules in response to a chemotactic stimulus (Wong et al. 1997). Recruitment of leukocytes in the post-sinusoidal venules of the liver follows a similar paradigm to the multi-step cascade with a rolling step before adhesion. But unlike in post-capillary venules, the migration within sinusoids occurs without any noticeable rolling (Lee and Kubes 2008). Leukocyte adhesion in sinusoids is selectin independent, probably as a consequence of the low levels of shear stress in the hepatic sinusoids and also little E- and P-selectin expression on the sinusoid endothelium (McNab et al. 1996).

In the rat liver at steady state, both the central venules and sinusoidal endothelium express ICAM-1 (Iigo et al. 1997). VCAM-1 and MAdCAM-1 is not expressed in normal liver tissue but can be upregulated on hepatic endothelium in inflammatory conditions (Volpes, Van Den Oord, and Desmet 1992; Ala, Dhillon, and Hodgson 2003).

β_2 integrins mediate adhesion of leukocytes in post-sinusoidal venules, but play a less obvious role in sinusoids (Lee and Kubes 2008). Activated CD8⁺ T cells adhere to liver sinusoidal endothelial cells via VCAM-1/VLA-4 interactions in the absence of antigen-dependent cues. If CD8⁺ T cells recognize antigens on the surface of hepatocytes or liver sinusoidal endothelial cells, CD8⁺ T cells adhere via ICAM-1/LFA-1 interactions (John and Crispe 2004). CXCL9 and CXCL10/CXCR3 interactions were reported to support the accumulation of virus-specific T cells in the murine liver (Hokeness et al. 2007).

Neutrophil adhesion within liver sinusoids is mediated by ICAM-1 and CD11b/CD18 in sterile inflammation, while CD44 rather than CD11b/CD18 interactions with hyaluronan (HA) have been found to mediate the recruitment of neutrophils to the liver in response to infectious stimuli (McDonald et al. 2008). CXCR2 expressed on the luminal surface of liver sinusoids around sites of necrosis can guide neutrophil to migrate to the site of injury (McDonald et al. 2010).

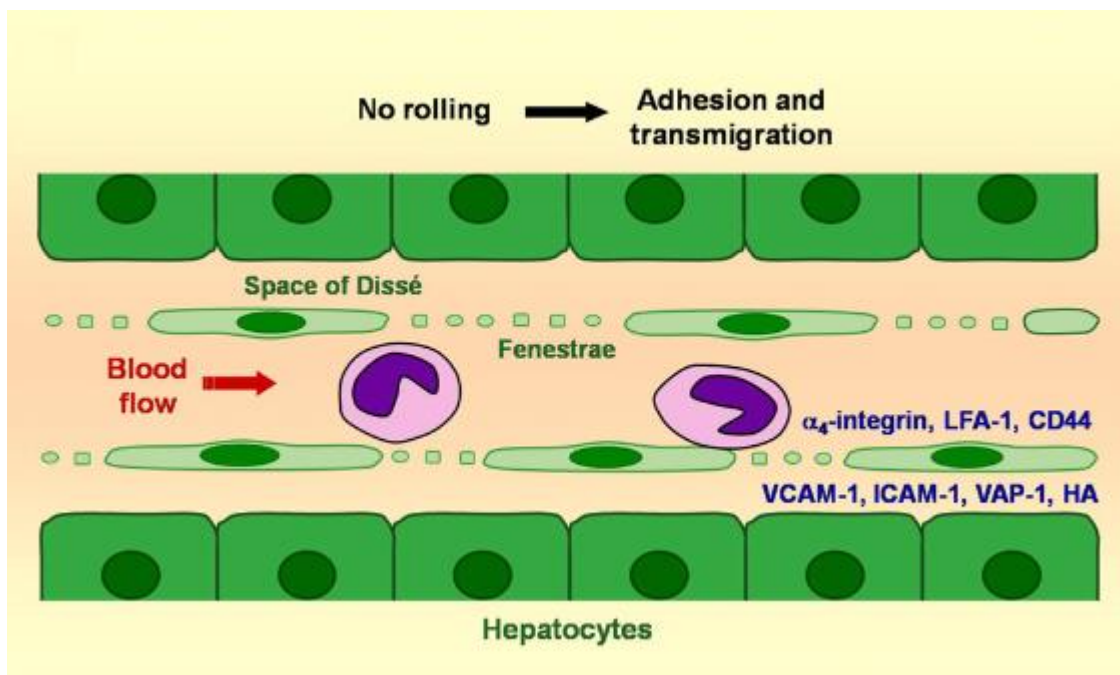


Figure 1.5 Leukocyte recruitment in liver in an inflammatory response

The structure of hepatic sinusoidal endothelium is fenestrated and lacks a basal membrane. Blood flow in the liver is slow. Leukocyte recruitment in liver sinusoids is selectin-independent. Cells adhere to liver endothelial cells by interaction between adhesion molecules, including α_4 integrins, LFA-1, CD44, VCAM-1, ICAM-1 and HA. In mice, very little VAP-1 was found in liver, but it can be significantly upregulated in all vessels of the inflamed liver (Lee and Kubes 2008).

In conclusion, leukocyte migration in liver is generally selectin-independent. ICAM-1 is expressed in liver endothelium and guides the CD8 T cell recruitment process, as well as that of neutrophils in sterile inflammation. VCAM/VLA-4 interactions contribute to CD8 T cell adhesion, although some studies suggest VCAM-1 was not expressed in liver under non-inflammatory conditions.

1.2.4.3. Leukocyte migration into lymph nodes

Lymphocytes are being recruited from blood to lymph nodes at the site of high endothelial venules (HEVs) (Marchesi and Gowans 1964). The interaction between lymphocytes and HEVs is initiated by L-selectin on the surface of lymphocytes. CD62L recognizes a family of mucin-like glycoprotein (also called peripheral nodal addressins, PNA_d), and the crucial carbohydrate determinant for recognition is called 6-sulpho sialyl Lewis X, which is abundantly expressed by HEVs. This apically expressed carbohydrate supports rolling of CD62L-high leukocytes and is crucial for homing, as blocking of this carbohydrate with the anti-PNA_d carbohydrate epitope antibody MECA-79 results in a functional block of leukocyte homing to the lymph node (Umemoto et al. 2006).

The next step for lymphocyte homing is to build firm adhesion due to a chemokine-induced activation of integrins. For T cells, the most important chemokines are CCL21/CCL19 and CXCL12, which can be recognized by the CCR7 and CXCR4 receptors respectively. In addition to these two receptors, B cells also express CXCR5, which is the receptor for CXCL13. HEV endothelial cells can abundantly express CCL21 (in mice, not humans) (Gunn et al. 1998), while lymph node stromal cells can produce CCL19, CXCL12 and CXCL13 and transcytose these molecules to the luminal surface of HEVs (Girard, Moussion, and Forster 2012; Okada et al. 2002; Baekkevold et al. 2001). These chemokine signals induce binding of LFA-1 to ICAM-1 and ICAM-2 in peripheral lymph nodes, or $\alpha 4\beta 7$ to MAdCAM-1 in mesenteric lymph nodes. By *in vivo* homing assays with lymphocytes as donor cells, overlapping effects of ICAM-1 and ICAM-2 were found. Blocking any of these molecules alone was shown not to influence the recruitment of lymphocytes, while simultaneous blockade of both adhesion molecules could drastically decrease recruitment (Lehmann et al. 2003). CXCR4 was found to support a low level of T cell homing when CCR7 ligands were absent (as found in the PLT mouse) (Bai et al. 2009), while blocking CCR7 and CXCR4 could block 90% of B cell migration to lymph nodes (Okada et al. 2002).

The firm adhesion of rolling cells on the inner luminal surface of HEV enables leukocytes to cross the tissue either via paracellular migration or transcellular transmigration (Engelhardt and Wolburg 2004). The transcellular route was found to

be preferentially used by lymphocytes (Nieminen et al. 2006) through ICAM-1 and VCAM-1 enriched endothelial projections (Carman and Springer 2004). Some transmigrated lymphocytes were shown to accumulate in HEV pockets for several minutes before entering the parenchyma as a way to control the lymphocyte entry flux (Mionnet et al. 2011).

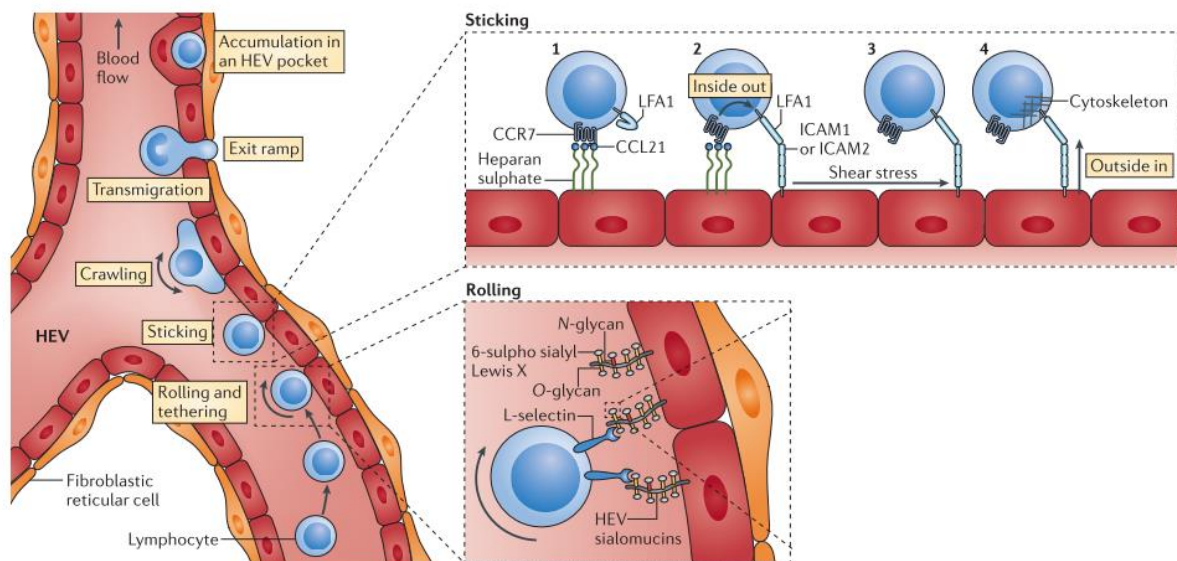


Figure 1.6 Lymphocytes migration to lymph nodes

Leukocyte recruitment from HEVs into lymph nodes through binding of CD62L to 6-sulpho sialyl Lewis X. Following rolling and tethering, firm adhesion by chemokine-induced activation of integrins is achieved by LFA-1 binding to ICAM-1 and ICAM-2. Finally, leukocytes transmigrate and accumulate in HEV pockets, and migrate into the lymph node parenchyma (Girard et al. 2012).

Neutrophils are largely excluded from lymph nodes under steady-state conditions, but can be recruited to draining lymph nodes in response to stimuli, such as inflammation, through both lymphatic and blood routes. L-selectin and PSGL-1, Mac-1 and LFA-1, and the chemokine receptor CXCR4 help neutrophils to migrate across HEVs, whereas Mac-1, LFA-1 and CXCR4 are also involved in the lymphatic trafficking route (Gorlino et al. 2014; Hampton and Chtanova 2016).

Taken together, lymphocytes migrate into lymph nodes from blood via HEVs. The recruitment process is initiated by L-selectin, followed by interaction between LFA-1 and ICAM-1/ICAM-2 and chemokines, including CCL21/CCL19, CXCL12 and CXCL13. Neutrophils are recruited to lymph nodes in response to inflammatory stimuli. L-selectin, PSGL-1, Mac-1, LFA-1 and CXCR4 were shown to be involved in this process.

1.2.4.4. Leukocyte migration to the spleen

The spleen is the largest secondary lymphoid organ and has a complex anatomy. It is composed of open-structured red pulp, which can filter blood and remove old red blood cell, and interwoven branches of white pulp, which is composed of lymphoid tissues. The red and white pulps are separated by the marginal zone, where follicular arteries terminate and form the sinus. Some lymphocytes together with non-lymphocytes pass to the outer region of the marginal zone and then to the red pulp or directly into venous sinuses. A fraction of lymphocytes enter the white pulp from the marginal zone and appear within the B and T cell areas of the white pulp cords (van Ewijk and Nieuwenhuis 1985; Lo, Lu, and Cyster 2003).

The white pulp is densely populated with lymphocytes. Lymphocytes can enter the spleen from the marginal sinus without the help of CD44, PSGL-1, L-selectin. But interactions through integrin LFA-1 and VLA-4, and their ligands ICAM-1 and VCAM-1 expressed by the sinus lining cells in the marginal zone are required. Blocking VLA-4 alone had no measurable effect on lymphocyte accumulation in the while pulp, but blocking both LFA-1 and VLA-4 generated a stronger blocking effect than blocking LFA-1 alone, suggesting the contribution of VLA-4 to lymphocyte homing is fully redundant to LFA-1, while LFA-1 is partially redundant with VLA-4 (Lo, Lu, and Cyster 2003). Although there is high expression of ICAM-1 on sinus lining cells, blocking LFA-1 can only partly block the recruitment of leukocytes to the while pulp, and no specific difference for T or B cells were found (Nolte et al. 2002).

Blocking ICAM-1 can partially reduce the number of B cells migration into white pulp cords. Blocking LFA-1 and VCAM-1 generated a reduction in B cells homing to the white pulp, better than blocking LFA-1 alone but not as severe as the combination of anti-VLA-4 and anti-LFA-1. MadCAM-1 is also expressed within the marginal zone, but no contribution was found for MAdCAM-1 or $\alpha_4\beta_7$ integrin (Lo, Lu, and Cyster 2003).

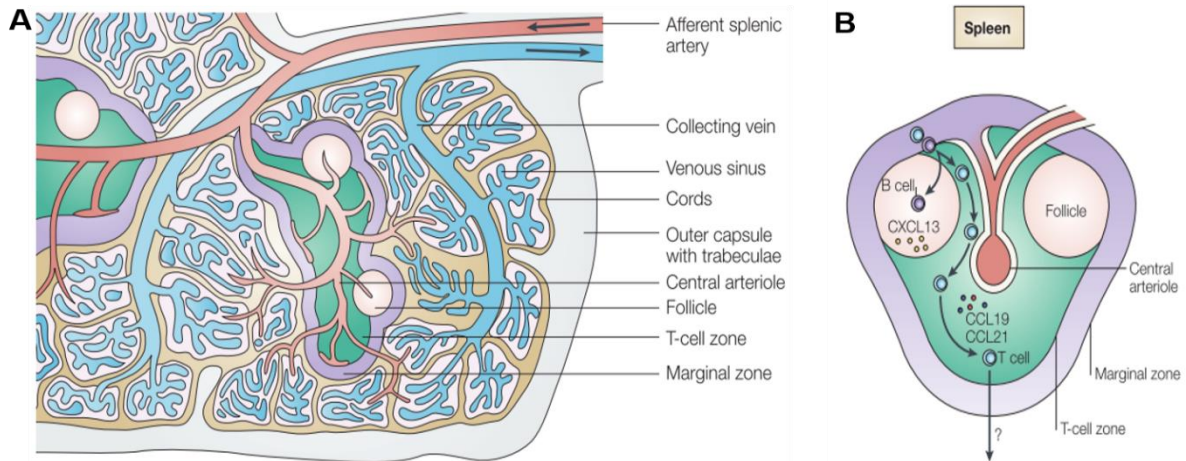


Figure 1.7 Spleen structure

(A) The afferent splenic artery enters the spleen and branches into central arterioles, which are sheathed by white-pulp areas consisting of the T-cell zone, B-cell follicles, and arterioles. The arterioles end in the red pulp which consists of a lot of venous sinuses. Blood from the arterioles and run into the sinuses, and finally collect into the efferent splenic vein. (B) Follicular arteries terminate in the marginal zone and form the marginal sinus. Leukocyte enter the white pulp through the marginal zone. Entry of the leukocyte is initiated by interaction of adhesion molecules. Leukocyte migrate into different zones by the guidance of different chemokines (Mebius and Kraal 2005).

The red pulp has an open connection with the blood stream, and serves as a filter to remove bacterial and senescent leukocytes from blood. Some lymphocytes can be found localized in the red pulp, which is regarded as a passive process, but selective retention may also occur (Nolte et al. 2002).

The spleen is also one of the sites to clear old neutrophils, together with the liver and the bone marrow. By pre-treatment of senescent neutrophils with pertussis toxin, the accumulation of neutrophils was decreased by 50%, indicating that neutrophil clearance via spleen is an active process mediated via Gai-coupled receptors (Gordy et al. 2011; Furze and Rankin 2008).

In conclusion, the spleen has two major structures, the white pulp and the red pulp. The migration to the white pulp is induced by the interactions of adhesion molecules, such as LFA-1/ICAM-1 and ICAM-2, VLA-4 and VCAM-1. However, the migration of leukocytes in the red pulp is considered to be a passive process.

1.2.4.5. Leukocyte migration to the bone marrow

The bone marrow has two distinct blood vessel types with different permeability properties, less permeable arterial blood vessels and more permeable sinusoids. The arterial bone marrow endothelial cells (BMEC) express higher level of VCAM-1, ICAM-1 and P-selectin, while sinusoidal BMEC express higher levels of E-selectin (Itkin et al. 2016). However, arterial blood vessels are less permeable and experience a higher blood flow (Spencer et al. 2014). This is likely one of the reasons why leukocyte trafficking from and to bone marrow occurs exclusively at the sinusoids (Itkin et al. 2016).

The bone marrow is the site to clear CXCR4^{high} senescent neutrophils, and therefore constitutes a major homing site for neutrophils (Furze and Rankin 2008). In vivo homing experiment with Indium-111 labelled neutrophils suggests that peripheral blood neutrophils homed significantly to both the bone marrow (approximately 31%) and the liver (approximately 32%) after 4 hours, and the percentage of neutrophils homed to bone marrow was even higher (approximately 62%) if bone marrow neutrophils were used as donor cells (Strydom and Rankin 2013; Suratt et al. 2001). Blocking CXCR4 impedes with neutrophil homing to the bone marrow (Martin et al. 2003), and CXCR4 deficient neutrophils failed to enter the bone marrow, but not the liver or the spleen (Casanova-Acebes et al. 2013), suggesting the recruitment process for neutrophils to bone marrow is CXCR4 dependent (Eash et al. 2009).

The bone marrow is also a major reservoir and site of recruitment for central memory CD8⁺ T cells. T_{cm} cells arrest in bone marrow microvessels mainly by interactions between VLA-4 and VCAM-1. The extravasation step is chemokine dependent, since PTX treatment can largely inhibit T_{cm} cells from emigrating (Mazo et al. 2005).

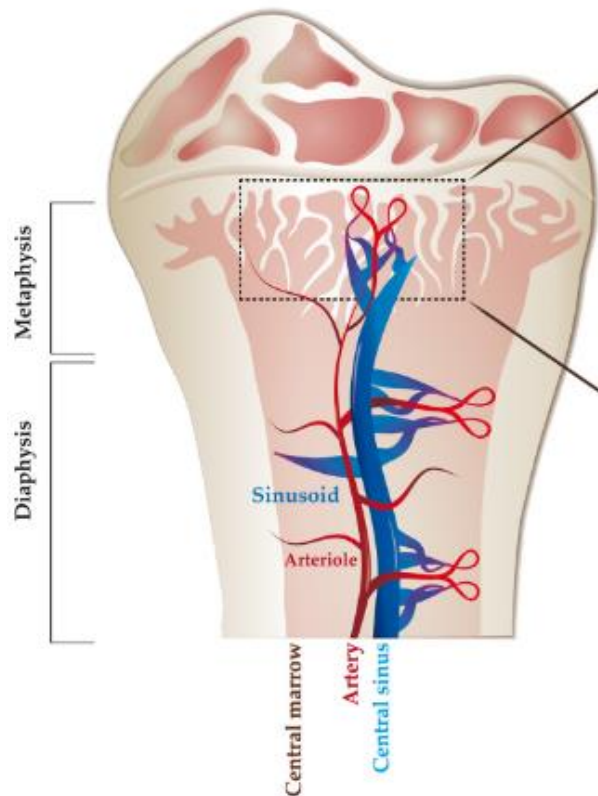


Figure 1.8 Bone marrow blood vessels model

The bone marrow vasculature has two main types of blood vessels which are arterial blood vessels and sinusoids. Blood enters the bone marrow via the arteries. The artery branches to smaller arterioles, and further branch into small-diameter endosteal arterioles which reconnect to downstream sinusoids. Blood flows into the central sinus and then out of the bone marrow (Itkin et al. 2016).

To conclude, bone marrow is the major site for neutrophil homing and this process is CXCR4 dependent. Central CD8+ T cells also home to bone marrow by VLA-4/VCAM-1 interactions. The leukocyte recruitment process occurs predominantly at the site of sinusoids where E-selectin is expressed at higher levels.

1.3. Homing zip code and circadian rhythmicity

There is evidence suggesting that rhythmic expression of pro-migratory molecules is responsible for leukocyte migration to specific tissues in a rhythmic manner. Scheiermann et al described rhythmic hematopoietic cell recruitment to the bone marrow to be mediated by expression of P-selectin, E-selectin and VCAM-1, and leukocyte recruitment to skeletal muscle in a circadian manner due to rhythmic

expression of ICAM-1 and *Ccl2* on skeletal muscle endothelium (Scheiermann et al. 2012). However, what specific cell type is recruited to which specific tissue at what time depending on which molecules is unknown. The aim of this thesis was to address this question by using circadian rhythms as a screening tool to focus on pro-migratory molecules on leukocytes and endothelial cells.

The rhythmic expression of some pro-migratory molecules is controlled by circadian genes (Scheiermann et al. 2012; Gibbs et al. 2014; Nguyen et al. 2013). Gibbs et al described pulmonary epithelial-specific ablation of *Bmal1* increased expression of CXCL5, which induced higher neutrophil recruitment to the lung in response to LPS (Gibbs et al. 2014). Nguyen et al found that the internal *Bmal1/Clock* cycles impact on expression of *Ccl2*, which was essential for rhythmic monocyte migration (Nguyen et al. 2013). Scheiermann et al described rhythmic hematopoietic stem cell recruitment to the bone marrow and leukocyte recruitment to skeletal muscle to be abolished in *Bmal1*^{-/-} mice (Scheiermann et al. 2012). Druzd et al found that *Bmal1*-deficient T cells lost rhythmic expression of CCR7, and lost overall rhythmicity in T cell homing to lymph nodes, suggesting that rhythmic expression of pro-migratory molecules guides leukocytes homing to lymph nodes at a specific time, and that expression of adhesion molecules is regulated by the circadian clock (Druzd et al. 2017).

3-10% of all mRNAs in a given tissue show circadian rhythms in steady state, but these are largely non-overlapping in each tissue. Indeed, about 60% of the genes cycling in liver or heart are also expressed in the other tissue, but they do not cycle there, suggesting each tissue to have its own mechanism for the circadian regulation of specific genes in order to perform cellular physiological function according to each cell type (Panda et al. 2002; Storch et al. 2002).

The rhythmic expression of pro-migratory molecules is not only mediated by intrinsic clocks, but also outside signals stemming from the SCN. Scheiermann et al found that enhanced adrenergic tone at night could upregulate expression of P-selectin, E-selectin and VCAM-1 (Scheiermann et al. 2012). Gibbs et al described that systemic adrenal glucocorticoids activating glucocorticoid receptor could act as a circadian repressor of CXCL5 expression on lung epithelial club cell (Gibbs et al. 2014). These findings suggest that the timely and tissue specific expression of pro-migratory

molecules is not only under the control of circadian genes inside the cells, but is also dependent on the environment.

The hypothesis of the thesis is that rhythmic recruitment of leukocytes from blood to tissues contributes to a dramatic drop in the number of leukocytes in murine blood at night. Migration of leukocytes in a circadian manner is due to the rhythmic expression of specific pro-migratory molecules, which form a homing zip code that can determine when and to which organ leukocytes migrate.

Table 1.1 Summary of homing zip code for leukocytes

Organs	Leukocyte	Ligands	conditions	Reference
Lung	Neutrophils	ICAM-1/CD11b	Inflammation	(Moreland et al. 2002)
	Lymphocytes	ICAM-1		(Lehmann et al. 2003)
Liver	Activated CD8 T cells	VCAM-1/VLA-4	No antigen recognition	(John and Crispe 2004)
		ICAM-1/LFA-1	Antigen recognition	(John and Crispe 2004)
	Neutrophil	ICAM-1/CD11b	Sterile inflammation	(McDonald et al. 2010)
		CD44/hyaluronan	Inflammation	(McDonald and Kubes 2015)
Lymph node	T cells	L-selectin, ICAM-1/LFA-1, ICAM-2/LFA-1, CCR7, CXCR4		(Girard, Moussion, and Forster 2012)
	B cells	L-selectin, ICAM-1/LFA-1, ICAM-2/LFA-1, CCR7, CXCR4, CXCR5		(Girard, Moussion, and Forster 2012)
	Neutrophils	L-selectin, PSGL-1, CD11b, LFA-1, CXCR4	Inflammation	(Gorlino et al. 2014; Hampton and Chtanova 2016)
Spleen	lymphocytes	ICAM-1/LFA-1, VCAM-1/VLA-4		(Lo, Lu, and Cyster 2003)
Bone marrow	Neutrophils	CXCR4		(Martin et al. 2003)
	Central memory CD8+ T cells	VCAM-1/VLA-4		(Mazo et al. 2005)

2. Materials

2.1. Animals

Male C57BL/6N mice aged 7-8 weeks were purchased from Charles River Laboratories (Sulzfeld, Germany). *Bmal1*^{flox/flox}, *CD19-cre*, *CD4-cre*, *Lyz2-cre* transgenic mice were purchased from Jackson Laboratories, and crossbred to obtain *CD19-cre Bmal1*^{flox/flox} mice, *CD4-cre Bmal1*^{flox/flox} mice, and *Lyz2-cre Bmal1*^{flox/flox} mice in-house. *Cdh5-cre/ERT2 Bmal1*^{flox/flox} mice were a gift from Eloi Montanez/Ralf Adams and were given intraperitoneal tamoxifen injection for five consecutive days to induce Cre recombinase expression. Experimental mice were male and used at 8-12 weeks of age, bred and fed in the Walter-Brendel Center for Experimental Medicine, LMU Munich, Germany. Mice were maintained in a 12-hour light/dark cycle with *ad libitum* access to food and water. For some experiment, mice were put in cabinets to change the light phase in order to perform experiments with animals on different light schedules at the same time. All animal procedures were in accordance with German Law of Animal Welfare and approved by the Regierung of Oberbayern.

2.2. Genotyping

Primers for genotyping

Table 2.1 Primer sequence and annealing temperature for genotyping

Primers	Sequence	Annealing(°C)
Generic <i>cre</i> Forward	GCG GTC TGG CAG TAA AAA CTA TC	62
Generic <i>cre</i> Reverse	GTG AAA CAG CAT TGC TGT CAC TT	
<i>Bmal1</i> flox Forward	ACT GGA AGT AAC TTT ATC AAA CTG	55
<i>Bmal1</i> flox Reverse	CTG ACC AAC TTG CTA ACA ATT A	

PCR reaction mix

Table 2.2 Reaction mix for genotyping

Dream Taq	10 μ l
H ₂ O	8.6 μ l
Forward primer	0.2 μ l
Reverse primer	0.2 μ l
DNA	1 μ l

2.3. Antibodies

2.3.1. Flow cytometry

Table 2.3 Antibody list of flow cytometry
h-human, m-mouse

Antibody	Dye	Reactivity	Isotype	Clone	Company
CD3	PE/DZL594	anti-m	Rat IgG2b, κ	17A2	Biolegend
CD3 ϵ	Alexa Fluor® 488	anti-m	Armenian Hamster IgG	145-2C11	Biolegend
CD4	Brilliant Violet 570™	anti-m	Rat IgG2a, κ	RM4-5	Biolegend
CD4	PE	anti-m	Rat IgG2b, κ	GK1.5	Biolegend
CD4	APC	anti-m	Rat IgG2b, κ	GK1.5	Biolegend
CD4	APC/Cy7	anti-m	Rat IgG2b, κ	GK1.5	Biolegend
CD8a	PE/Cy7	anti-m	Rat IgG2a, κ	53-6.7	Biolegend
CD8a	APC/Cy7	anti-m	Rat IgG2a, κ	53-6.7	Biolegend
CD8a	PE-CF594	anti-m	LOU/M IgG2a, κ	53-6.7	BD Bioscience
CD8a	Alexa Fluor® 700	anti-m	Rat IgG2a, κ	53-6.7	Biolegend
CD11b	Alexa Fluor® 700	anti-m/h	Rat IgG2a, κ	M1/70	Biolegend
CD115	PE	anti-m	Rat IgG2a, κ	AFS98	Biolegend
CD115	APC	anti-m	Rat IgG2a, κ	AFS98	ebioscience
Gr-1	PerCP/Cy5.5	anti-m	Rat IgG2b, κ	RB6-8C5	Biolegend
Gr-1	FITC	anti-m	Rat IgG2b, κ	RB6-8C5	Biolegend

CD45R/B220	Alexa Fluor® 488	anti-m/h	Rat IgG2a, κ	RA3-6B2	Biolegend
CD45R/B220	PE/Cy7	anti-m/h	Rat IgG2a, κ	RA3-6B2	Biolegend
CD45R/B220	APC-Cy7	anti-m/h	Rat IgG2a, κ	RA3-6B2	Biolegend
Siglec-F	Alexa Fluor® 647	anti-m	Rat IgG2a, κ	E50-2440	BD bioscience
Siglec-F	APC-Cy™7	anti-m	LOU/M IgG2a, κ	E50-2440	BD Bioscience
NK1.1	APC	anti-m	Mouse IgG2b, κ	PK136	Biolegend
NK1.1	Alexa Fluor® 700	anti-m	Mouse IgG2a, κ	PK136	ebioscience
NK1.1	PE/Cy7	anti-m	Mouse IgG2a, κ	PK136	Biolegend
NK1.1	PE/Cy5	anti-m	Mouse IgG2a, κ	PK136	Biolegend
CD45	PE/Dazzle™ 594	anti-m	Rat IgG2b, κ	30-F11	Biolegend
CD45	PE	anti-m	Rat IgG2b, κ	30-F11	Biolegend
CD45	APC	anti-m	Rat IgG2b	I3/2.3	Biolegend
Ly6C	PE	anti-m	Rat IgG2c, κ	HK1.4	Biolegend
Ly6G	PerCP/Cy5.5	anti-m	Rat IgG2a, κ	1A8	Biolegend
I-A/I-E	PE/Cy7	anti-m	Rat IgG2b, κ	M5/114.15. 2	Biolegend
CCR1	PE	anti-m	Rat IgG2b, κ	643854	R&D
CCR2	Alexa Fluor® 700	anti-m	Rat IgG2b, κ	475301	R&D
CCR3	FITC	anti-m	Rat IgG2a, κ	J073E5	Biolegend
CCR3	PE	anti-m	Rat IgG2a, κ	J073E5	Biolegend
CCR4	PE/Cy7	anti-m	Armenian Hamster IgG	2G12	Biolegend
CCR5	PE	anti-m	Armenian Hamster IgG	HM-CCR5	Biolegend
CCR6	PerCp/Cy5.5	anti-m	Armenian Hamster IgG	29-2L17	Biolegend
CCR7	PE	anti-m	Rat IgG2a, κ	4B12	Biolegend
CCR8	PE	anti-m	Rabbit IgG	1035c	R&D
CCR9	PE	anti-m	Rat IgG2a, κ	9B1	Biolegend
CCR10	Alexa Fluor® 700	anti-m	Rat IgG2b, κ	248918	R&D
CXCR2	PE	anti-m	Rat IgG2a, κ	242216	R&D
CXCR3	PE/Cy7	anti-m	Armenian Hamster IgG	CXCR3-173	Biolegend
CXCR4	PE	anti-m	Rat IgG2b, κ	L276F12	Biolegend

CXCR4	PerCP/Cy5.5	anti-m	Rat IgG2b, κ	L276F12	Biolegend
CXCR5	PE	anti-m	Rat IgG2b, κ	L138D7	Biolegend
CXCR6	PerCP	anti-m	Rat IgG2b	221002	R&D
CX3CR1	PerCP Cy 5.5	anti-m	Mouse IgG2a, κ	SA011F11	Biolegend
CD11a	PerCP/Cy5.5	anti-m	Rat IgG2a, κ	M17/4	Biolegend
CD11b	Alexa Fluor® 700	anti-m/h	Rat IgG2a, κ	M1/70	Biolegend
CD11c	Alexa Fluor® 700	anti-m	Armenian Hamster IgG	N418	Biolegend
CD44	PE-CF594	anti-m	Rat IgG2b, κ	IM7	BD Bioscience
CD62L	APC/Cy7	anti-m	Rat IgG2a, κ	MEL-14	Biolegend
CD162	PE	anti-m	Rat IgG1 κ	2PH1	BD bioscience
CD18	PerCP-Cy™5.5	anti-m	Rat IgG2a, κ	C71/16	BD Bioscience
CD29	Alexa Fluor® 700	anti-m/r	Armenian Hamster IgG	HMβ1-1	Biolegend
CD49b	PE/Cy7	anti-m	Rat IgM, κ	DX5	Biolegend
CD49d	PerCP/Cy5.5	anti-m	Rat IgG2b, κ	R1-2	Biolegend
CD49e	PE-CF594	anti-m	Rat IgG2a, κ	5H10-27 (MFR5)	BD Bioscience
CD49f	PE/Cy7	anti-m/h	Rat IgG2a, κ	GoH3	Biolegend
Isotypes					
Isotype control	Alexa Fluor® 700	anti-m	Armenian Hamster IgG	HTK888	Biolegend
Isotype control	PE	anti-m	Armenian Hamster IgG	HTK888	Biolegend
Isotype control	Pe/Cy7	anti-m	Armenian Hamster IgG	HTK888	Biolegend
Isotype control	PerCp/Cy5.5	anti-m	Armenian Hamster IgG	HTK888	Biolegend
Isotype control	PE	anti-m	Mouse IgG 1, κ	P3.6.2.8.1	eBioscience
Isotype control	PE	anti-m	Rat IgG 1, κ	R3-34	BD bioscience
Isotype control	Alexa Fluor® 488	anti-m	Rat IgG 2a, κ	RTK2758	Biolegend
Isotype control	Alexa Fluor® 700	anti-m	Rat IgG 2a, K	eBR2a	eBioscience
Isotype control	APC/Cy7	anti-m	Rat IgG 2a, κ	RTK2758	Biolegend

Isotype control	PE	anti-m	Rat IgG 2a, κ	RTK2758	Biolegend
Isotype control	PE-CF594	anti-m	Rat IgG2a, κ	R35-95	BD Bioscience
Isotype control	PE/Cy7	anti-m	Rat IgG2a, κ	RTK2758	Biolegend
Isotype control	PerCp/Cy5.5	anti-m	Rat IgG 2a, κ	RTK2758	Biolegend
Isotype control	PerCp/Cy5.5	anti-m	Mouse IgG2a, κ	MOPC-173	Biolegend
Isotype control	Alexa Fluor® 700	anti-m	Rat IgG 2b, κ	RTK4530	Biolegend
Isotype control	PE	anti-m	Rat IgG2b, κ	RTK4530	Biolegend
Isotype control	PE/Cy7	anti-m	Rat IgG 2b, κ	RTK4530	Biolegend
Isotype control	PE CP594	anti-m	Rat IgG 2b, κ	A95-1	R&D
Isotype control	PerCP/Cy5.5	anti-m	Rat IgG 2b, κ	RTK4530	Biolegend

2.3.2. Blocking Antibodies

Table 2.4 Blocking antibodies

Antibody	Reactivity	Isotype	Clone	Company
anti-ICAM-1	anti-m	Rat IgG2b	YN1/1.7.4	BioXcell
anti-ICAM-2	anti-m	Rat Lewis IgG2a, κ	3C4(mIC2/4)	BD bioscience
anti-VCAM-1	anti-m	Rat IgG1	M/K-2.7	BioXcell
anti-P-selectin	anti-m	Rat Lewis IgG1, λ	RB40.34	BD bioscience
anti-E-selectin	anti-m	Rat Lewis IgG2a, κ	10E9.6	BD bioscience
anti-L-selectin	anti-m	Rat IgG2a	Mel-14	BioXcell
anti-CD162	anti-m	Rat IgG1	4RA10	BioXcell
anti-CD18	anti-m	Rat IgG2a	M18/2	BioXcell
anti-CD29	anti-m	Rat IgG2a	KMI6	BioXcell
anti-CD49d	anti-m	Rat IgG2b	PS/2	BioXcell

anti-CD11a	anti-m	Rat IgG2a	M17/4	BioXcell
Isotypes				
Isotype control	anti-m	Rat IgG2a	2A3	BioXcell
Isotype control	anti-m	Rat IgG1	HRPN	BioXcell

All blocking antibodies are in no azide, low endotoxin format.

2.3.3. Antibodies for fluorescence microscopy

Table 2.5 Antibodies for fluorescence microscopy

Antibody	Dye	Reactivity	Isotype	Clone	Company
ICAM-1	PE	anti-m	Rat IgG2b, κ	YN1/1.7.4	Biologend
VCAM-1	PE	anti-m	Rat IgG2a, κ	429 (MVCAM.A)	Biologend
E-selectin	PE	anti-m	Rat IgG2a, κ	10E9.6 (RUO)	BD Bioscience
P-selectin	PE	anti-m/h	Mouse IgG1, κ	Psel.KO2.3	eBioscience
MadCAM	Alexa Fluor® 488	anti-m	Rat IgG2a, κ	MECA-367	Biologend
ICAM-2	Alexa Fluor® 488	anti-m	Rat IgG2a, κ	3C4 (MIC2/4)	Biologend
PNAd	Biotin	anti-m/h	Rat IGM, κ	MECA-79	Biologend
PECAM-1	Alexa Fluor® 647	anti-m	Rat IgG2a, κ	MEC13.3	Biologend
CD44	PE	anti-m/h	Rat IgG2b, κ	IM7	Biologend
Streptavidin	Cy3				Biologend
Isotypes					
Isotype control	Biotin	anti-m	Rat IgM, κ	RTK2118	Biologend
Isotype control	PE	anti-m	Rat IgG 2a, κ	RTK2758	Biologend
Isotype control	PE	anti-m	Rat IgG2b, κ	RTK4530	Biologend
Isotype control	Alexa Fluor® 488	anti-m	Rat IgG 2a, κ	RTK2758	Biologend
Isotype control	PE	anti-m	Rat IgG 1, κ	P3.6.2.8.1	eBioscience

2.4. Blocking chemicals

Table 2.6 Blocking chemicals

Antagonist	Product name	Company
CCR1	J113863	Tocris
CCR2	RS 504393	Tocris
CCR3	SB 328437	Tocris
CCR4	C 021 dihydrochloride	Tocris
CXCR2	SB 265610	Tocris
CXCR3	(±)-AMG 487	Tocris
CXCR4	AMD 3100 octahydrochloride	Tocris

2.5. Primers for qPCR

Table 2.7 Primer list for qPCR

Primers	Sequence	Annealing(°C)
<i>Bmal1</i> Forward	AGA GGT GCC ACC AAC CCA TA	62
<i>Bmal1</i> Reverse	TGA GAA TTA GGT GTT TCA GTT CGT CAT	
<i>Clock</i> Forward	CAA AAT GTC ACG AGC ACT TAA TGC	62
<i>Clock</i> Reverse	ATA TCC ACT GCT GGC CTT TGG	
<i>Per1</i> Forward	TGA GAG CAG CAA GAG TAC AAA CTC A	60
<i>Per1</i> Reverse	CTC GCA CTC AGG AGG CTG TAG	
<i>Per2</i> Forward	GTC CAC CTC CCT GCA GAC AA	60
<i>Per2</i> Reverse	TCA TTA GCC TTC ACC TGC TTC AC	
<i>Cry1</i> Forward	CTC GGG TGA GGA GGT TTT CTT	62
<i>Cry1</i> Reverse	GAC TTC CTC TAC CGA GAG CTT CAA	
<i>Nr1d1</i> Forward	GAT AGC TCC CCT TCT TCT GCA TCA TC	60
<i>Nr1d1</i> Reverse	TTC CAT GGC CAC TTG TAG ACT TC	

*All primers were purchased from Eurofins Genomics.

2.6. Cell and RNA isolation Kits

Table 2.8 Cell and RNA isolation kits

EasySep mouse neutrophil enrichment Kit	STEMCELL Technologies
EasySep mouse monocyte isolation Kit	STEMCELL Technologies
EasySep mouse B cell isolation kit	STEMCELL Technologies
RNeasy Plus mini Kit	Qiagen Hilden Germany

2.7. Buffers

Table 2.9 RBC lysis buffer

RBC lysis buffer(1X)	1000 ml
NH ₄ Cl	8.26 g
KHCO ₃	1.00 g
0.5M EDTA (pH8)	100 µl
H ₂ O	1000 ml
pH 7.2-7.4	

Table 2.10 PEB buffer

PEB buffer	1 L
EDTA	2 mM
Bovin Serum Albumin	5 g
20%NaN ₃	2.5 ml
PBS	1L

Table 2.11 Tissue digestion buffer

Tissue digestion buffer	60 ml
12mg/ml Collagenase IV	4 ml
10ml/ml DNase	1.2 ml
PBS	54.8 ml

Table 2.12 Cell incubation buffer

Cell incubation buffer	500 ml
0.5M EDTA	2 ml
BSA	1 g
PBS	500 ml

Table 2.13 DAPI buffer

DAPI buffer	50 ml
DAPI (5mg/ml)	13.76 μ l
PEB buffer	50 ml

Table 2.14 Tissue digestion buffer

Animal tissue digestion buffer for genotyping	1000 ml
100 ml Tris (1M) pH8.5	100 ml
10 ml 0.5M EDTA	10 ml
10%SDS	20 ml
5M NaCl	40 ml

2.8. Software

Table 2.15 Software used for analyses

Software	Application
GraphPad Prism7	Statistical analysis
Flowjo	Flow cytometry data analysis
Zeiss	Quantification of images

2.9. Equipment

Table 2.16 Equipment used for experiments

StepOnePlus Real-Time RCR System	Applied Biosystems
Gallios Flow Cytometer	Beckman Coulter
IDEXX ProCyte DX cell counter	IDEXX Ludwigsburg Germany
Cryostat	Leica
NanoDrop 2000	Thermo Scientific
Z-Series Coulter Counter	Beckman coulter
2702 thermal cycler	Applied Biosystem

2.10. Other substances

Table 2.17 Other substances used in experiments

CFSE	Thermo Fisher Scientific
Cell tracker Deep red	Thermo Fisher Scientific
EDTA	Invitrogen
DMSO	Sigma
BSA	Sigma
DAPI	Biolegend
Gel red	Biotrend
Dreamtaq	Thermo Fisher Scientific
Gene ruler 6X	Thermo Fisher Scientific
Loading buffer	Thermo Fisher Scientific
OCT	Laborversand.de and Science services
Collagenase IV	Sigma
DNase	Roche

3. Methods

3.1. Flow cytometry

3.1.1. Preparation of samples for flow cytometry

3.1.1.1. Peripheral blood

Mice were anesthetized by inhalation of isoflurane. Blood was collected by bleeding from the retro-orbital plexus into EDTA-coated capillary tubes. Leukocyte counts were obtained using an IDEXX ProCyte DX cell counter. Blood samples were subjected to erythrocyte lysis by incubation in 5ml RBC lysis buffer for 5 min at room temperature. 5ml PBS were added to stop the lysis reaction. Leukocytes were spun down at 1300 rpm for 5min at 4°C, and resuspended in 5ml RBC lysis buffer for a second lysis process on ice. After the second centrifugation, leukocytes were resuspended in PEB buffer, and stained with fluorescence-conjugated antibodies for 30 min on ice. After washing with PBS, cells were resuspended in DAPI buffer, and analyzed by flow cytometry using a Gallios Flow Cytometer.

3.1.1.2. Lymph node and thymus

Lymph nodes and thymi were harvested from animals and processed through a cell strainer (40 µm, Thermo Fisher Scientific). Cells were spun down at 1300 rpm for 5 min at 4°C. Cells were resuspended in PEB buffer and stained with fluorescence-conjugated antibodies for 30 min on ice. After washing with PBS, cells were resuspended in DAPI buffer and analyzed by flow cytometry using a Gallios Flow Cytometer.

3.1.1.3. Spleen and bone marrow

Spleens were harvested from animals and processed through a cell strainer (40 µm, Thermo Fisher Scientific). Bone marrow cells were harvested from either one femur only or two femurs and two tibiae by flushing the bone gently with cold PBS. Cells were spun down at 1300 rpm for 5 min at 4°C. The supernatant was removed and cells were resuspended in 5 ml RBC lysis buffer. After 5 min, 5 ml PBS was added and the white blood cell population was separated by centrifugation at 1300 rpm for 5 min at 4°C. Cells were resuspended in PEB buffer and stained with fluorescence-conjugated antibodies for 30 min on ice. Cells were washed with PBS, resuspended in DAPI buffer and analyzed by flow cytometry using a Gallios Flow Cytometer.

3.1.1.4. Lung and liver

Lung and liver were first chopped into small pieces in DPBS with calcium and magnesium (Sigma), incubated for 1 h in digestion buffer with 1 mg/ml collagenase IV (Sigma) and 0.2 mg/ml DNase (Roche) at 37°C with gentle agitation. After digestion, cells were filtered through a 40 µm cell strainer (Thermo Fisher Scientific) and spun down at 1300 rpm for 5 min at 4°C. The supernatant was removed, cells were resuspended in 5 ml RBC lysis buffer and incubated for 5 min on ice. After adding 5 ml PBS, cells were spun down at 1300 rpm for 5 min at 4°C and resuspended in PBS supplemented with 2% FBS. Cells were stained with fluorescence-conjugated antibodies for 30 min and washed with PBS, resuspended in DAPI buffer and analyzed by flow cytometry using a Gallios Flow Cytometer.

All organ numbers were quantified using an automated cell counter (Z2 Coulter Particle Counter, Beckman Coulter).

3.1.2. Surface expression analyses of leukocytes

Expression levels of adhesion molecules and chemokine receptors on blood leukocytes were measured by flow cytometry at multiple time points across the day and compared with isotype control using mean fluorescence intensity (MFI). Blood was collected and prepared as described before. Major leukocyte subsets in blood were identified by specific surface markers.

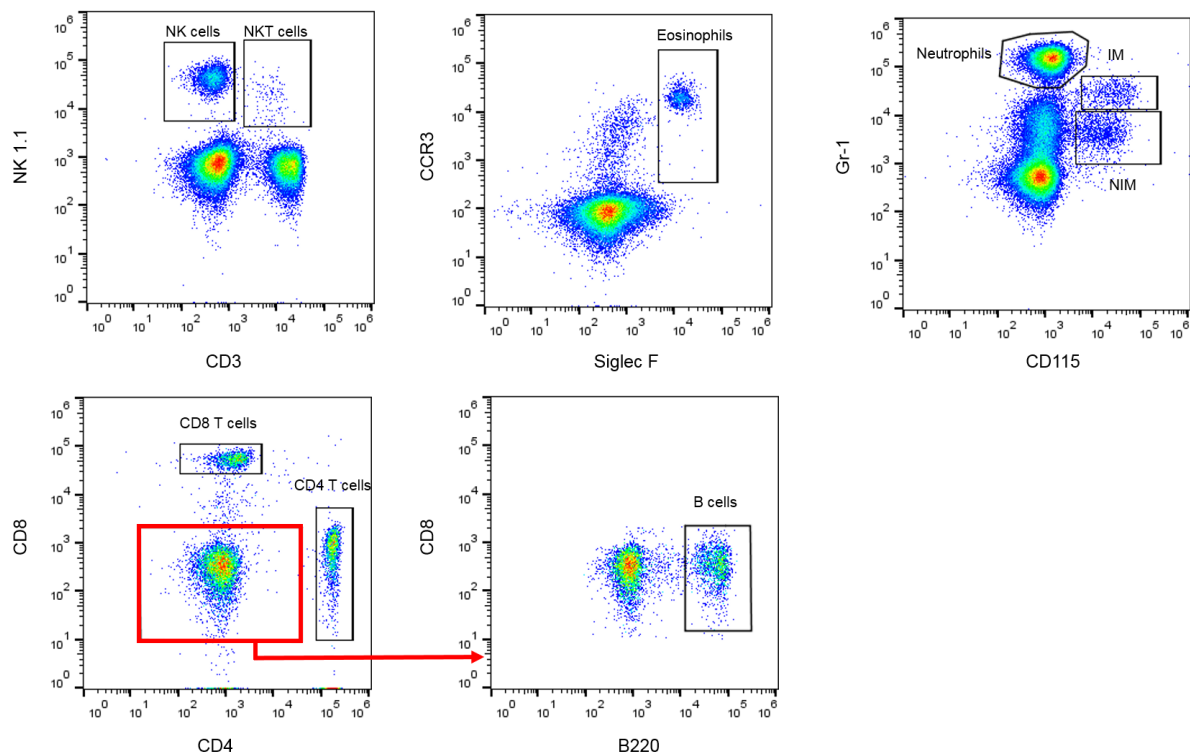


Figure 3.1 Gating leukocyte subsets

Blood cells were gated from live cells and singlets. Then leukocyte subsets were identified by different combinations of antibodies. CD115 and Gr-1 for differentiation of neutrophils; inflammatory monocytes (IM) and non-inflammatory monocytes (NIM); CD4, CD8 and B220 for identifying lymphocytes; NK1.1 and CD3 for NK cells and NKT cells; Siglec-F and CCR3 were used for eosinophil.

Table 3.1 Antibodies for surface expression of adhesion molecules and chemokine receptors.

Antibody	Dye	Reactivity	Isotype	Clone	Company
Siglec F	Alexa 647	anti-m	Rat IgG2a, κ	E50-2440 RUO	BD bioscience
CCR3	FITC	anti-m	Rat IgG2a, κ	J073E5	Biologend
NK1.1	APC	anti-m	Mouse IgG2b, κ	PK136	Biologend

CD3ε	Alexa Fluor® 488	anti-m	Armenian Hamster IgG	145-2C11	Biolegend
CD115	APC	anti-m	Rat IgG2a, κ	AFS98	ebioscience
Gr-1	FITC	anti-m	Rat IgG2b, κ	RB6-8C5	Biolegend
CD45R/B220	Alexa Fluor® 488	anti-m/h	Rat IgG2a, κ	RA3-6B2	Biolegend
CD4	APC	anti-m	Rat IgG2b, κ	GK1.5	Biolegend
CD8a	PE/Cy7	anti-m	Rat IgG2a, κ	53-6.7	Biolegend
CCR1	PE	anti-m	Rat IgG2b, κ	643854	R&D
CCR2	Alexa Fluor® 700	anti-m	Rat IgG2b, κ	475301	R&D
CCR3	FITC	anti-m	Rat IgG2a, κ	J073E5	Biolegend
CCR3	PE	anti-m	Rat IgG2a, κ	J073E5	Biolegend
CCR4	PE/Cy7	anti-m	Armenian Hamster IgG	2G12	Biolegend
CCR5	PE	anti-m	Armenian Hamster IgG	HM-CCR5	Biolegend
CCR6	PerCp/Cy5.5	anti-m	Armenian Hamster IgG	29-2L17	Biolegend
CCR7	PE	anti-m	Rat IgG2a, κ	4B12	Biolegend
CCR8	PE	anti-m	Rabbit IgG	1035c	R&D
CCR9	PE	anti-m	Rat IgG2a, κ	9B1	Biolegend
CCR10	Alexa Fluor® 700	anti-m	Rat IgG2b, κ	248918	R&D
CXCR2	PE	anti-m	Rat IgG2a, κ	242216	R&D
CXCR3	PE/Cy7	anti-m	Armenian Hamster IgG	CXCR3-173	Biolegend
CXCR4	PE	anti-m	Rat IgG2b, κ	L276F12	Biolegend
CXCR4	PerCP/Cy5.5	anti-m	Rat IgG2b, κ	L276F12	Biolegend
CXCR5	PE	anti-m	Rat IgG2b, κ	L138D7	Biolegend
CXCR6	PerCP	anti-m	Rat IgG2b	221002	R&D
CX3CR1	PerCP Cy 5.5	anti-m	Mouse IgG2a, κ	SA011F11	Biolegend
CD11a	PerCP/Cy5.5	anti-m	Rat IgG2a, κ	M17/4	Biolegend
CD11b	Alexa Fluor® 700	anti-m/h	Rat IgG2a, κ	M1/70	Biolegend
CD11c	Alexa Fluor® 700	anti-m	Armenian Hamster IgG	N418	Biolegend
CD44	PE-CF594	anti-m	Rat IgG2b, κ	IM7	BD Bioscience
CD62L	APC/Cy7	anti-m	Rat IgG2a, κ	MEL-14	Biolegend
CD162	PE	anti-m	Rat IgG1 κ	2PH1	BD bioscience
CD18	PerCP-Cy™5.5	anti-m	Rat IgG2a, κ	C71/16	BD Bioscience
CD29	Alexa Fluor® 700	anti-m/r	Armenian Hamster IgG	HMβ1-1	Biolegend

CD49b	PE/Cy7	anti-m	Rat IgM, κ	DX5	Biolegend
CD49d	PerCP/Cy5.5	anti-m	Rat IgG2b, κ	R1-2	Biolegend
CD49e	PE-CF594	anti-m	Rat IgG2a, κ	5H10-27 (MFR5)	BD Bioscience
CD49f	PE/Cy7	anti-m/h	Rat IgG2a, κ	GoH3	Biolegend

3.1.3. Adoptive transfer and homing assay of leukocytes

3.1.3.1. Adoptive transfer and peripheral blood

To investigate the recruitment of leukocytes from the blood to tissues, adoptive transfer experiments were performed and donor cells left in blood were measured as a negative indicator of how many cells had migrated into tissues. First, donor cells were obtained from bone marrow and spleen from donor mice. Single cell suspensions were made by flushing bone marrow with cold PBS and smashing spleen gently through a 40 μm cell strainer (Thermo Fisher Scientific). Cells were lysed with red cell lysis buffer for 5 min, then 5 ml PBS were added to stop the lysis reaction. Cells were spun down at 1300 rpm for 5 min and resuspended in cell incubation buffer (PBS, 0.2%BSA, 2mM EDTA) and counted on a cell counter (ProCyte DX cell counter). Bone marrow and spleen cells were mixed with a ratio of 50:50, and labeled with 1.5 μM CFSE or 0.1 μM CellTracker Deep Red dye for 20 min at 37 °C. After washing 3 times with PBS, cells were resuspended in PBS and 20X10⁶ cells were injected intravenously in each recipient mouse. After one hour, blood was harvested from recipient mice and processed as described before for flow cytometry analyses.

For identifying different leukocyte subsets of remaining injected cells in blood, cells were gated from total CFSE or CellTracker Deep Red positive cells, from which various leukocyte subsets were differentiated by specific surface markers as below.

Table 3.2 Flow cytometry panel for blood staining with CFSE donor cells

Antibody	Dye	Reactivity	Isotype	Clone	Company
Siglec-F	Alexa Fluor® 647	anti-m	Rat IgG2a, κ	E50-2440	BD bioscience
NK1.1	Alexa Fluor® 700	anti-m	Mouse IgG2a, κ	PK136	ebioscience
CD3	PE/DZL594	anti-m	Rat IgG2b, κ	17A2	Biolegend
CD115	PE	anti-m	Rat IgG2a, κ	AFS98	Biolegend
Gr-1	PerCP/Cy5.5	anti-m	Rat IgG2b, κ	RB6-8C5	Biolegend
CD45R/B220	PE/Cy7	anti-m/h	Rat IgG2a, κ	RA3-6B2	Biolegend
CD4	Brilliant Violet 570™	anti-m	Rat IgG2a, κ	RM4-5	Biolegend
CD8a	APC/Cy7	anti-m	Rat IgG2a, κ	53-6.7	Biolegend
DAPI					Biolegend

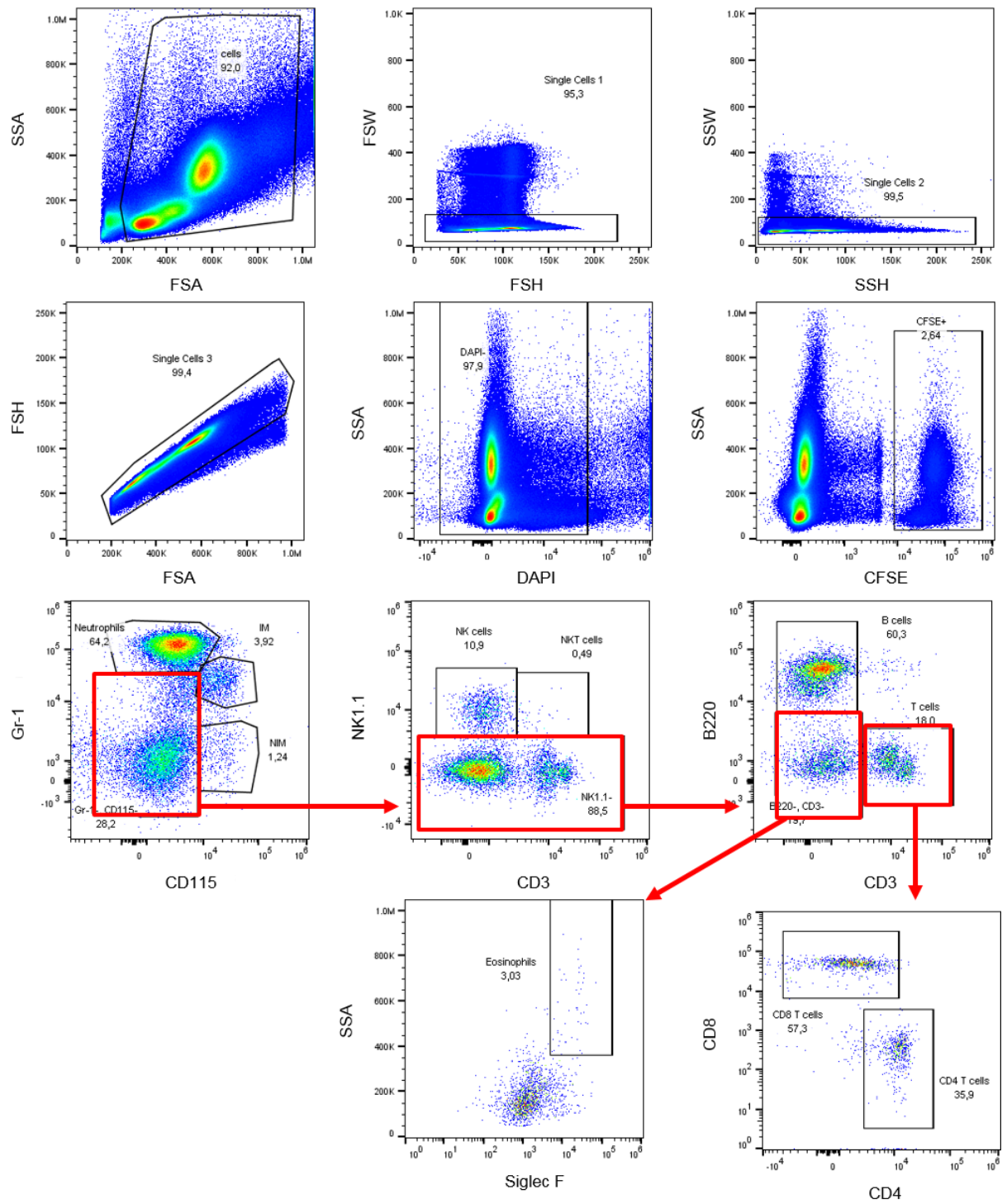


Figure 3.2 Gating strategy of adoptive transfer experiment with CFSE donor cells

Table 3.3 Flow cytometry panel for blood staining with CFSE and CellTracker Deep Red donor cells

Antibody	Dye	Reactivity	Isotype	Clone	Company
Siglec-F	APC-Cy™7	anti-m	LOU/M IgG2a, κ	E50-2440	BD Bioscience
NK1.1	Alexa Fluor® 700	anti-m	Mouse IgG2a, κ	PK136	ebioscience
CD115	PE	anti-m	Rat IgG2a, κ	AFS98	Biolegend
Gr-1	PerCP/Cy5.5	anti-m	Rat IgG2b, κ	RB6-8C5	Biolegend
CD45R/B220	PE/Cy7	anti-m/h	Rat IgG2a, κ	RA3-6B2	Biolegend
CD4	Brilliant Violet 570™	anti-m	Rat IgG2a, κ	RM4-5	Biolegend
CD8a	PE-CF594	anti-m	LOU/M IgG2a, κ	53-6.7	BD Bioscience
DAPI					Biolegend

3.1.3.2. Homing assay and organ analysis

For homing assays to organs, donor cells were prepared as describe before (3.1.3.1). One hour after the injection of cells, organs were harvested. Various leukocyte subsets were identified by surface makers, and then donor cells were differentiated by CFSE and Deep red dyes. For the spleen, bone marrow and lymph nodes, we used the same panel as for blood (Table 3.3). For the Lung and liver, two flow cytometry panels were applied (Table 3.4 and Table 3.5).

Table 3.4 Antibody panel for homing experiment to lung and liver group 1

Antibody	Dye	Reactivity	Isotype	Clone	Company
CFSE					
CD45	PE/Dazzle™ 594	anti-m	Rat IgG2b, κ	30-F11	Biolegend
Ly6C	PE	anti-m	Rat IgG2c, κ	HK1.4	Biolegend
Ly6G	PerCP/Cy5.5	anti-m	Rat IgG2a, κ	1A8	Biolegend
I-A/I-E	PE/Cy7	anti-m	Rat IgG2b, κ	M5/114.15.2	Biolegend
NK1.1	PE/Cy7	anti-m	Mouse IgG2a, κ	PK136	Biolegend
Deep red					
CD11b	Alexa Fluor® 700	anti-m/h	Rat IgG2a, κ	M1/70	Biolegend
Siglec-F	APC-Cy™7	anti-m	LOU/M IgG2a, κ	E50-2440	BD Bioscience
DAPI					

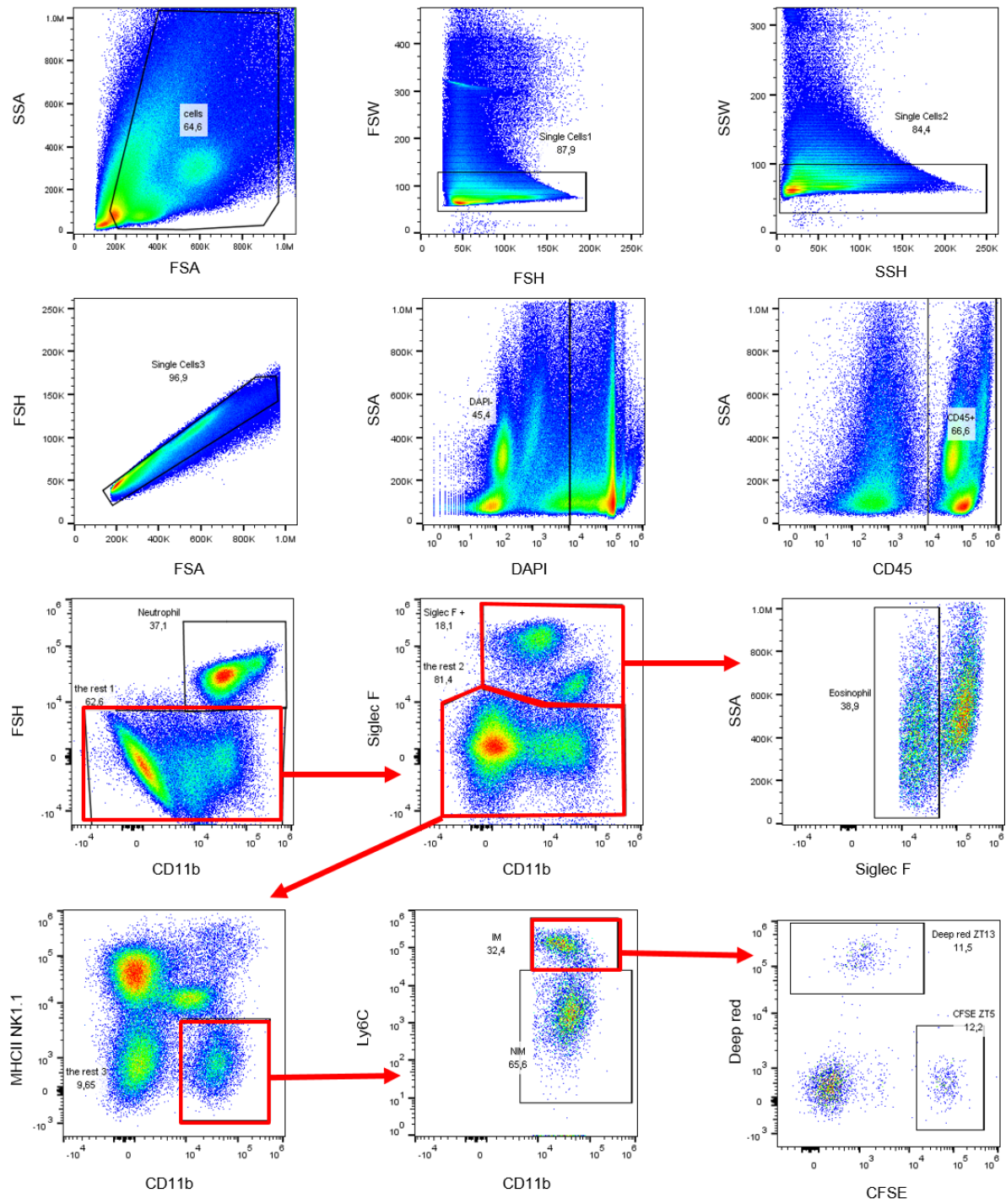


Figure 3.3 Gating strategy of organs to identify homed myeloid cells : lung

Table 3.5 Antibody panel for homing experiment to lung and liver group 2

Antibody	Dye	Reactivity	Isotype	Clone	Company
CFSE					
CD8a	PE-CF594	anti-m	LOU/M IgG2a, κ	53-6.7	BD Bioscience
CD4	PE	anti-m	Rat IgG2b, κ	GK1.5	Biolegend
NK1.1	PE/Cy5	anti-m	Mouse IgG2a, κ	PK136	Biolegend
CD45	PE-cy7	anti-m	Rat IgG2b, κ	30-F11	Biolegend
Deep red					
CD45R/B220	APC-Cy7	anti-m/h	Rat IgG2a, κ	RA3-6B2	Biolegend
DAPI					

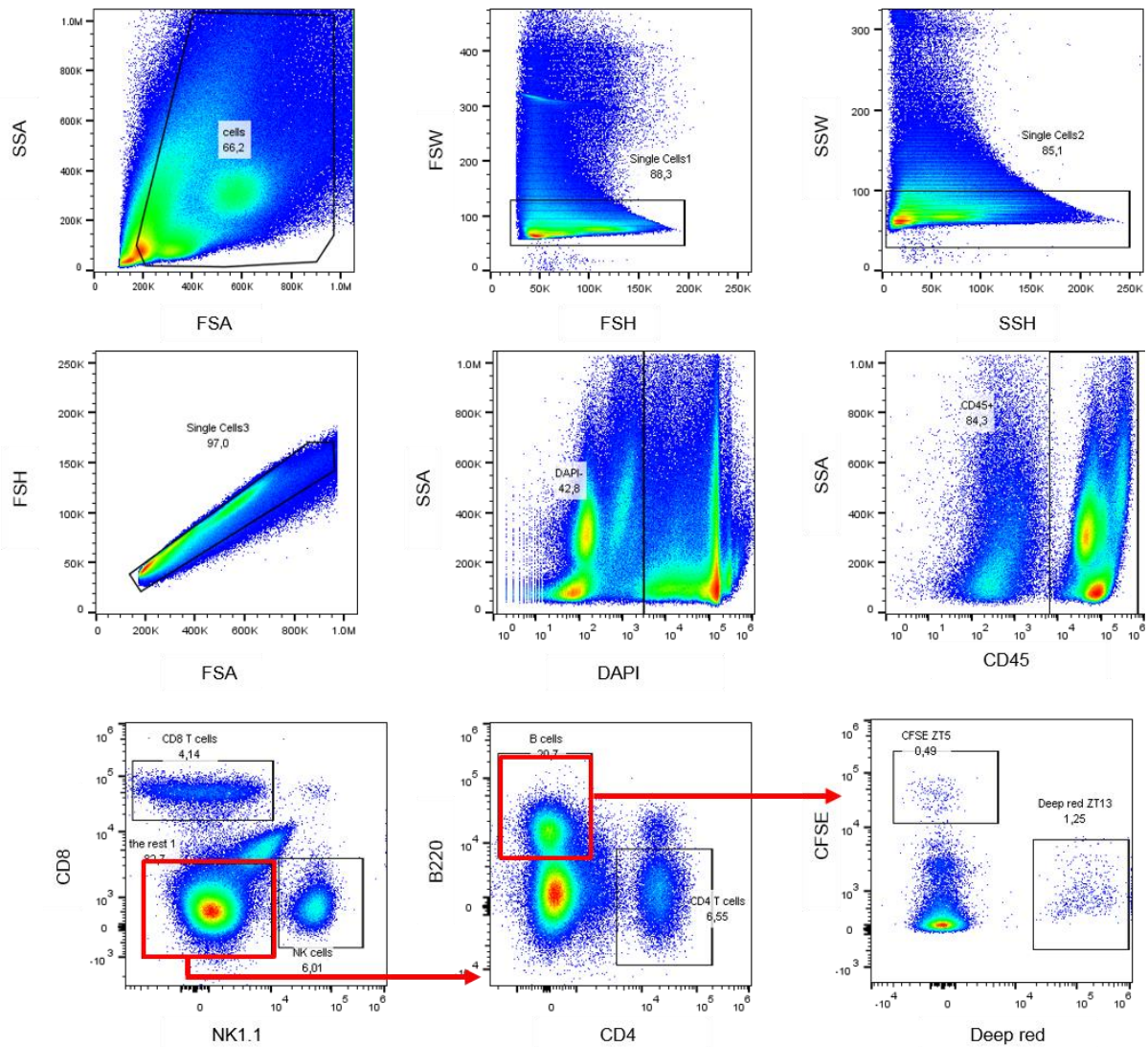


Figure 3.4 Gating strategy of organs to identify homed lymphocytes and NK cells: lung

In some experiment, injection of CD45 antibody (clone I3/2.3) followed by perfusion were performed in order to clean organs from blood and distinguish between cells adherent to the vascular endothelium or located extravascularly. Injection of donor cells was performed as described before. After one hour, 10 μ l CD45 (clone I3/2.3) in 200 μ l PBS were injected intravenously to recipient mice. 3 minutes later, mice were killed using an overdose of isoflurane and perfused with 10 ml PBS, 5 ml from the left ventricle and 5 ml from the right ventricle in order to perfuse the whole body and the lung, respectively. Organs were harvested and processed as described before. CD45 PE/Dazzle™ 594 FL3 (clone 30-F11) antibody was use for staining total CD45 positive cells, while cells only adherent to vessel endothelium were identified by staining with an injected i.v. CD45 APC FL6 (clone I3/2.3) antibody. Total injected donor cells were further differentiated into various leukocyte subsets by specific surface markers as below (Table 3.6 Figure 3.5).

Table 3.6 Flow cytometry panel for homing assay staining

Antibody	Dye	Reactivity	Isotype	Clone	Company
Ly6C	PE	anti-m	Rat IgG2c, κ	HK1.4	Biolegend
CD45	PE/Dazzle™ 594	anti-m	Rat IgG2b, κ	30-F11	Biolegend
Ly6G	PerCP/Cy5.5	anti-m	Rat IgG2a, κ	1A8	Biolegend
CD45R/B220	PE/Cy7	anti-m/h	Rat IgG2a, κ	RA3-6B2	Biolegend
CD45	APC	anti-m	Rat IgG2b	I3/2.3	Biolegend
CD8a	Alexa Fluor® 700	anti-m	Rat IgG2a, κ	53-6.7	Biolegend
CD4	APC/Cy7	anti-m	Rat IgG2b, κ	GK1.5	Biolegend
DAPI					Biolegend

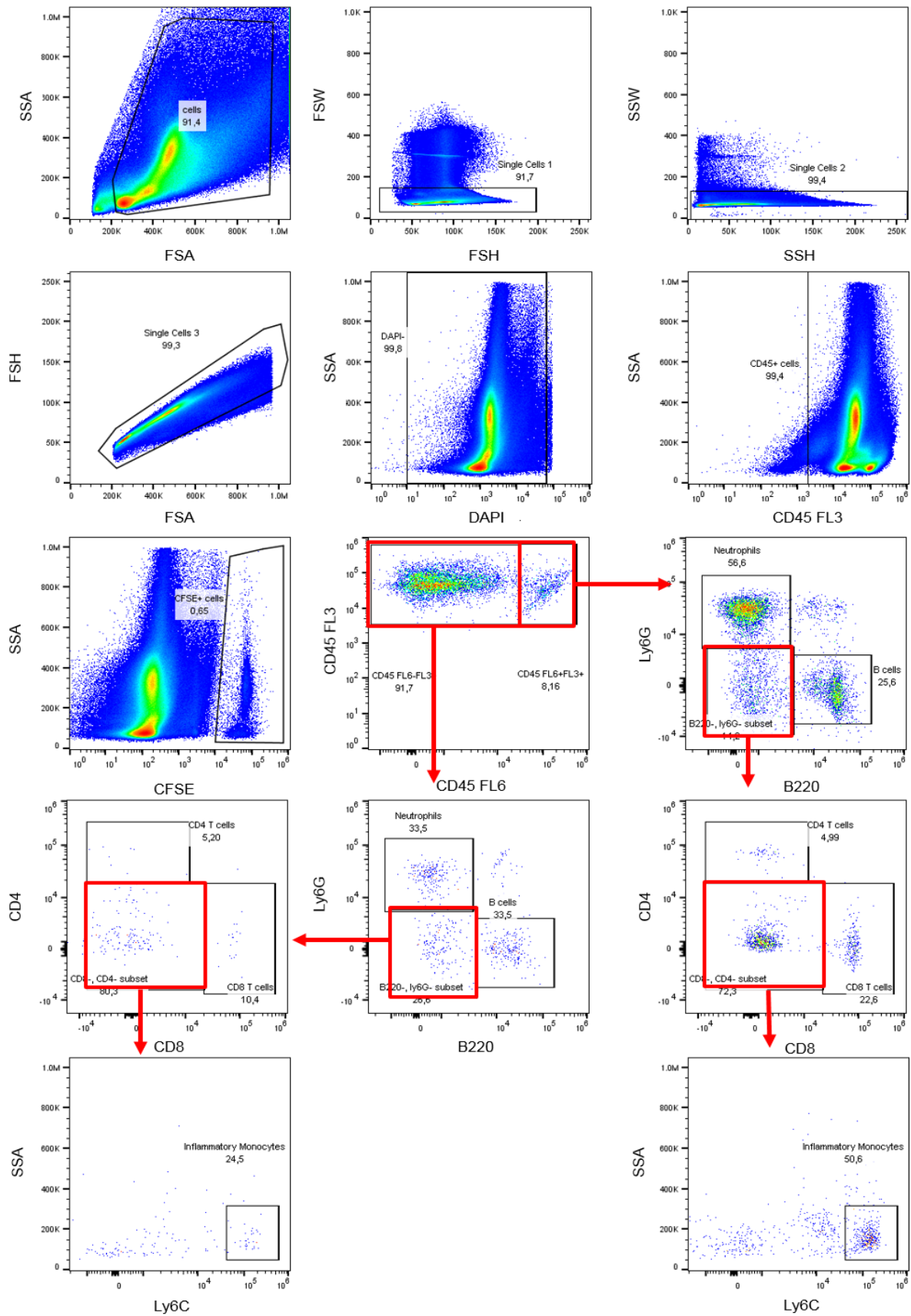


Figure 3.5 Gating strategy of homing experiment to organs

3.1.3.3. Blocking functions of pro-migratory molecules

To investigate the role of specific pro-migratory molecules in a rhythmic homing process, antibody or antagonist experiments were performed in combination with adoptive transfer experiments or homing assays. Blocking antibodies or chemokine antagonists were diluted into working concentrations with PBS or 5% DMSO with 1% Tween80 (Sigma) and injected i.v. or i.p. to recipient mice 2 hours before injection of donor cells. The following steps were performed as described above. The volumes of each antibody or chemical were listed as below:

Table 3.7 Antibodies and chemicals for function blocking experiments

Antibodies or chemicals	Volume	medium	Injection
anti-ICAM-1	200 µg/mouse	PBS	i.v.
anti-ICAM-2	60 µg/mouse	PBS	i.v.
anti-VCAM-1	200 µg/mouse	PBS	i.v.
anti-P-selectin	30 µg/mouse	PBS	i.v.
anti-CD62E	50 µg/mouse	PBS	i.v.
anti-CD62L	200 µg/mouse	PBS	i.v.
anti-PSGL-1	200 µg/mouse	PBS	i.v.
anti-CD18	200 µg/mouse	PBS	i.v.
anti-CD29	200 µg/mouse	PBS	i.v.
anti-CD49d	100 µg/mouse	PBS	i.v.
anti-CD11a	100 µg/mouse	PBS	i.v.
Isotype control	200 µg/mouse	PBS	i.v.
CCR1	125 µg/mouse	5% DMSO with 1% Tween80	i.p.
CCR2	125 µg/mouse	5% DMSO with 1% Tween80	i.p.
CCR3	125 µg/mouse	5% DMSO with 1% Tween80	i.p.
CCR4	125 µg/mouse	PBS	i.p.
CXCR2	125 µg/mouse	5% DMSO with 1% Tween80	i.p.
CXCR3	125 µg/mouse	5% DMSO with 1% Tween80	i.p.
CXCR4	125 µg/mouse	PBS	i.p.
control	200 µl	5% DMSO with 1% Tween80	i.p.
control	200 µl	PBS	i.p.

3.1.4. Human peripheral blood experiment

Human blood was taken by finger puncture and collected into a EDTA coated tube (SARSTEDT, Germany). Blood was prepared as described before (3.1.1.1) and stained with antibodies (Table 3.8) in room temperature for 30 min. Human experiment was conducted according to the ethical principles.

Table 3.8 Antibodies for human blood staining

Antibody	Dye	Reactivity	Isotype	Clone	Company
CD8	Alexa Fluor® 488	anti-human	Mouse IgG1, κ	HIT8a	Biolegend
CD19	PE	anti-human	Mouse IgG1, κ	HIB19	Biolegend
CD56	PE/Dazzle™ 594	anti-human	Mouse IgG1, κ	HCD56	Biolegend
CD14	PerCP/Cy5.5	anti-human	Mouse IgG1, κ	HCD14	Biolegend
CD16	PE/Cy7	anti-human	Mouse IgG1, κ	3G8	Biolegend
CD49d	APC	anti-human	Mouse IgG1, κ	9F10	Biolegend
CD4	Alexa Fluor® 700	anti-human	Mouse IgG1, κ	SK3	Biolegend
CXCR4	APC/Cy7	anti-human	Mouse IgG2a, κ	12G5	Biolegend
CD3	Brilliant Violet 570™	anti-human	Mouse IgG1, κ	UCHT1	Biolegend
DAPI					Biolegend

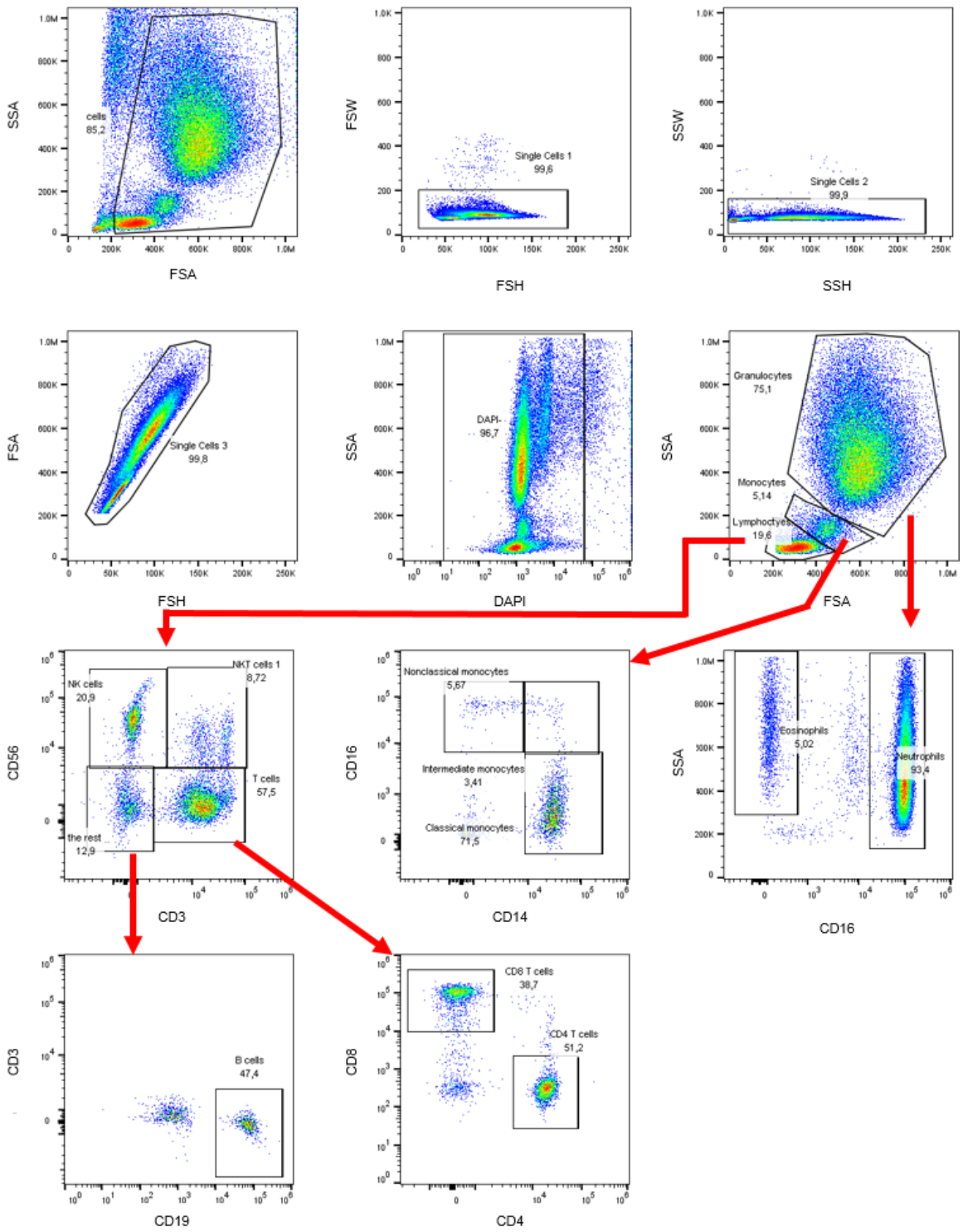


Figure 3.6 Gating strategy of human blood.

3.2. Cell isolation

Spleen B cells were purified from *CD19-cre Bmal1^{flox/flox}* or littermate control mice using a EasySep mouse B cell isolation kit (STEMCELL Technologies) according to the manufacturer's protocol, and purity (~92%) was assessed by flow cytometry. Bone marrow monocytes and neutrophils were purified from *Lyz2-cre Bmal1^{flox/flox}* or littermate control mice using a monocyte isolation kit and a neutrophil enrichment kit (STEMCELL Technologies) respectively. Purity of monocytes was about 93% and of neutrophils around 82%.

3.3. Q-PCR

RNA was extracted from isolated cells using RNeasy Plus mini Kit (Qiagen Hilden Germany) following the manufacturers' instructions. RNA samples were analyzed using NanoDrop2000 (Thermo Scientific) to determine RNA concentration and quality. RNA was stored at -80°C.

For reverse transcription, 150-200 ng RNA was added for reverse transcription, using the High Capacity cDNA Reverse Transcription Kit (Applied Biosystems). cDNA samples were stored at -20°C prior to use in quantitative PCR (Q-PCR). Q-PCR was performed with StepOnePlus Real-Time PCR System (Applied Biosystems) in 96-well plates with SYBR green compatible primers. The cycling conditions are listed below. Duplicates or triplicates were performed for each qPCR samples. The total reaction volume was 10 µl, containing 5 µl SYBR green, 1 µl primer mix (5 µM), 2 µl H₂O and 2 µl cDNA. Gene expression levels were normalized to the housekeeping gene GAPDH.

Table 3.9 Cycling conditions for qPCR

Cycling conditions	Temperature	Time
Initial denaturation	95°C	10 min
Denaturation	95°C	15 s
Annealing	60-62°C	1 min
Extension	72°C	15 s
Final extension	72°C	7 min

3.4. Immunofluorescence staining and quantitative imaging analyses

To measure adhesion molecule expression levels on endothelial cells, animal organs were put in to OCT, frozen at -80°C and sectioned with a thickness of 10 µm on a cryostat (Leica). Sections were fixed with cold methanol for 10 min at room temperature, incubated in PBS containing Triton X-100 (0.5%), and normal goat serum (20%). Sections were stained with antibodies and incubated at 4°C overnight.

For investigation of protein expression levels on the endothelium, images were obtained using a Zeiss Axio Examiner.D1 microscope equipped with 405, 488, 563 and 655 nm LED excitation light sources. All quantifications were performed using mask analyses with Zeiss software based on PECAM-1 expression as shown below. First, vascular endothelium was identified by PECAM-1+ expression, and this area was then covered by a mask. Quantifying expression of other florescent channels within this mask was then performed (Figure 3.7).

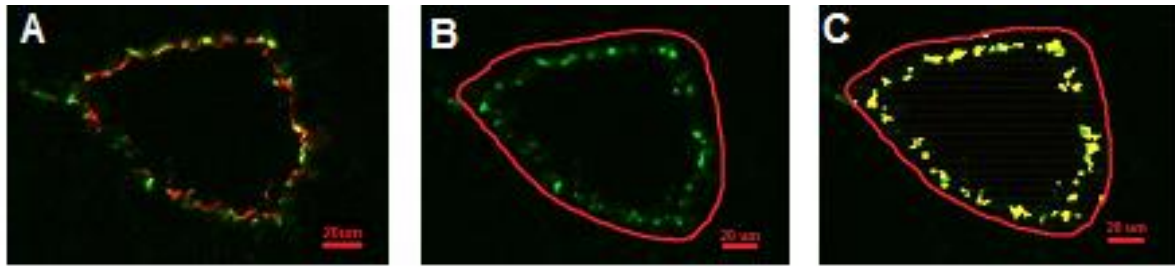


Figure 3.7 Surface expression measurements on liver endothelium

(A) Representative image of a frozen section from liver stained for PECAM-1 (Green) and ICAM-1 (Red) (B) The endothelial area for the mask analysis is indicated by a red shape. (C) The PECAM-1+ endothelial cell area (yellow area) was created as a mask by for further analysis.

PECAM-1+ areas (see Figure 3.3C) smaller than $10 \mu\text{m}^2$ were excluded from analysis to minimize non-specific signals. Protein expression levels were presented as mean fluorescence intensity (MFI) within the mask area and after subtraction of isotype controls (Figure 3.8).

	ID	Area[μm^2]	Intensity...	Intensity...
	A	B	C	D
1	2	3.641	218.600	494.000
2	3	0.728	355.000	820.000
3	4	8.010	866.545	3,095.818
4	5	1.456	851.000	4,784.500
5	6	0.728	754.000	4,617.000
6	7	29.854	1,192.537	2,818.341

Figure 3.8 MFI data results

Adhesion molecule expression levels in PECAM-1+ areas are represented by mean fluorescence intensities (MFI) of the stained antibody. Column B shows the size of the PECAM+ endothelium area, column C shows the MFI of ICAM-1, and column D shows the MFI of PECAM-1 in this area.

3.5. Genotyping

Genotyping samples from transgenic mice were collected by ear punches. Tissue samples were stored at -20°C prior to DNA extraction

DNA extraction began with incubation of tissue samples in 250 μl animal tissue lysis buffer and 1 μl proteinase K in a thermomixer at 55°C at 500 rpm overnight. Following incubation, the pellet of the digested tissue was centrifuged down, the supernatant was

transferred to 100 µl isopropanol. After shaking a few times, DNA samples were centrifuged down for 10 min, and supernatant was discarded before adding 100 µl EB buffer. Samples were put in thermomixer at 37°C for 1 hour for dissolving. DNA samples were stored at -20°C prior to use in genotyping PCR reactions.

PCR were performed using a PCR machine (2702 thermal cycler, Applied Biosystem). And the reverse transcription protocols were listed below.

Table 3.10 RCR conditions for *cre*

<i>Cre</i>	
Number of cycles	35
Initial denaturation 95°C	3 min
Denaturation 95°C	20 sec
Annealing 62°C	30 sec
Extension 72°C	30 sec
Final extension 72°C	10 min

Table 3.11 PCR conditions for *Bmal1*

<i>Bmal1</i>	
Number of cycles	35
Initial denaturation 94°C	3 min
Denaturation 94°C	30 sec
Annealing 55°C	30 sec
Extension 72°C	30 sec
Final extension 72°C	2 min

All PCR products were run on a 1% agarose-TAE gel containing gel red (Biotrend) to visualize DNA bands. Electrophoresis was performed in TAE buffer at 120V for 30 min. Gene ruler 6X was used to allow determination of fragment sizes.

3.6. Statistics

Data was analyzed using Prism 7 (GraphPad), and presented as mean +/- standard error of mean (SEM). A p value less than 0.05 was considered as statistically significant. Comparison between two groups were performed using unpaired Student's t test. One-way ANOVA analysis followed by Tukey's multiple comparison test was used for multiple group comparison. One-way ANOVA analysis followed by Dunnett's test was used for comparison between control and treatment groups. Human data was analyzed by repeated measures of one-way ANOVA.

4. Results

4.1. Oscillations in circulating leukocyte subsets are governed by a rhythmic homing process

4.1.1. Circulating subsets oscillate during 24 hours

All work presented in this thesis is currently prepared for submission as a first author publication.

To first assess whether leukocyte subsets oscillate over 24 hours, blood was harvested every four hours from mice which were kept in 12h light:12h dark cycles. Total white blood cell numbers were counted and leukocyte subset percentages were obtained by flow cytometry analysis. We found that the total white blood cell count showed dramatic oscillations during 24 hours, with a trough at ZT13 (i.e. 8pm), which is one hour after lights off, when mice become active, and a peak at ZT5 (i.e. 12pm), when mice are in their resting phase (Figure 4.1). Numbers of neutrophils, B cells, CD8 and CD4 T cells, Natural Killer (NK) cells, Natural Killer T (NKT) cells, inflammatory monocytes (IM) and non-inflammatory monocytes (NIM) as well as eosinophils showed similar oscillation patterns (Figure 4.1).

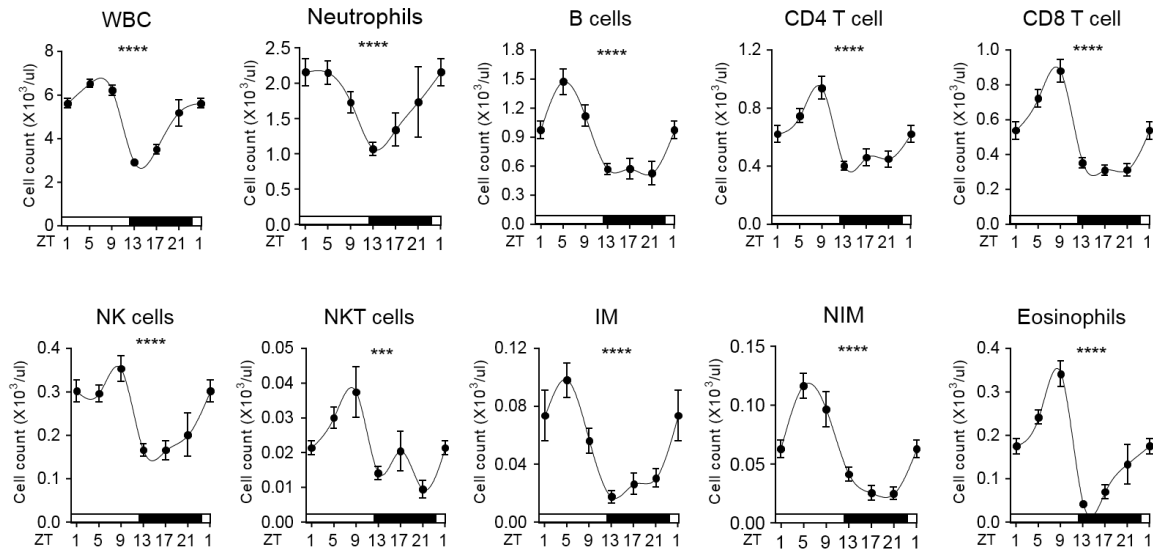


Figure 4.1 Oscillations in total white blood cell and leukocyte subset counts

Total leukocyte counts and leukocyte subsets, including neutrophils, B cells, CD8 T cells, CD4 T cells, NK cells, NKT cells, IM (inflammatory monocytes), NIM (non-inflammatory monocytes), and eosinophils, exhibit circadian number changes. *Zeitgeber time* (time after light onset). ZT1 is double plotted to facilitate viewing. n=9-62, one-way ANOVA. *p<0.05, ***p<0.001, ****p<0.0001 (manuscript in preparation).

4.1.2. The microenvironment contributes to rhythmic leukocyte homing

We next investigated whether the oscillation of leukocyte blood counts was due to rhythmic homing, and furthermore, whether the microenvironment contributes to this process. We performed ‘negative’ homing assays where we collected donor cells from ZT1 mice, incubated these with CFSE, and injected them at the same time into 6 groups of mice kept at different light phases (ZT1, ZT5, ZT9, ZT13, ZT17 and ZT21). After letting donor cells circulate for one hour, we measured the number of donor cells left in recipients’ blood (Figure 4.2). By keeping the donor constant and changing the recipients only, we were able to decipher the role of time-dependent microenvironment factors.



Figure 4.2 Adoptive transfer experiment with recipients kept at different phases

Spleen and bone marrow cells were collected from donor mice at the ZT1 time point. After incubation with CFSE, cells were injected into recipients at various time points, namely ZT1, ZT5, ZT9, ZT13, ZT17, ZT21. One hour later, blood was harvested and analyzed by flow cytometry.

Donor cells left in recipients' blood showed lowest numbers at ZT13, indicating that a rhythmic microenvironment contributes to cells leaving the circulation either by having migrated into tissues or by being in firm contact with the endothelium. There were more than 2-fold time-of-day differences in the capacity of every leukocyte subset to emigrate out from blood, suggesting that the microenvironment at the ZT13 time point was most permissive to the cells' migration (Figure 4.3).

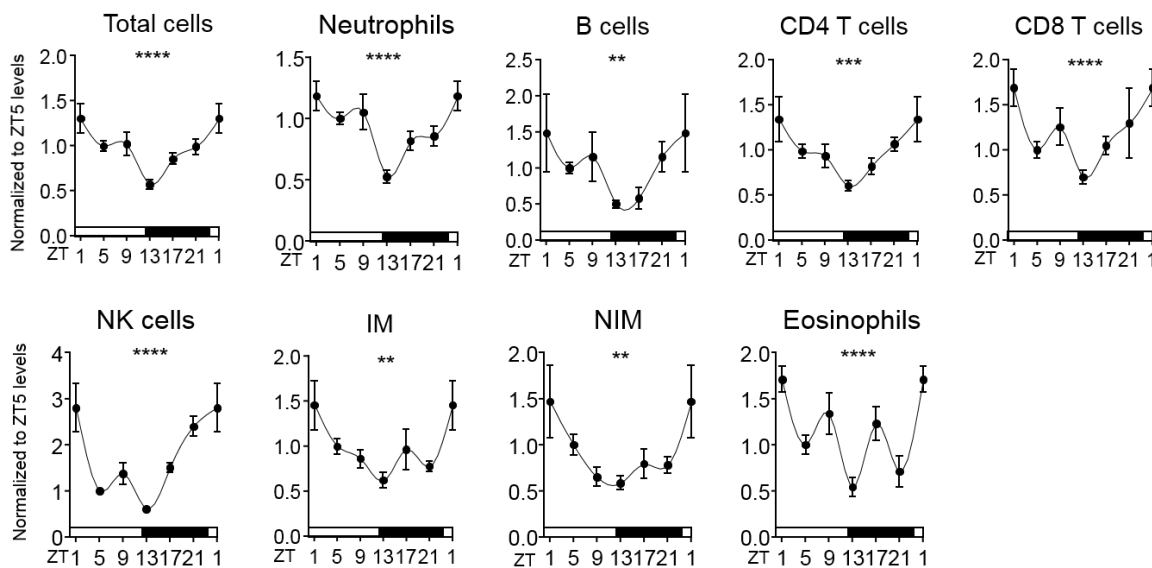


Figure 4.3 A rhythmic microenvironment contributes to leukocyte number oscillation in peripheral blood

Donor cells left in blood showed differences between different time points. Total donor cells as well as neutrophils, B cells, CD4 T cells, CD8 T cells, NK cells, IM (inflammatory monocytes), NIM (non-inflammatory monocytes), eosinophils, all leave the circulation at a higher rate at ZT13. $n=3-25$, one-way ANOVA. ** $p<0.01$, *** $p<0.001$, **** $p<0.0001$ (manuscript in preparation).

4.1.3. Leukocytes contribute to rhythmic homing

In addition to the microenvironment, migration of leukocytes also depends on various pro-migratory molecules expressed on the surface of leukocytes themselves. Therefore, we next investigated whether leukocytes also play an important role in rhythmic migration. This time we changed the time of donor cells but kept the recipients constant. Donor cells from mice were harvested at ZT1, 5, 9, 13 and 21, incubated with CFSE and injected i.v. into ZT5 recipient mice (Figure 4.4).

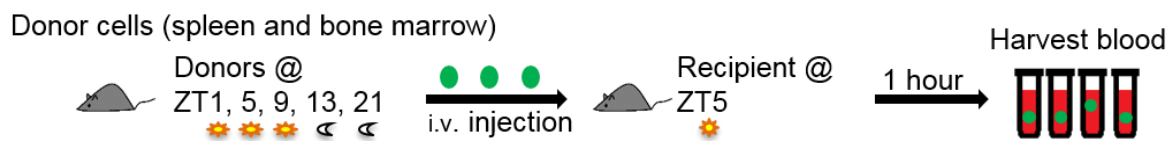


Figure 4.4 Adoptive transfer experiment with recipients kept in one phase

Spleen and bone marrow cells were collected from mice at ZT1, ZT5, ZT9, ZT13, ZT21 time points as donor cells. After incubation in CFSE, donor cells were injected into ZT5 recipients. One hour later, blood was harvested and analyzed by flow cytometry.

The donor cells left in blood showed the lowest number at ZT13, suggesting that donor cells at the ZT13 time point can leave blood more easily than at any other time of the day. The same phenomenon was found for each leukocyte subset (Figure 4.5). This finding indicates that donor cells at different time points have distinct recruitment capacities.

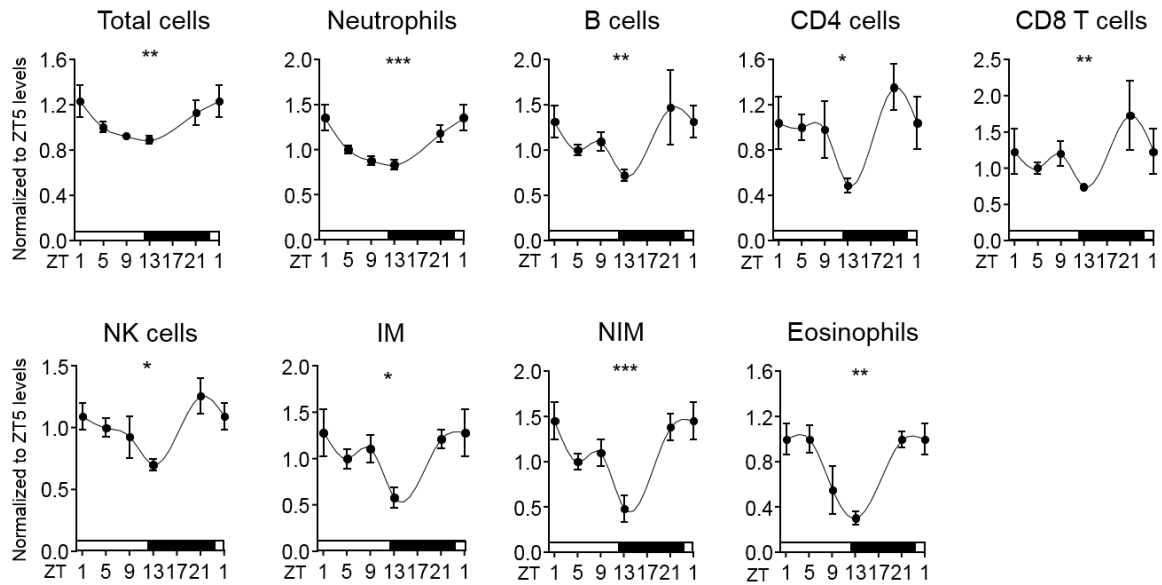


Figure 4.5 Rhythmic recruitment governed by donor cells contributes to the leukocyte number oscillation in peripheral blood
 Donor cells left in blood showed oscillations during 24 hours. Donor cells from ZT13 mice leave the circulation better than at any other time point. This was observed for neutrophils, B cells, CD4 T cell, CD8 T cells, NK cells, IM (inflammatory monocytes), NIM (non-inflammatory monocytes), eosinophils. n=3-17, one-way ANOVA. *p<0.05, **p<0.01, ***p<0.001 (manuscript in preparation).

4.1.4. Both the microenvironment and the leukocyte contribute to rhythmic leukocyte migration

Both the microenvironment and the leukocytes contribute to the rhythmic migration of leukocytes. We confirmed these observations by using reciprocal homing assays. We labeled ZT5 and ZT13 donor cells with CFSE (green) or Cell tracker deep red (red), and then injected them together into ZT5 or ZT13 recipients (Figure 4.6).

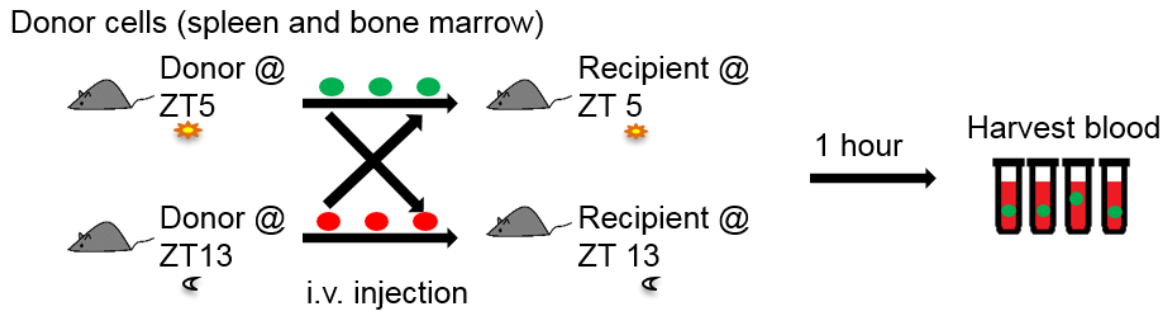


Figure 4.6 Reciprocal homing assays

Spleen and bone marrow cells were collected from mice at ZT5 and ZT13 time points as donor cells. After incubation in CFSE (green) or Cell tracker deep red (red), donor cells were mixed and injected into ZT5 and ZT13 recipients. One hour later, blood was harvested and analyzed by flow cytometry.

The data showed that ZT13 donor cells in a ZT13 recipients' microenvironment exhibited the lowest number of donor cells in the circulation, indicating that highest homing had occurred in this combination, while ZT5 donor cells in ZT5 recipients showed the lowest homing capacity. The homing of ZT13 to ZT5 and ZT5 to ZT13 groups were at intermediate levels, indicating that both the microenvironment and the leukocyte contribute to rhythmic leukocyte exit from the circulation (Figure 4.7).

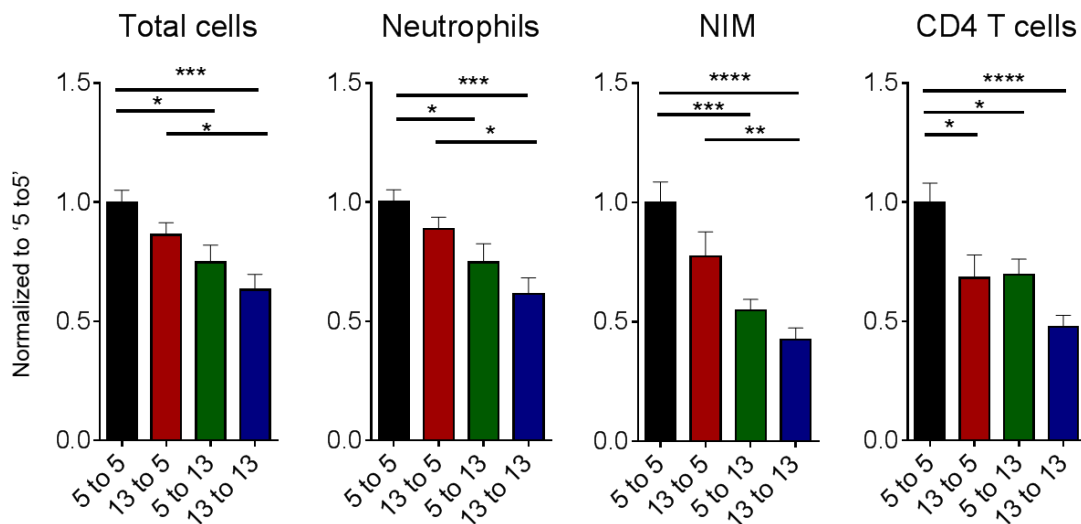


Figure 4.7 Reciprocal homing assays: leukocyte subsets

ZT5 and ZT13 donor cells were mixed and labeled differently and injected into ZT5 and ZT13 recipients. Donor cell numbers were normalized to '5 to 5' (ZT5 donor cells transferred to ZT5 recipients). ZT13 donor cells to ZT13 recipients showed the fewest cells left in the circulation. n=21-24, one-way ANOVA followed by Tukey's multiple comparison test. *p<0.05, **p<0.01, ***p<0.001, ****p<0.0001 (manuscript in preparation).

4.2. Tissue-specific oscillations in adhesion molecules expressed on endothelial cells contribute to the recruitment process

4.2.1. Expression of endothelial adhesion molecules in various organ is oscillatory

The endothelium is one of the major cell types that governs leukocyte migration. We therefore assessed which molecules expressed by these cells contributed to rhythmic leukocyte migration. We performed time course analyses of surface protein expression levels of eight key adhesion molecules expressed by endothelial cells, known to be important in leukocyte migration, using imaging-based approaches.

We found expressions and oscillations of adhesion molecules on endothelial cells vary between organs, with some molecules being expressed at constant levels (represented by purple squares), other molecules' expression levels fluctuated during 24 hours (represented by red squares), while some were not expressed (represented by grey squares). Combining the results together, we detected the existence of a rhythmic tissue-specific molecular signature in the expression of pro-migratory factors. ICAM-1, ICAM-2, VCAM-1 and P-selectin were the most widely expressed adhesion molecules on the endothelial cells (Figure 4.8).

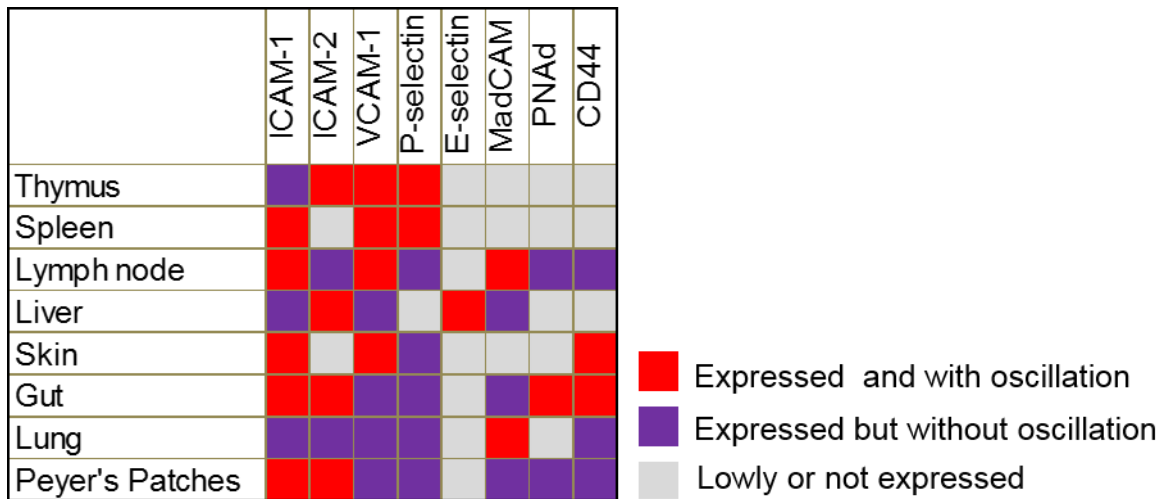


Figure 4.8 Expression of adhesion molecules in endothelial cells of various organs
 Expression of adhesion molecules on endothelial cells was measured by an image-based approach. Red squares represent higher expression levels than isotype controls and with a daily oscillation. Purple squares represent higher expression levels than isotype controls but without an oscillation. Grey squares represent expression levels equal to or lower than isotype control. n=3-6 with 6 time points measured each, one-way ANOVA.

4.2.2. Blocking endothelial cells adhesion molecules abolishes rhythmic recruitment

We next tested the involvement of specific molecules in the recruitment process focusing on a rhythmic microenvironment. We performed antibody blocking approaches together with adoptive transfer experiments. Blocking antibodies were injected into two groups of mice at ZT22 and ZT10, two hours before the transfer of donor cells. Donor cells from ZT1 donor mice were harvested and incubated with CFSE and injected into the two groups of mice simultaneously. One hour after the injection of donor cells, blood was harvested and analyzed by flow cytometry (Figure 4.9). Donor cell numbers were presented as percentage of injected donor cells, leukocyte subsets number were presented as percentage of injected leukocyte subsets, since the leukocyte subset number injected were not exactly the same for every experiment.

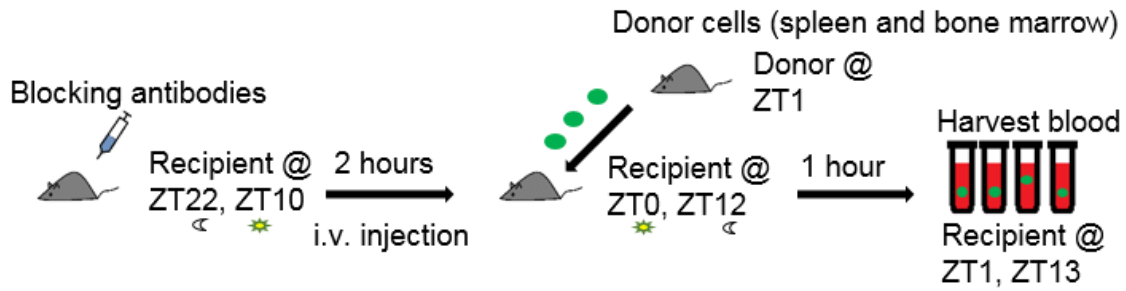


Figure 4.9 Antibody blocking in combination with adoptive transfer experiments

Recipient mice were treated with blocking antibodies two hours before the injection of donor cells. Spleen and bone marrow cells were collected from donor mice at the ZT1 time point. After incubation in CFSE, donor cells were injected into ZT0 and ZT12 recipients. One hour later, blood was harvested from ZT1 and ZT13 recipients.

We previously showed that the ZT13 microenvironment was more permissive for donor cells to leave the circulation. However, after antibody injection, the recruitment difference between ZT1 and ZT13 recipients was abolished for some leukocyte subsets. Our data suggest that the VCAM-1 antibody abolished recruitment rhythmicity of the total injected cells as well as leukocyte subsets. Blocking ICAM-1 diminished the recruitment rhythmicity of B cells, CD4 T cells, CD8 T cells, NK cells, non-inflammatory monocytes and eosinophils. In contrast, blocking ICAM-2, E-selectin, P-selectin had no effects on the rhythmic recruitment process (Figure 4.10).

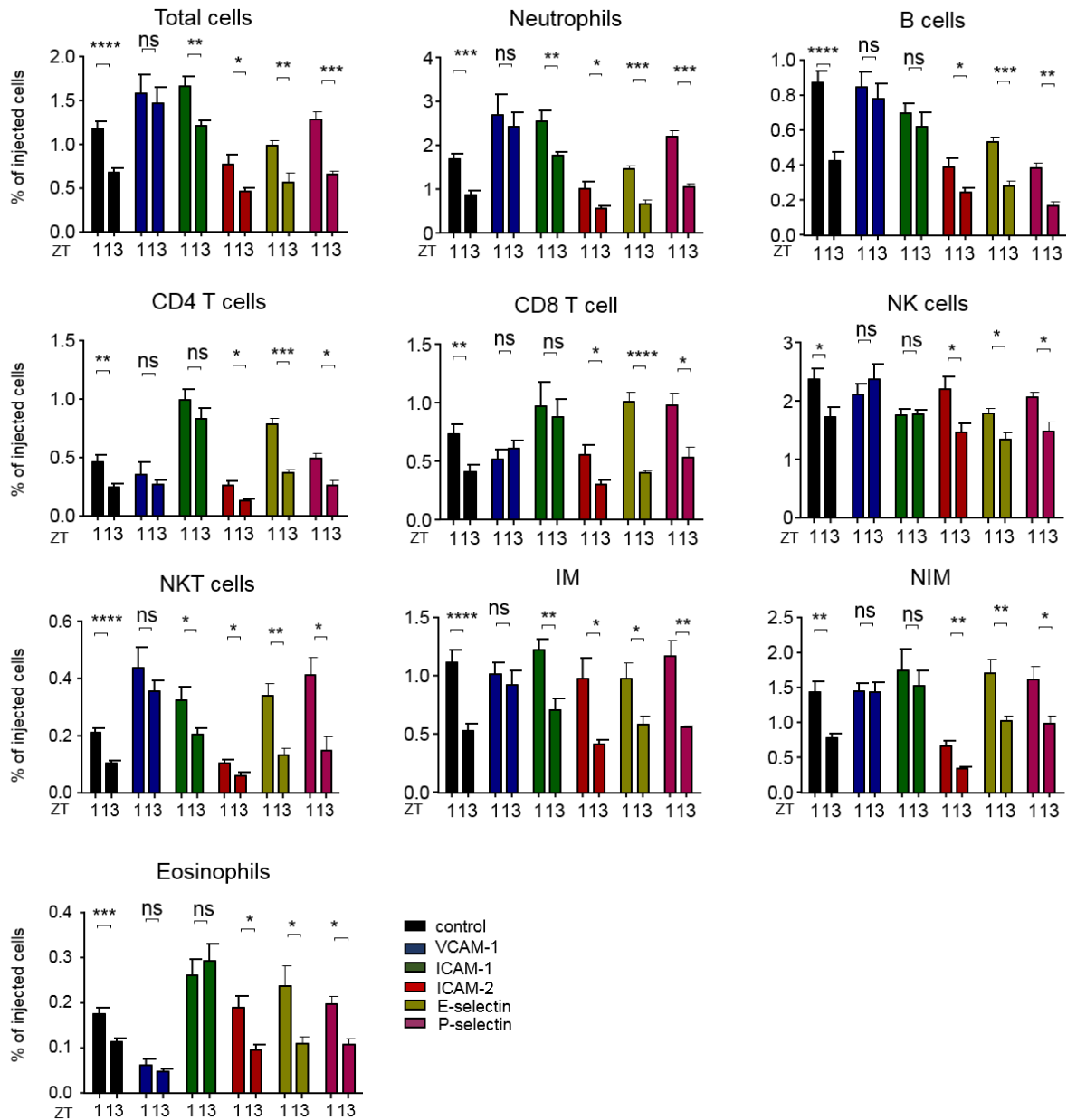


Figure 4.10 Antibody blocking experiment with adoptive transfer experiments

Blood of recipient mice treated with blocking antibodies or isotype control was analyzed by flow cytometry. Total donor numbers were presented as percentage of injected cells. Subset numbers were presented as percentage of injected leukocyte subsets. $n=4-12$, unpaired Student's t-test. * $p<0.05$, ** $p<0.01$, *** $p<0.001$, **** $p<0.0001$ (manuscript in preparation).

Next, we confirmed the blocking effects of the anti-ICAM-1 antibody genetically using ICAM-1 knockout mice as recipients. In the knockout mice, recruitment rhythmicity between ZT1 and ZT13 recipients was abolished in total cells, neutrophils, B cells, CD4 T cells, CD8 T cells, NK cells, NKT cells, non-inflammatory monocytes and eosinophils. However, the recruitment rhythmicity still existed for inflammatory monocytes (Figure 4.11).

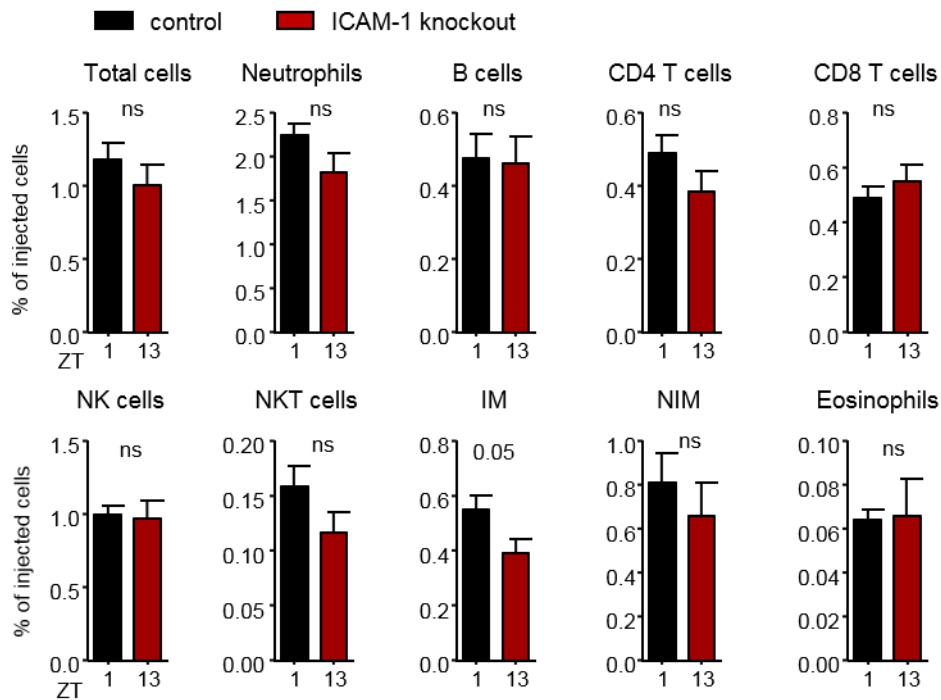


Figure 4.11 Adoptive transfer experiment with ICAM-1 knockout mice at ZT1 and ZT13 time points

Blood of recipient mice was analyzed by flow cytometry. Total CFSE numbers were presented as percentage of injected cells. Subset numbers were presented as percentage of injected leukocyte subsets. n=6-8, unpaired Student's t-test. *p<0.05 (manuscript in preparation).

From the experiments above, we found both anti-VCAM-1 and anti-ICAM-1 antibodies to exert blocking effects. Moreover, the blocking effects were stronger at the ZT13 time point, as a bigger fold change was found at this time point for total injected cells, as well as neutrophils, B cells, and NK cells for both VCAM-1 and ICAM-1 blockade. In addition, VCAM-1 blocking generated a higher effect at ZT13 also for CD8 T cells, inflammatory monocytes, non-inflammatory monocytes, CD8 T cells, and NKT cells. A bigger blocking effect was found in CD4 T cells and eosinophils after ICAM-1 blockade (Figure 4.12).

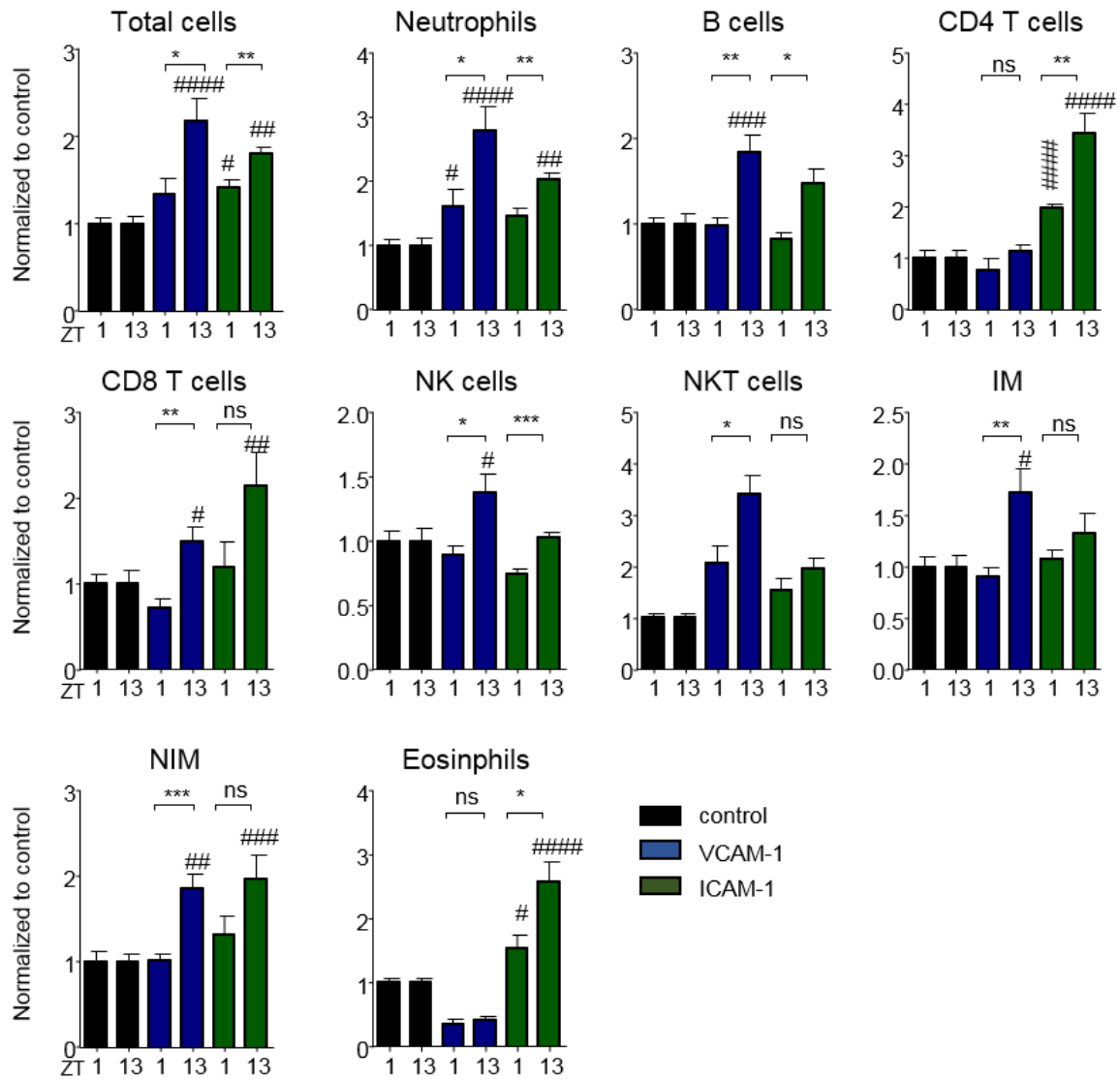


Figure 4.12 Fold change of antibody blocking experiment

The donor cell number left in blood was normalized to control mice. ZT1 groups were normalized to the ZT1 control group, and ZT13 groups were normalized to the ZT13 control group. n=7-12, one-way ANOVA followed by Dunnett comparison was performed to compare the control with treatment groups, #p<0.05, ##p<0.01, ###p<0.001, ####p, #####p<0.0001; unpaired Student's t-test was performed to compare the fold change between ZT1 and ZT13 groups after injection of antibodies. *p<0.05, **p<0.01, ***p<0.001 (manuscript in preparation).

4.3. Leukocyte subset specific oscillations in adhesion molecules contribute to the recruitment process

4.3.1. Leukocyte subsets have distinctly rhythmic expression patterns of adhesion molecules and chemokine receptors

On the leukocyte side, we used flow cytometry to assess the expression levels of adhesion molecules and chemokine receptors of blood leukocytes at different time points. We found expression levels and oscillations of adhesion molecules and chemokine receptors on the surface of leukocytes to vary between subsets, with some molecules being expressed at constant levels (represented by purple squares), other molecules' expression levels fluctuated during 24 hours (represented by red squares), while some were not expressed (represented by grey squares). Together, each leukocyte subset had its distinctive expression profile of these pro-migratory molecules. Adhesion molecules were widely expressed on leukocyte subsets, while chemokine receptors exhibited a more restricted expression profile (Figure 4.13).

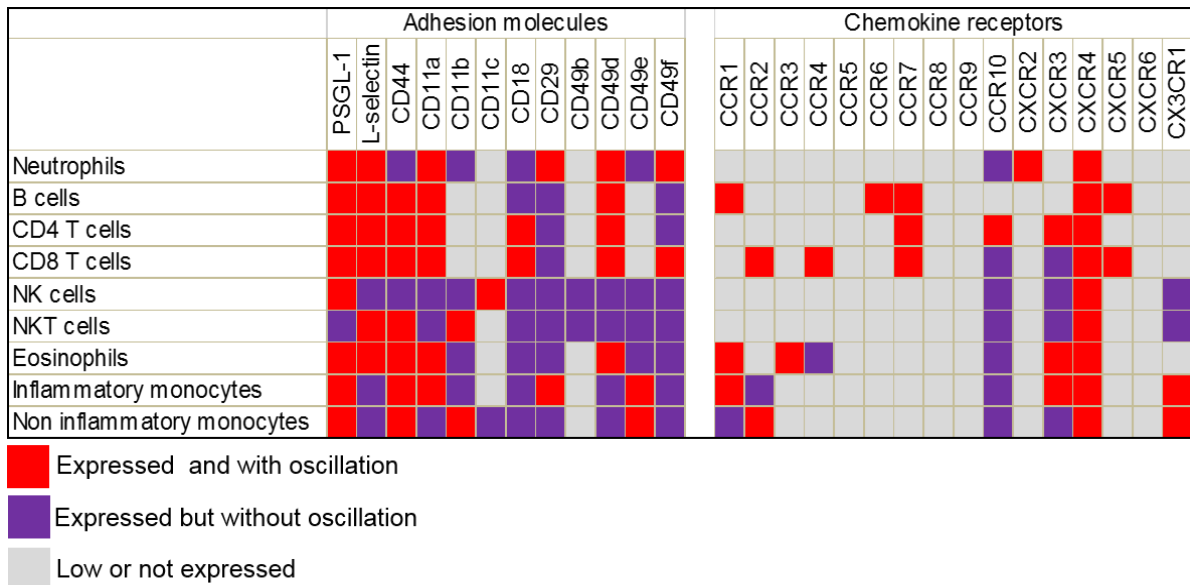


Figure 4.13 Expression levels of adhesion molecules and chemokine receptors on leukocytes
 Adhesion molecules and chemokine receptor expression levels of blood leukocytes were measured by flow cytometry. Red squares represent molecules' expression levels higher than isotype and being oscillatory. Purple squares represent molecules' expression levels higher than isotype but without oscillation. Grey squares represent molecules' expression levels equal to or lower than isotype control. n=3-6 with 4-6 time points measured each, one-way ANOVA.

4.3.2. Functional blocking experiments using antibodies or functional inhibitors inhibit the rhythmic recruitment process in a time-dependent manner

4.3.2.1. Adhesion molecules

To investigate the critical molecules involved in the rhythmic recruitment process, we performed antibody blocking experiments against adhesion molecules. ZT0 and ZT12 donor cells were transferred to ZT0 and ZT12 recipient mice that were treated with blocking antibodies two hours before. One hour after donor cell injection, blood was

harvested from ZT1 and ZT13 recipients, and analyzed by flow cytometry. Donor cell numbers were presented as percentage of injected donor cells, and leukocyte subsets numbers were presented as percentage of injected leukocyte subsets (Figure 4.14).

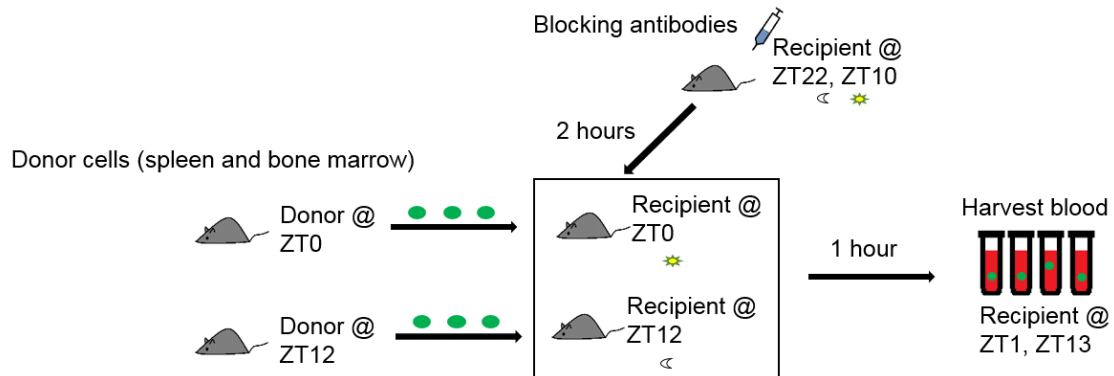


Figure 4.14 Antibody blocking with adoptive transfer experiment at one time point

Recipient mice were treated with blocking antibodies two hours before injection of donor cells. Spleen and bone marrow cells were collected from mice at ZT0 and ZT12 time points as donor cells. After incubation in CFSE, donor cells were injected into ZT0 and ZT12 recipients. One hour later, blood was harvested from ZT1 and ZT13 recipients.

The results demonstrated that L-selectin, CD11a (LFA-1) and CD49d (VLA-4) are the molecules that mediated the homing of total donor cells or some leukocyte subsets as more donor cells were found in blood after antibody blockade. Blocking CD49d inhibited the homing of neutrophils, B cells, CD4 T cells, CD8 T cells, NK cells, and inflammatory monocytes. Blocking L-selectin decreased the emigration process of B cells, CD4 T cells, CD8 T cells, and non-inflammatory monocytes. CD11a blockade inhibited emigration of neutrophils. A higher blockade effect at ZT13 was found in B cells after CD11a blocking, in inflammatory monocytes and eosinophils after CD49d blocking (Figure 4.15).

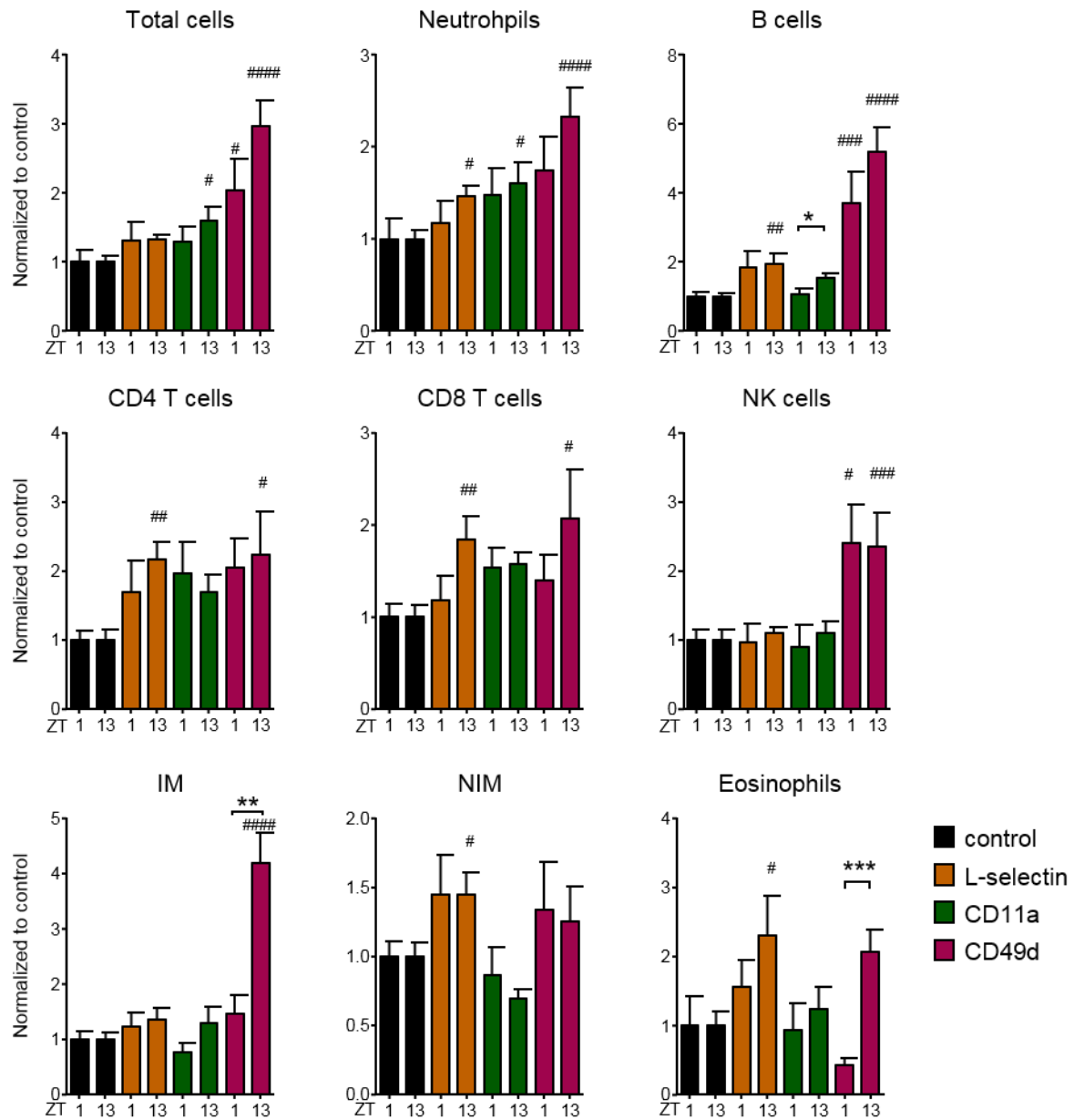


Figure 4.15 Antibody blocking with adoptive transfer experiment

Blood of recipient mice was analyzed by flow cytometry. The donor cell number left in blood was normalized to control mice. ZT1 groups were normalized to ZT1 controls, and ZT13 groups were normalized to ZT13 controls. n=3-12, one-way ANOVA followed by Dunnett comparison was performed to compare the control and treatment groups, #p<0.05, ##p<0.01, ###p<0.001, ####p, #####p<0.0001; unpaired Student's t-test was performed compare the fold change between ZT1 and ZT13 groups after injection of antibodies, *p<0.05, **p<0.01, ***p<0.001 (manuscript in preparation).

4.3.2.2. Chemokine receptors

We next investigated the function of chemokine receptors in rhythmic recruitment process. We first injected functional antagonists i.p. to ZT22 and ZT10 recipients. Two hours later, donor cells were injected into recipients. After one hour, blood was harvested and analyzed (Figure 4.16).

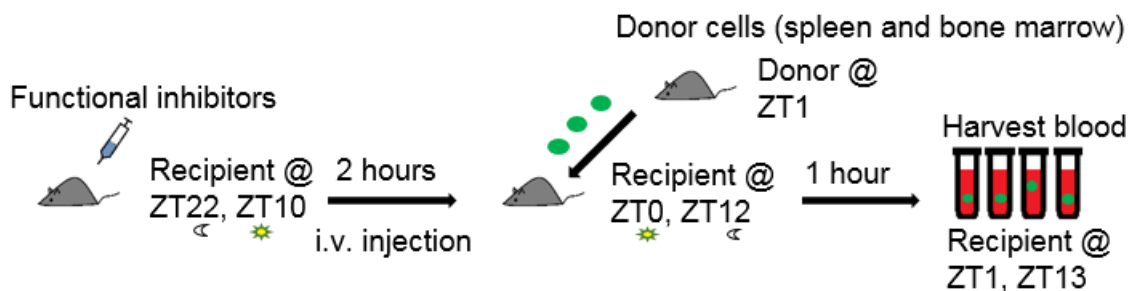


Figure 4.16 Antibody blocking with adoptive transfer experiment

Recipient mice were treated with antagonist two hours before injection of donor cells. Spleen and bone marrow cells were collected from mice at ZT1 time point as donor cells. After incubation in CFSE, donor cells were injected into ZT0 and ZT12 recipients. One hour later, blood was harvest from ZT1 and ZT13 recipients.

Our data showed that an antagonist to CXCR4 can block rhythmic homing of total donor cells, neutrophils, CD4 T cells, CD8 T cells, NK cells, NKT cells, non-inflammatory monocytes and eosinophils, but not including inflammatory monocytes, as for the latter the homing differences between ZT1 and ZT13 recipients still existed. This suggested that CXCR4 is critical for the homing of most but not all leukocyte subsets. A CXCR3 inhibitor affected the recruitment process of neutrophils, CD4 T cells, CD8 T cells, NK cells, NKT cells, inflammatory monocytes and eosinophils. A CCR1 inhibitor affected the migration of CD4 T cells, CD8 T cells, NK cells, inflammatory monocytes, and non-inflammatory monocytes. Blocking CCR2 affected rhythmic homing of neutrophils, B cells, CD4 T cells, CD8 T cells, NK cells, NKT cell, non-inflammatory monocytes and eosinophils. In contrast, the CXCR2 and CCR4 inhibitors did not exert effects on the recruitment process of most subsets (Figure 4.17). Since the blocking effects of the CXCR3, CCR2 or CCR1 inhibitor were not as strong as CXCR4 inhibitor, we therefore focused on the CXCR4 inhibitor in subsequent studies.

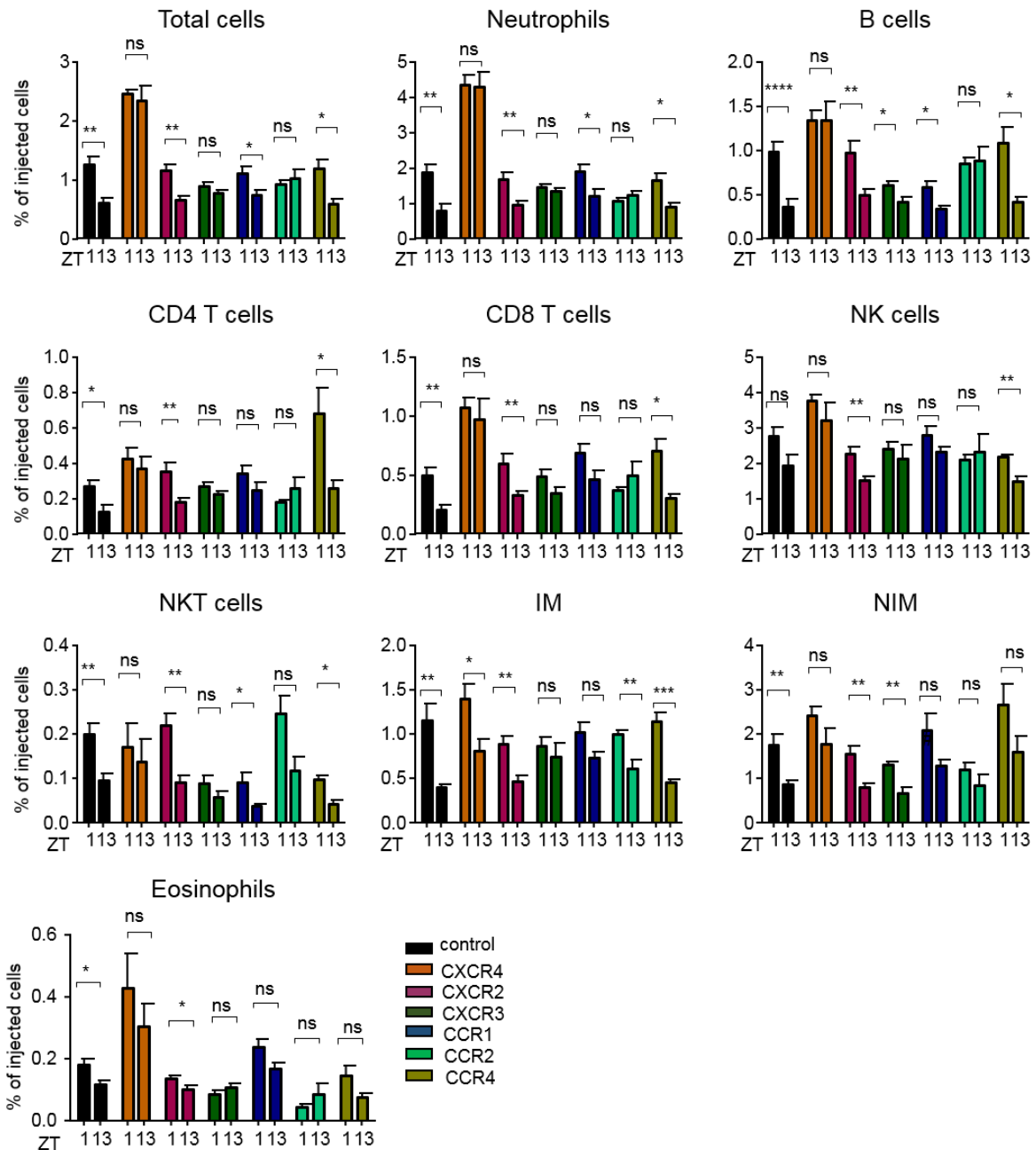


Figure 4.17 Antagonist blocking with adoptive transfer experiment

Blood of recipient mice which were treated with blocking antibodies or control reagents was analyzed by flow cytometry. Total CFSE numbers were presented as percentage of injected cells. Subset numbers were presented as percentage of injected leukocyte subsets. n=3-10, unpaired Student's t-test was performed between ZT1 and ZT13 groups. *p<0.05, **p<0.01, ****p<0.0001 (manuscript in preparation).

These experiments demonstrated CXCR4 to be a critical factor in homing. Moreover, the blocking effects was much more obvious at ZT13 compared to ZT1, as a bigger

fold change was detected at this time point, indicating that a more active recruitment process occurred at night (Figure 4.18).

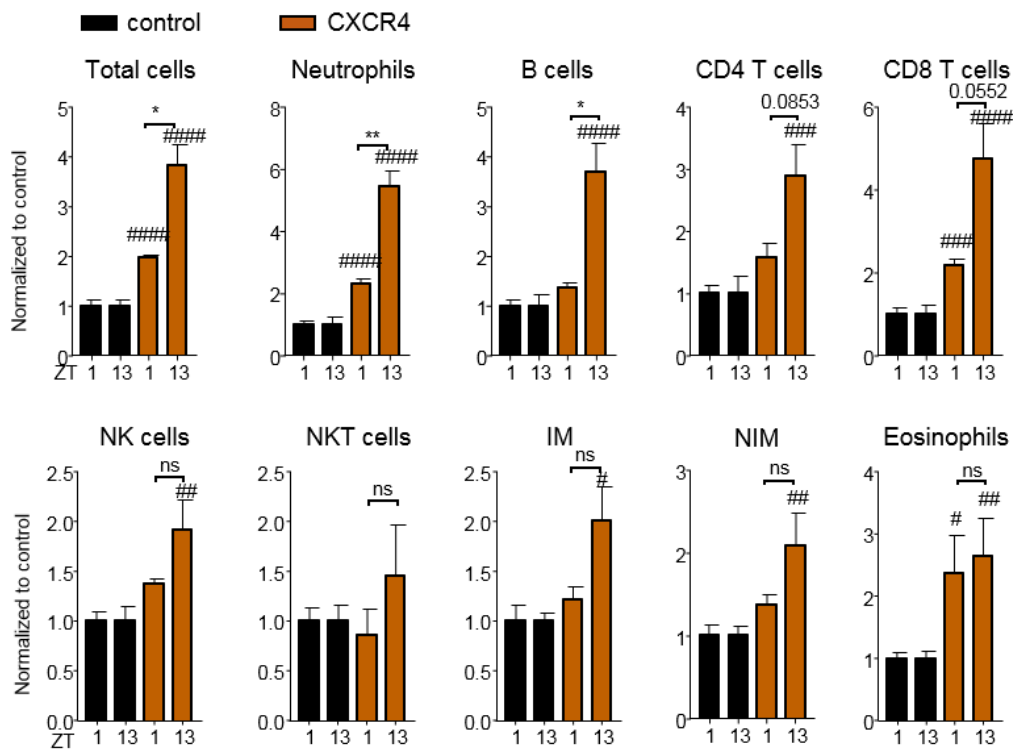


Figure 4.18 Fold change of CXCR4 antagonist experiments

The donor cell number left in blood was normalized to control mice. ZT1 groups were normalized to ZT1 controls, and ZT13 groups were normalized to ZT13 controls. n=3-6, one-way ANOVA followed by Dunnett comparison was performed to compare the control and treatment groups, #p<0.05, ##p<0.01, ###p<0.001, ####p, #####p<0.0001; unpaired Student's t-test was performed to compare the fold change between ZT1 and ZT13 groups after CXCR4 blockade. *p<0.05, **p<0.01 (manuscript in preparation).

4.4. The homing of leukocyte subsets to specific organs is time-of-day dependent

Our data indicated that leukocyte leave the circulation in a time-dependent manner. We next investigated where the cells went. To address this, homing experiments were performed. Donor cells were collected from ZT5 and ZT13 recipients and incubated with CFSE. Then, donor cells were injected into ZT5 and ZT13 recipients. After one

hour, spleen, bone marrow, lymph nodes, lung and liver were harvested and measured by flow cytometry (Figure 4.19).

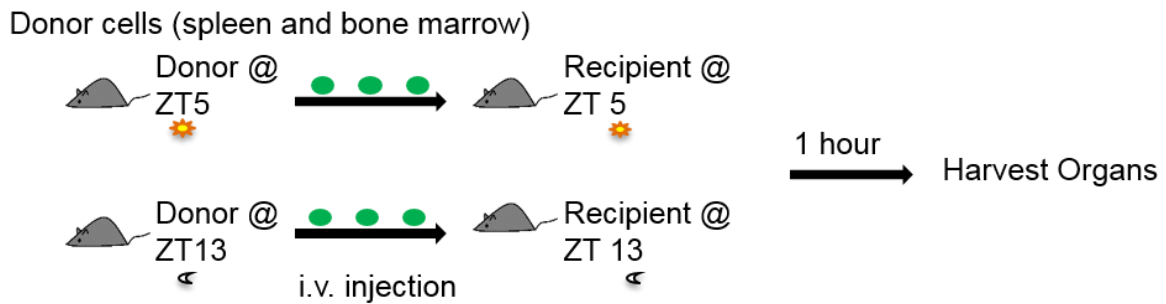


Figure 4.19 Homing experiment to organs

Spleen and bone marrow cells were collected from mice at ZT5 and ZT13 time points as donor cells. After incubation with CFSE, donor cells were injected into recipient at ZT5 and ZT13, respectively. One hour later, organs were harvested and analyzed by flow cytometry.

Homed cells to organs exhibited an inverse trend to the cells left in blood with more cells having migrated to organs at ZT13 compared with ZT1 (Figure 4.20). The homed donor cell numbers in lymph nodes were presented as absolute numbers, since the total lymph node numbers were reported to change over time (Druzd et al. 2017). For all other organs, the total cellularity was stable at the investigated time points, therefore, the homed donor cell numbers were represented as percentage of CD45+ cell numbers in this organ. The major recruited leukocyte populations to organs were tissue specific. In lymph nodes, CD4 T cells, CD8 T cells and B cells were the three major populations. In spleen, neutrophils, B cells and CD8 T cells were the three major populations. In bone marrow, neutrophils, B cells and inflammatory monocytes were the major populations. In liver, inflammatory monocytes, neutrophils and B cells, for lung, neutrophils, B cells and inflammatory monocytes were the three biggest populations (Figure 4.20).

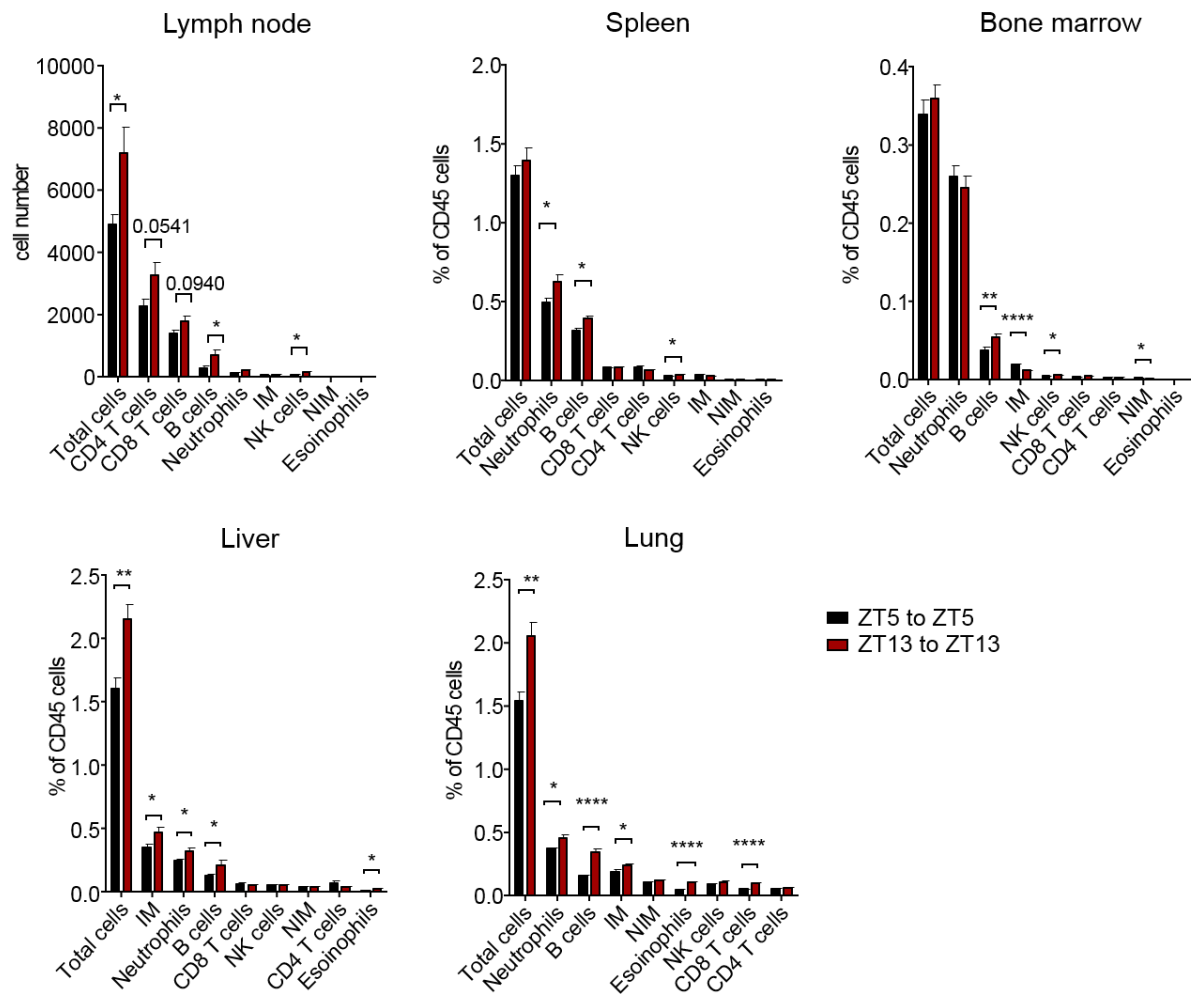


Figure 4.20 Homing experiment to various organs

Organs were harvested and analyzed by flow cytometry. The first column represents ZT5 recipients, and the second one represents ZT13 recipients. Lymph node, n=11-14; spleen, n=24-25; Bone marrow, n=24-25; Liver, n=10; Lung, n=10, unpaired Student's t-test. *p<0.05, **p<0.01, ***p<0.001, ****p<0.0001 (manuscript in preparation).

4.5. Time-dependent leukocyte migration of organs is adhesion molecule- and leukocyte subset-specific

To investigate the specific effects of pro-migratory molecules on rhythmic homing, we performed antibody or functional inhibitor blocking in combination with homing

experiments using ZT13 mice as recipients. To identify the precise location of cells, namely whether donor cells in the organ were inside or outside the vasculature, we injected an anti-CD45 antibody (clone I3/2.3), five minutes before perfusion of the recipient mice (Figure 4.21).

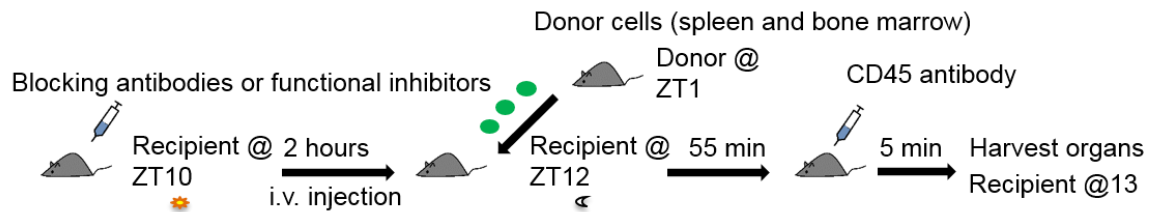


Figure 4.21 Antibody or functional inhibitor blocking experiments

Recipient mice were treated with blocking antibodies or functional inhibitors two hours before injection of donor cells. Spleen and bone marrow cells were collected from mice at ZT1 time point as donor cells. After incubation in CFSE, donor cells were injected into ZT12 recipients. After 55 minutes, CD45 antibody was injected i.v. into recipient mice. Five minutes later, mice were perfused and organs were harvested and analyzed by flow cytometry.

We performed a perfusion to remove free-flowing cells in the circulation. Using two different anti-CD45 antibody clones, we were able to identify whether donor cells were still inside or outside the vasculature. If donor cells were positive for the injected anti-CD45 clone, they were located in the vasculature. In liver and lung, more than 97% of donor cells were thus shown to be inside the vasculature. In contrast, in bone marrow, spleen and lymph node, only 3-9% of donor cells were found inside the vessel, as most of the donor cells migrated already into the tissues and were negative for the i.v. injected anti-CD45 antibody (Figure 4.22).

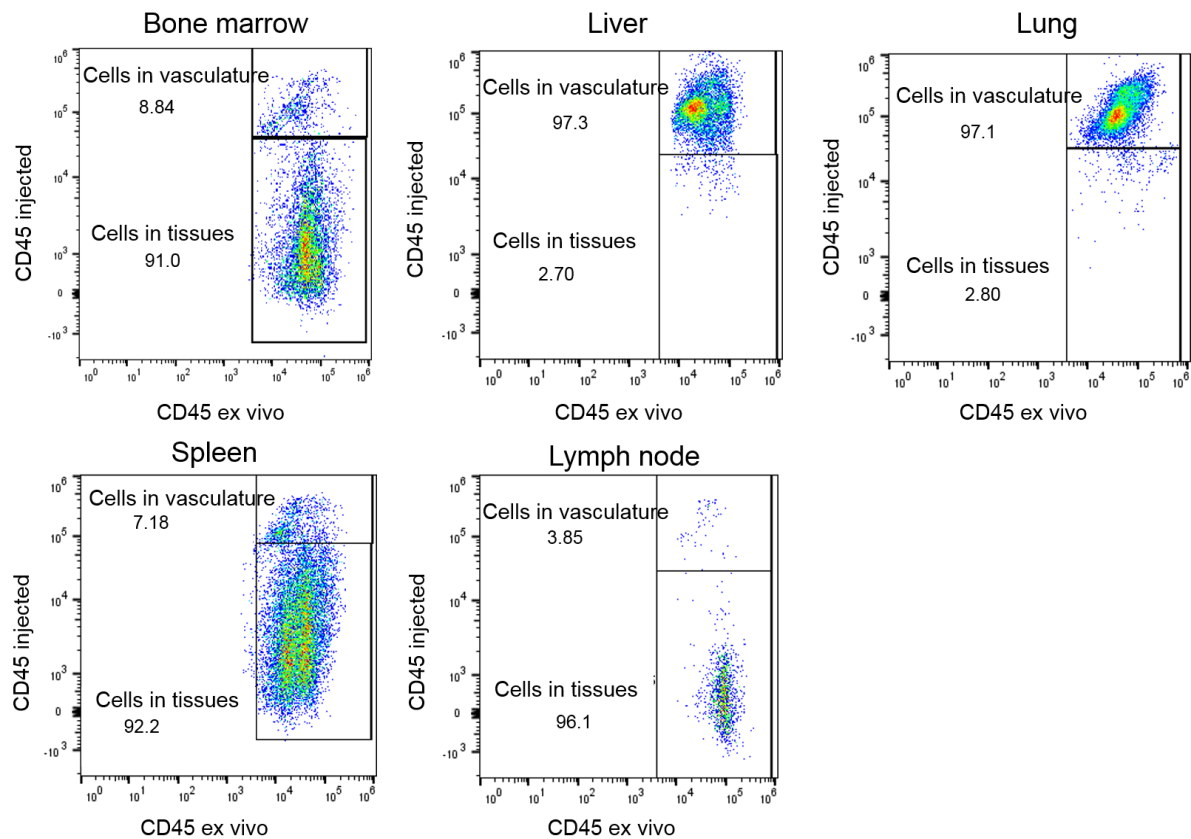


Figure 4.22 Flow cytometry of organs in homing experiment after i.v. injection of CD45
 Injected anti-CD45 (clone I3/2.3) identified cells' firm attachment to the vasculature. Ex vivo staining of CD45 (clone 30-F11) stained for all the CD45+ cells. The CD45 injected positive population thus represents the attached donor cells, while the CD45 injected negative population represents cells that had migrated into the tissues. In bone marrow, spleen and lymph node, most of the donor cells had migrated into the tissues, while in liver and lung, the majority of the donor cells were attached to the vasculature (manuscript in preparation).

4.5.1. Migration of donor cells to the lung

In order to identify the blocking effect of each inhibitor and which leukocyte subset they targeted, we compared donor cell numbers in different antibody treatment groups with control groups. For total donor cells, blockade of VCAM-1, ICAM-1, CXCR4, CD11a showed decreased donor cell numbers in the lung. In contrast, anti-L-selectin did not inhibit the homing of donor cells. The blocking effects of these inhibitors was mainly due to an effect on B cells and inflammatory monocytes (Ly6C^{high}), since these were the two biggest populations that migrated to the lung (Figure 4.20). Blocking VCAM-1, ICAM-1, CXCR4, CD49d decreased CD4 T cell numbers. Anti-VCAM-1 and anti-ICAM-

1 antibodies showed a blocking effect for CD8 T cell migration. However, the biggest population, neutrophils, was not affected by any of these functional blockers (Figure 4.23).

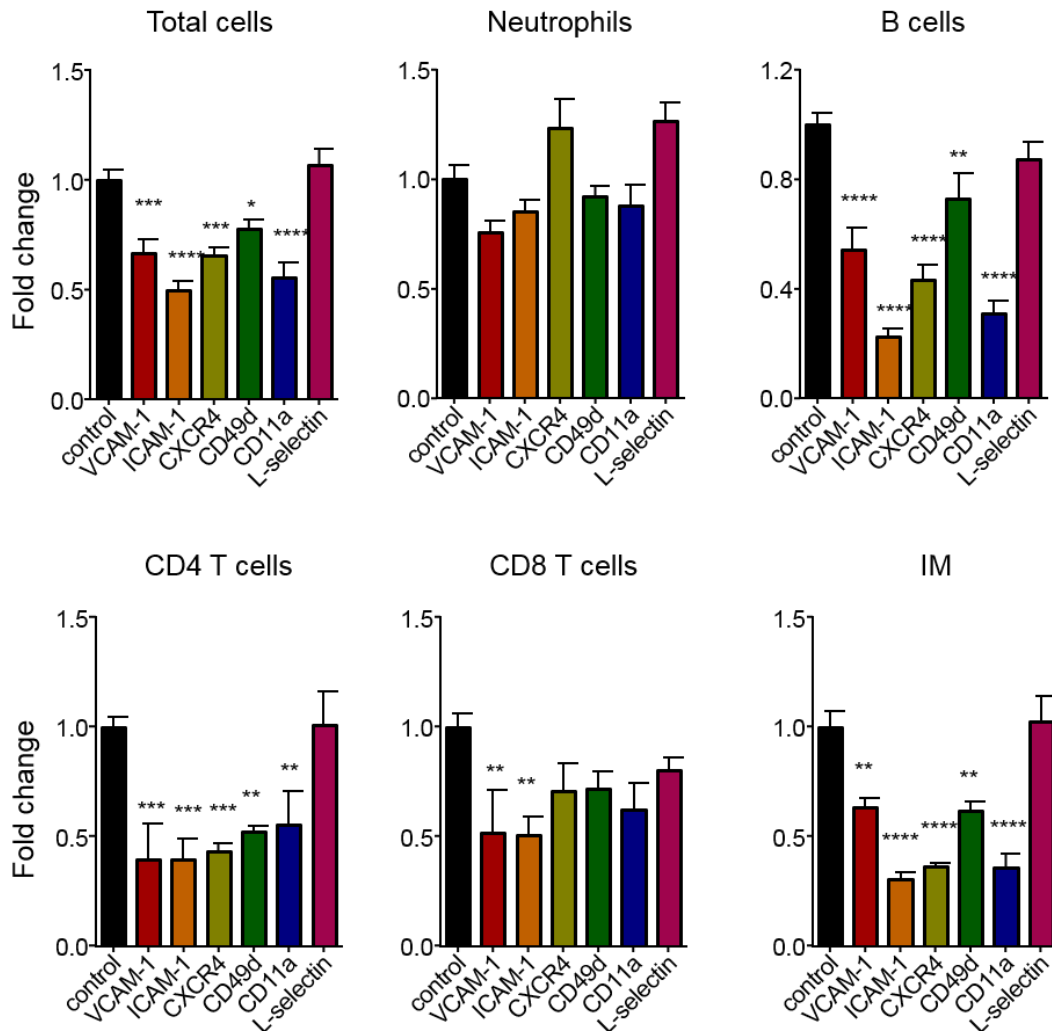


Figure 4.23 Recruited donor cells in the lung in antibody blocking with homing experiment

Lung was harvested from ZT13 recipients after injection of antibodies or PBS and given donor cells. Recruited donor cells were compared with control groups. n=4-8, unpaired Student's t-test. *p<0.05, **p<0.01, ***p<0.001 (manuscript in preparation).

Since more than 97% of donor cells attached to the vessel in the lung (Figure 4.22), the change of leukocyte number was mostly due to effects inside the vasculature (Figure 4.24).

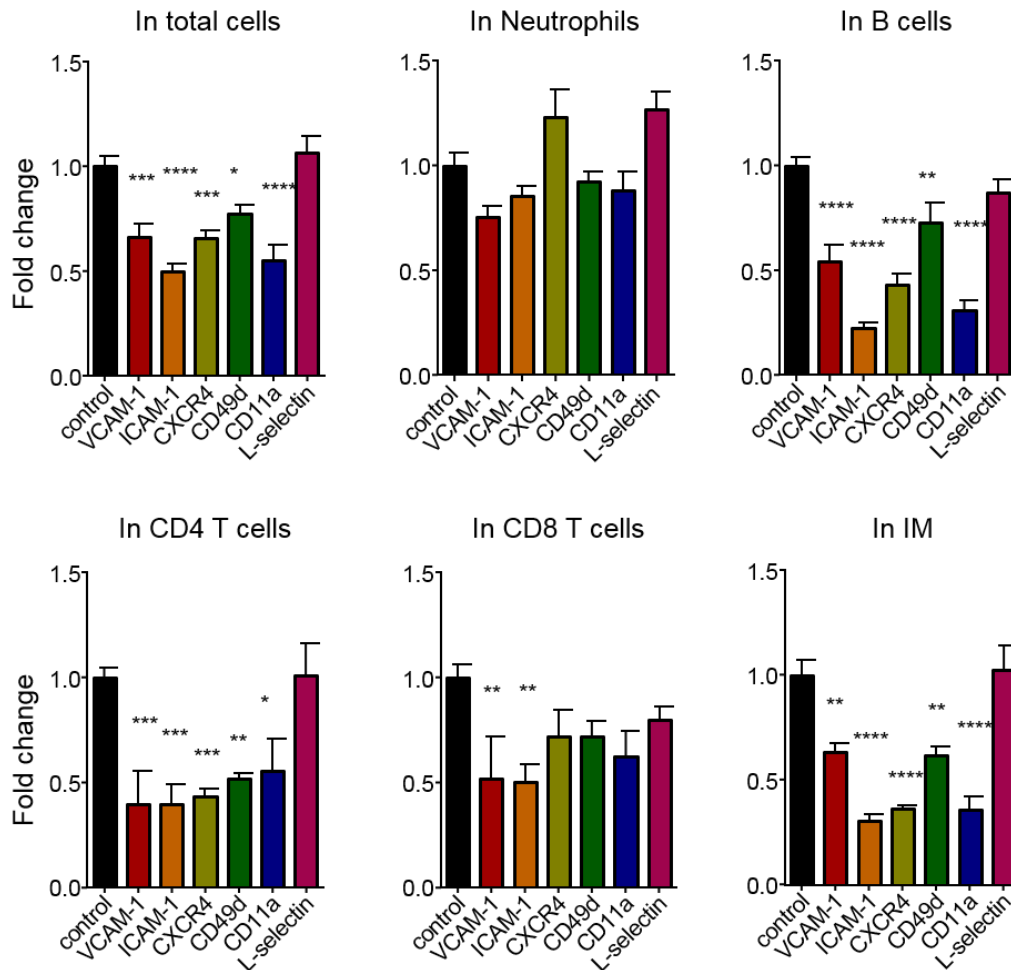


Figure 4.24 Recruited donor cells inside the lung vasculature

Lung was harvested from ZT13 recipients after injection of antibodies or PBS and donor cells. Recruited donor cells were compared with control groups. 'In' means cells in the vasculature. n=4-8, unpaired Student's t-test. *p<0.05, **p<0.01, ***p<0.001 (manuscript in preparation).

4.5.2. Migration of donor cells to the liver

Donor cells recruited to the liver were decreased by VCAM-1, ICAM-1 or CXCR4 blockade. This effect was mainly due to an effect on neutrophils, B cells and inflammatory monocytes (Ly6C^{high}), and only slightly due to CD4 T cells and CD8 T cells, as the latter represent only small populations in the liver. Blocking VCAM-1 or ICAM-1 decreased numbers of inflammatory monocytes and CD4 T cells. VCAM-1

but not ICAM-1 was involved in neutrophil homing to liver, while homing for B cells and CD8 T cells were ICAM-1 dependent. Targeting CXCR4 inhibited the recruitment process of inflammatory monocytes, CD4 T cells and probably CD8 T cells. While blocking L-selectin showed a trend to decrease the numbers of inflammatory monocytes, it increased the numbers of neutrophils and B cells in the vasculature of the liver. Anti-CD49d antibody also showed an inverse effect for different leukocyte subsets. While blocking CD49d decreased the number homed inflammatory monocytes, it increased the number of B cells which may be recruited to the liver in an unspecific manner. CD11a did not play any function role in the liver recruitment process for total leukocyte numbers as well as for the individual leukocyte subsets (Figure 4.25).

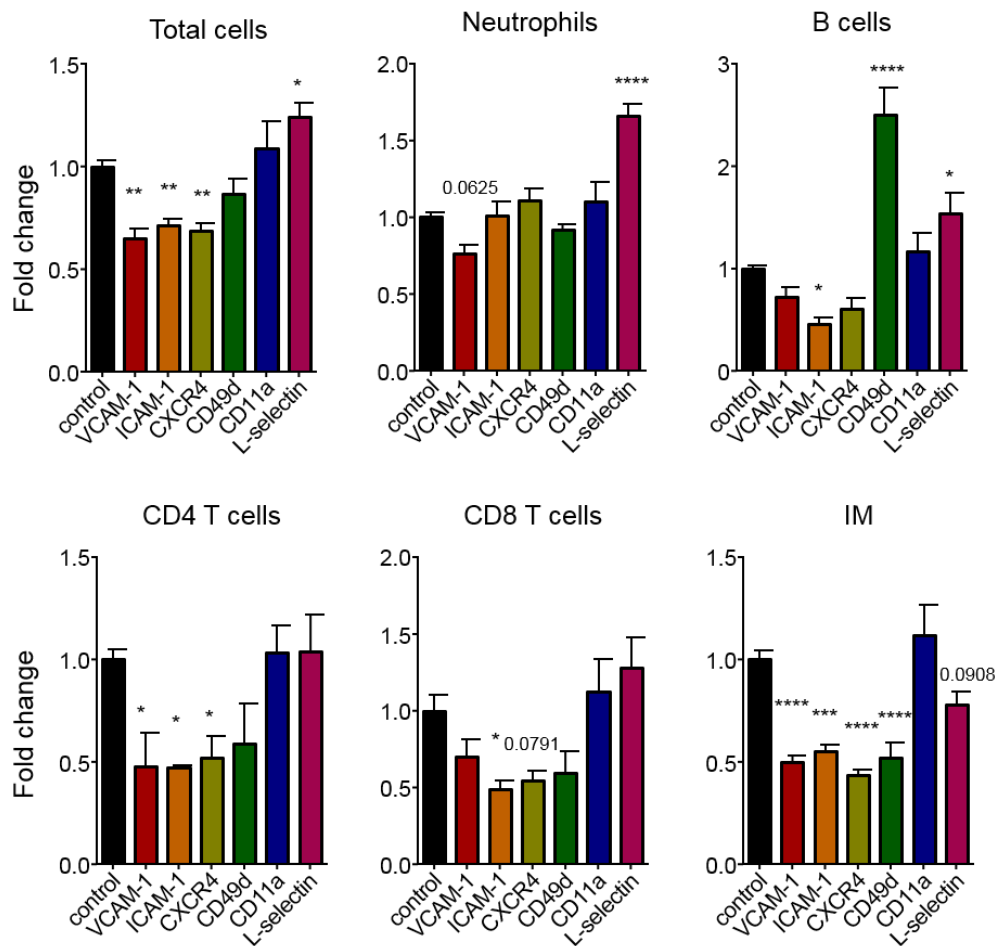


Figure 4.25 Recruited donor cells in the liver in antibody blocking with homing experiment

Liver was harvested from ZT13 recipients after injection of antibodies or PBS and donor cells. Recruited donor cells were compared with control groups. n=4-8, unpaired Student's t-test. *p<0.05, **p<0.01, ***p<0.001 (manuscript in preparation).

In the liver, more than 97% donor cells remained in the vasculature. Therefore, the effects we saw above was mostly due to the cell number change in the vasculature (Figure 4.26).

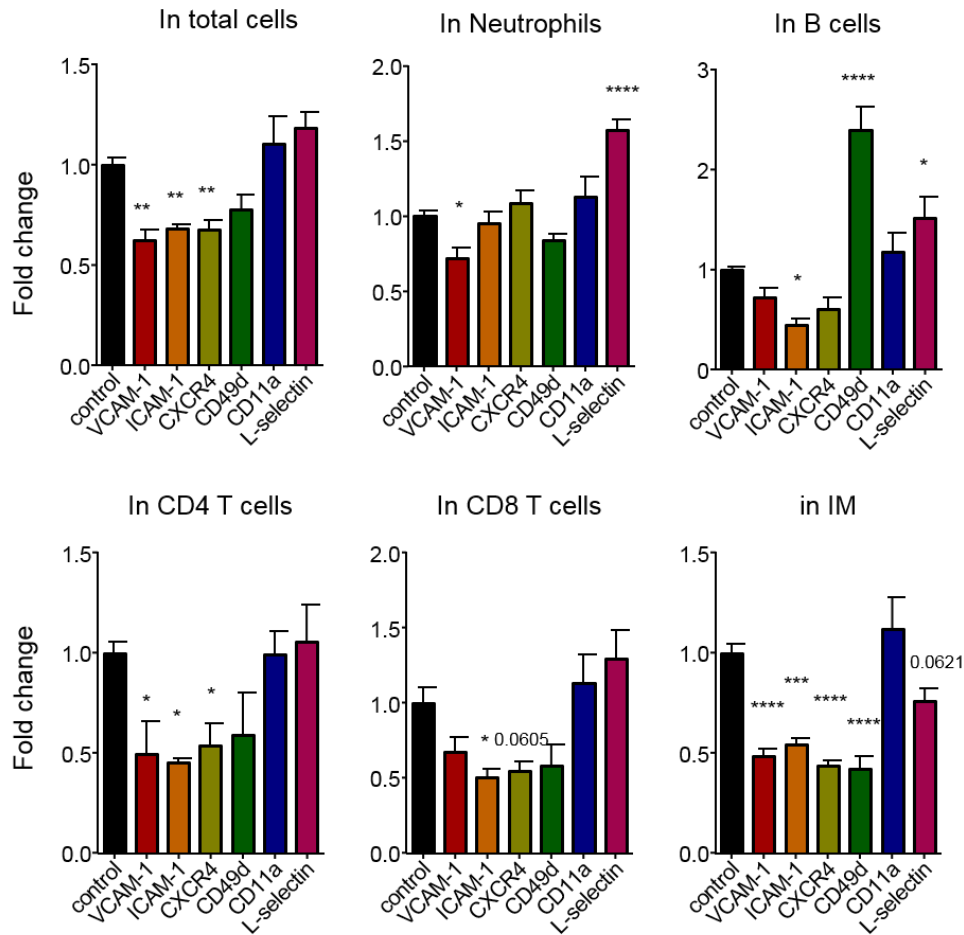


Figure 4.26 Recruited donor cells inside the liver vasculature

Liver was harvested from ZT13 recipients with injection of antibodies or PBS and donor cells. Recruited donor cells were compared with control groups. 'In' means cells in the vasculature. n=4-8, unpaired Student's t-test. *p<0.05, **p<0.01, ***p<0.001, ****p<0.0001 (manuscript in preparation).

4.5.3. Migration of donor cells to the lymph node

Total donor cell numbers in the lymph node were strongly decreased by blocking ICAM-1, CD11a or L-selectin. This effect was found for the lymphocyte subsets, including B cell, CD4 T cells, CD8 T cells, neutrophils as well as inflammatory monocytes. In addition, neutrophils, B cells and inflammatory monocytes were decreased by the CXCR4 antagonist, while CD8 T cell numbers increased. Neutrophils could also be blocked with the anti-CD49d antibody. (Figure 4.27).

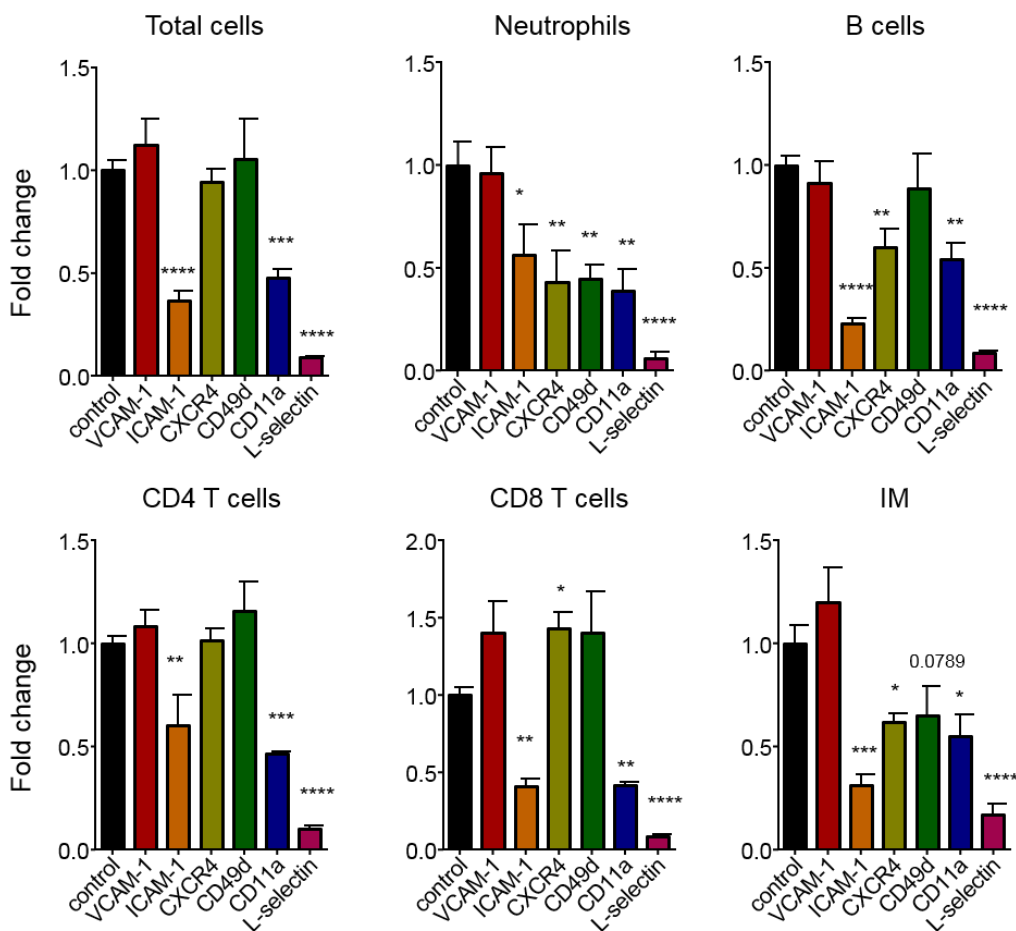


Figure 4.27 Recruited donor cells in the lymph nodes in antibody blocking with homing experiment

Lymph nodes were harvested from ZT13 recipients after injection of antibodies or PBS and donor cells. Recruited donor cells were compared with control groups. n=4-8, unpaired Student's t-test. *p<0.05, **p<0.01, ***p<0.001, ****p<0.0001 (manuscript in preparation).

In lymph nodes, most of the adoptive transferred cells had migrated into the organ, with less than 5% being adherent to the vascular endothelium (Figure 4.22). Donor cells were divided into two populations, cells inside or outside the vessel. The results showed that both the cells that had migrated into the tissues or were attached to the vessels were greatly decreased after injection of blocking antibody against ICAM-1, CD11a or L-selectin. The transmigrated donor cell numbers of major populations, CD4 T cells, CD8 T cells, and B cells, were greatly decreased by ICAM-1, CD11a or L-selectin blockade. The intravascular numbers of B cells decreased after ICAM-1 or L-selectin blockade. CD4 T cells showed decreased numbers in the vessel after L-selectin blockade. Neutrophils and monocytes were very minor populations in lymph nodes. Neutrophil numbers were decreased by blocking CXCR4, CD49d, CD11a or L-selectin, and intravascular neutrophil numbers were decreased by targeting CD49d or L-selectin. Monocyte migration into the tissues of lymph nodes was inhibited by ICAM-1 or L-selectin blockade, while the cells adherent to the vessel were affected by blocking VCAM-1, ICAM-1 CXCR4, CD11a, CD49d or L-selectin (Figure 4.28).

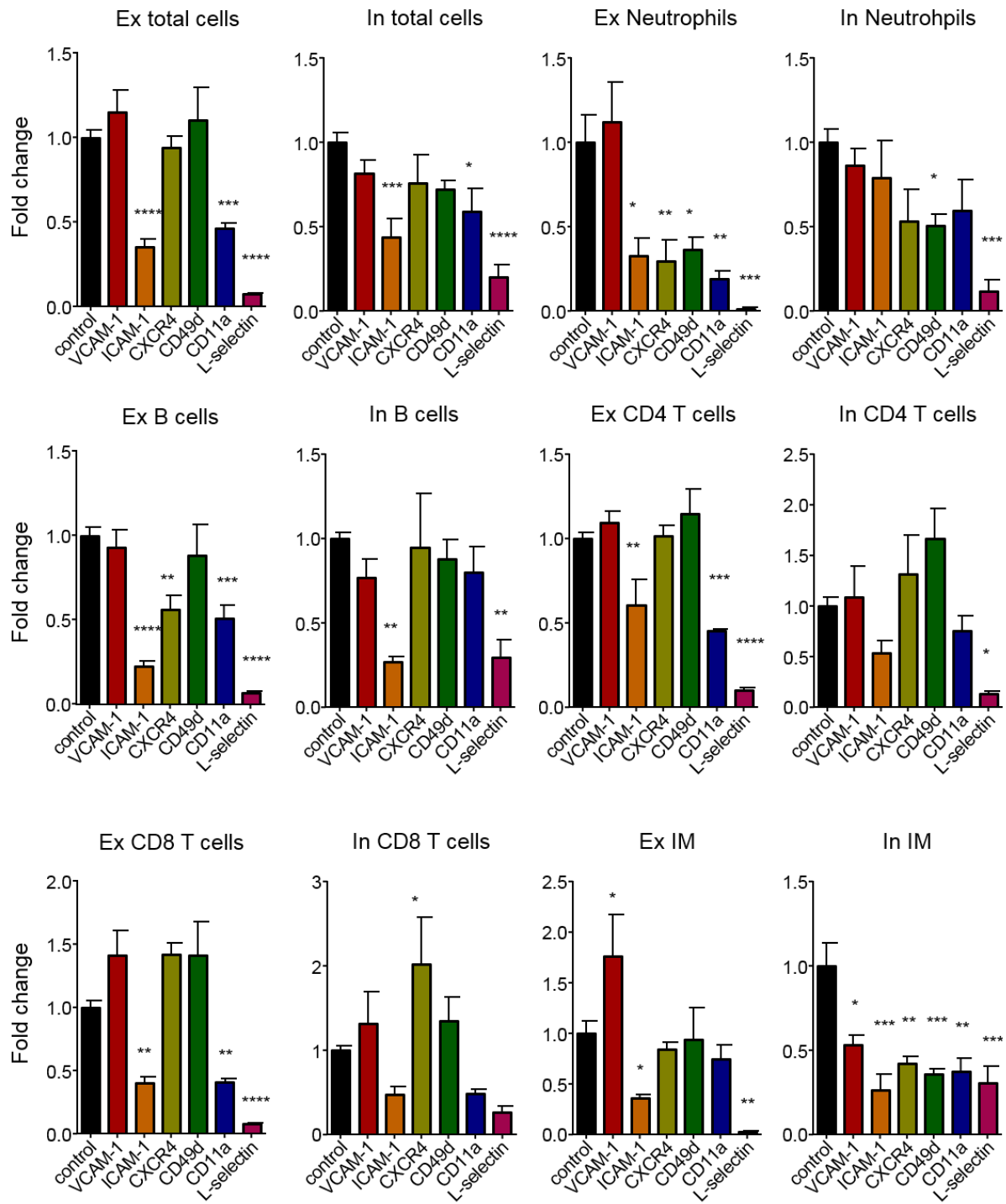


Figure 4.28 Recruited donor cells inside or outside the lymph node vasculature

Lymph nodes were harvested from ZT13 recipients after injection of antibodies or PBS and donor cells. 'Ex' refers to as cells outside the vasculature, while 'In' refers to cells inside the vasculature. n=4-8, unpaired Student's t-test. *p<0.05, **p<0.01, ***p<0.001, ****p<0.0001 (manuscript in preparation).

4.5.4. Migration of donor cells to the spleen

Migration of total injected donor cells to the spleen was inhibited by blocking L-selectin. Anti-L-selectin antibody showed a wide blocking effect for neutrophils, B cells, CD4 T cells and CD8 T cells. Anti-ICAM-1 antibody targeted B cells and inflammatory monocytes. Blocking CXCR4 or CD49d inhibited CD4 T cells homing to spleen (Figure 4.29).

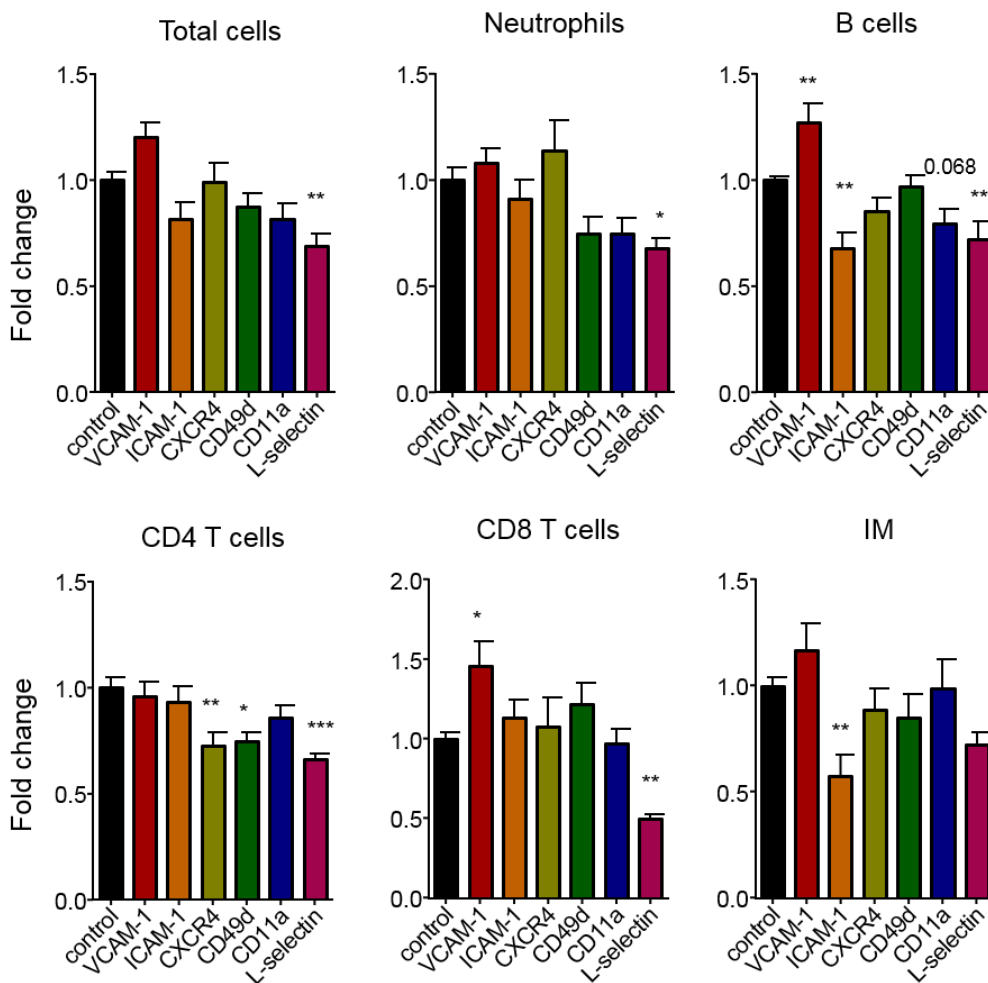


Figure 4.29 Recruited donor cells in the spleen in antibody blocking with homing experiment
Spleens were harvested from ZT13 recipients after injection of antibodies or PBS and donor cells. Recruited donor cells were compared with control groups. n=4-8, unpaired Student's t-test. *p<0.05, **p<0.01, ***p<0.001, ****p<0.0001 (manuscript in preparation).

Donor cells that had migrated to the spleen were mostly located outside the vasculature (more than 90%) (Figure 4.22). L-selectin blockade decreased the total number of migrated leukocytes into the spleen. The biggest migratory population in the spleen was neutrophils, which were affected by CD49d and L-selectin blockade, while more neutrophils were attached to the vessel endothelium after blockade of CXCR4. The second major population migrated to spleen was B cells. Migration of B cells into the spleen was decreased by ICAM-1, CD11a or L-selectin blockade, but increased by VCAM-1 blocking. Blocking CD11a or CD49d increased the number of intravascular B cells. CD4 T cells were inhibited from homing to spleen by CXCR4, CD49d or L-selectin blockade, while intravascular CD4 T cells numbers were increased by CD11a blockade. Extravascular CD8 T cells numbers were increased by VCAM-1 blockade, but decreased by L-selectin blockade. Homing of inflammatory monocytes to spleen was inhibited by ICAM-1 blockade (Figure 4.30).

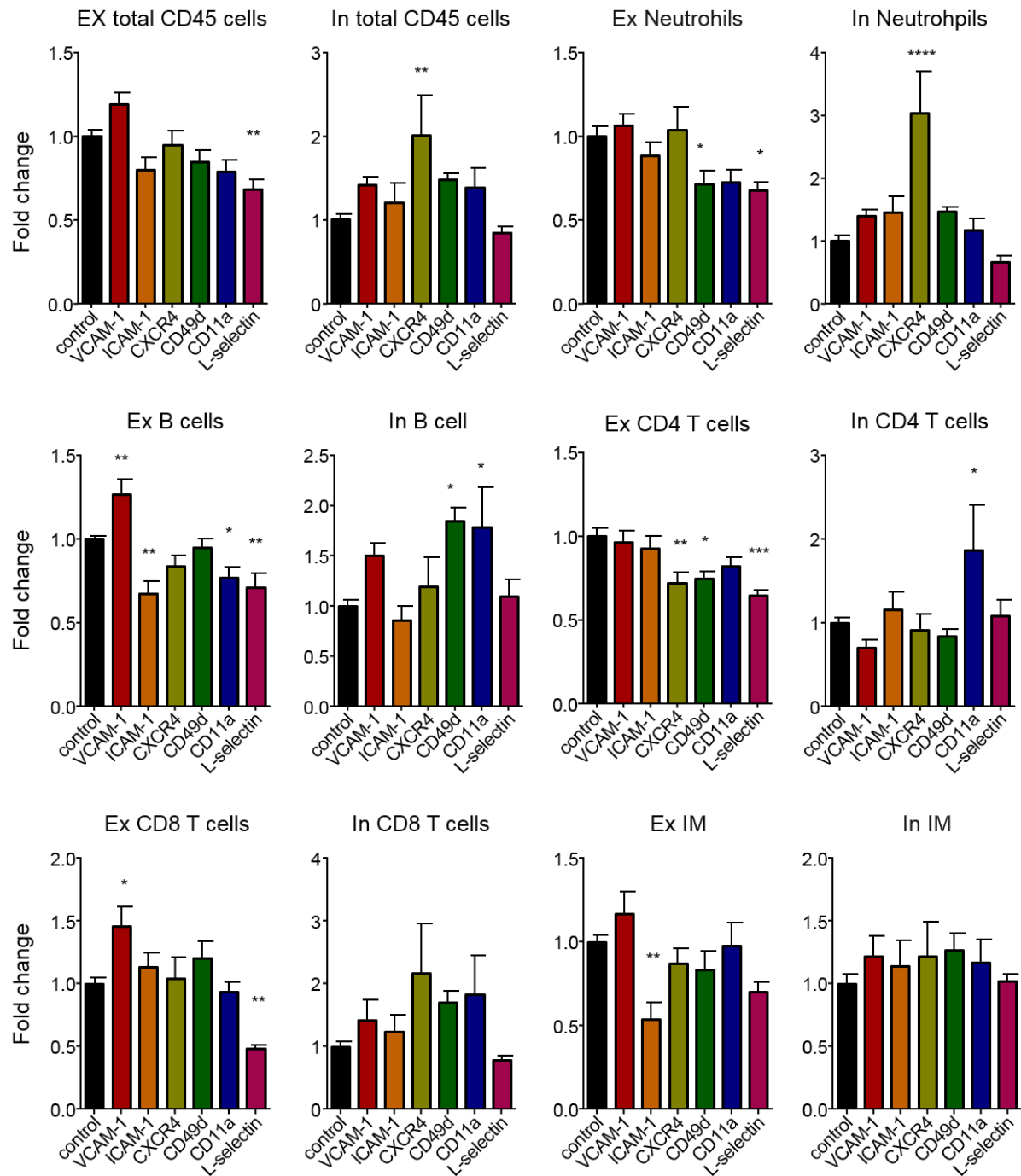


Figure 4.30 Recruited donor cells inside or outside the spleen vasculature

Spleens were harvested from ZT13 recipients after injection of antibodies or PBS and donor cells. Recruited donor cells were compared with control groups. 'Ex' refers to as cells outside the vasculature, while 'In' refers to cells inside the vasculature. n=4-8, unpaired Student's t-test. *p<0.05, **p<0.01, ***p<0.001, ****p<0.0001 (manuscript in preparation).

4.5.5. Migration of donor cells to the bone marrow

For the bone marrow, the number of total recruited cells could be inhibited by blocking VCAM-1, ICAM-1, CXCR4, CD49d, but the strongest blocking effect was found after CXCR4 antagonist injection. Both VCAM-1 and ICAM-1 targeted B cells and CD8 T cells, but only VCAM-1 had an impact on CD4 T cell migration to this tissue. L-selectin blocking decreased neutrophil migration, but increased CD4 T cells migration. Anti-CD49d antibody affected B cells, CD4 T cells and CD8 T cells. The CXCR4 antagonist had a strong effect on B cells, neutrophils, CD4 T cells, CD8 T cells, but not inflammatory monocytes (Figure 4.31).

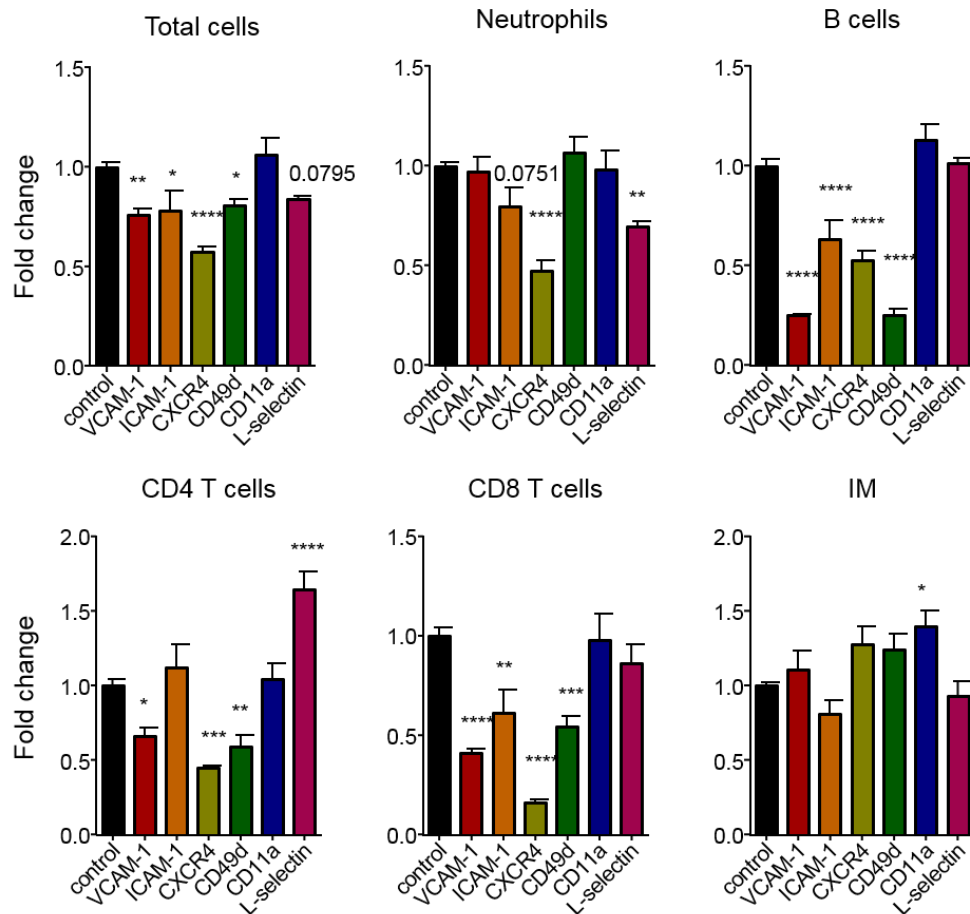


Figure 4.31 Recruited donor cells in the bone marrow in antibody blocking with homing experiment

Bone marrow was harvested from ZT13 recipients after injection of antibodies or PBS and donor cells. Recruited donor cells were compared with control groups. n=4-8, unpaired Student's t-test. *p<0.05, **p<0.01, ***p<0.001, ****p<0.0001 (manuscript in preparation).

CXCR4 inhibition decreased the number of migrated cells into the bone marrow, except for inflammatory monocytes. Neutrophil recruitment to bone marrow was strongly decreased by CXCR4 blockade, while a lot of neutrophils were blocked at the transmigration stage and remained at the stage of adhesion, therefore the intravascular neutrophil number increased. Besides CXCR4, neutrophils homing to bone marrow was inhibited by ICAM-1 or L-selectin blockade. B cells were greatly affected by VCAM-1, ICAM-1, CXCR4 or CD49d interference. Blocking CXCR4 increased intravascular B cells, while blocking VCAM-1 or CD49d decreased the numbers of intravascular B cells. Inflammatory monocytes migration in to the bone marrow tissue was inhibited by ICAM-1, while increased by CD11a blockade. Inflammatory monocytes remained in the vasculature increased after CXCR4 blockade. CD8 T cells migration could be decreased by VCAM-1, ICAM-1, CXCR4 or L-selectin blockade. CD4 T cells migration into the bone marrow could be inhibited by VCAM-1 or CXCR4 blockade, while CD4 T cells numbers were increased in bone marrow tissue and vessel after L-selectin blockade, and increased only in the vessel after ICAM-1 blockade (Figure 4.32).

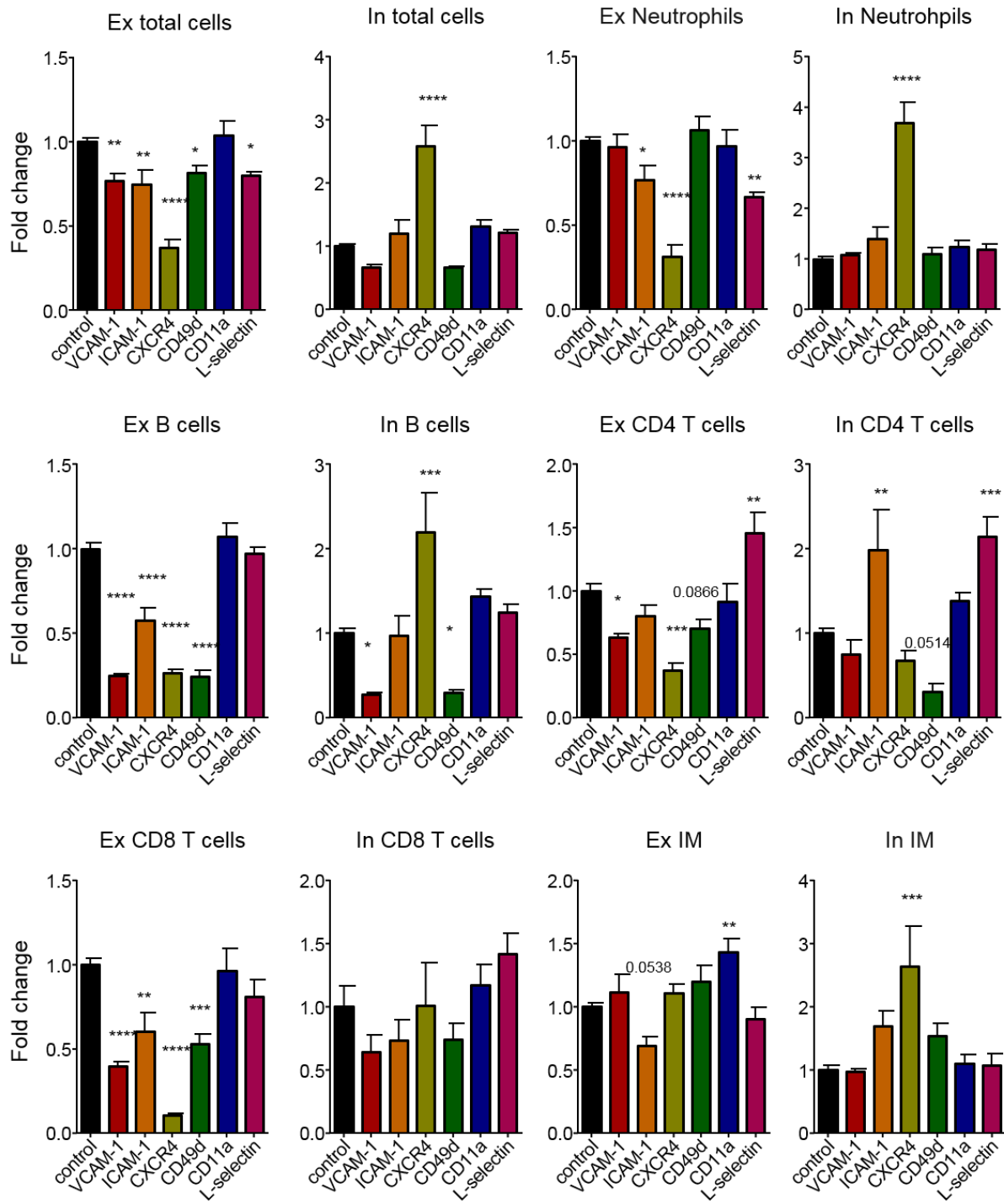


Figure 4.32 Recruited donor cells inside or outside the bone marrow vasculature

Bone marrow was harvested from ZT13 recipients after injection of antibodies or PBS and donor cells. Recruited donor cells were compared with control groups. 'Ex' refers to as cells outside the vasculature, while 'In' refers to cells inside the vasculature. n=4-8, unpaired Student's t-test. *p<0.05, **p<0.01, ***p<0.001, ****p<0.0001 (manuscript in preparation).

To summarize the results, two matrixes were created as below, showing the blocking effect of each blocker for every organ (Figure 4.33). The figure B is a different representation of figure A.

A

	Spleen					Bone marrow				Lymph node					Lung				Liver													
	Total cells	Neutrophil	B cell	CD4 T cells	CD8 T cells	Total cells	Neutrophil	B cell	CD4 T cells	CD8 T cells	Total cells	Neutrophil	B cell	CD4 T cells	CD8 T cells	Total cells	Neutrophil	B cell	CD4 T cells	CD8 T cells	Total cells	Neutrophil	B cell	CD4 T cells	CD8 T cells	IM						
VCAM-1																																
ICAM-1																																
CXCR4																																
CD49d																																
CD11a																																
L-selectin																																

B

	VCAM-1					ICAM-1					CXCR4					CD49d					CD11a					L-selectin										
	Total cells	Neutrophil	B cell	CD4 T cells	CD8 T cells	Total cells	Neutrophil	B cell	CD4 T cells	CD8 T cells	Total cells	Neutrophil	B cell	CD4 T cells	CD8 T cells	Total cells	Neutrophil	B cell	CD4 T cells	CD8 T cells	Total cells	Neutrophil	B cell	CD4 T cells	CD8 T cells	IM	Total cells	Neutrophil	B cell	CD4 T cells	CD8 T cells	IM				
Spleen																																				
Bone marrow																																				
Lymph node																																				
Lung																																				
Liver																																				

Figure 4.33 Matrix of molecular dependency of leukocyte subtype homing to specific organs
 Donor cells in each organ after antibody or inhibitor blocking were compared with the control group. Blue squares: donor cell number lower than the isotype or PBS control, red square: donor cells number higher than the control. (A) Donor cell numbers changes were presented for each organ. (B) Donor cells number changes were presented according to the treatment. For each subset, either the intravascular or the extravascular numbers were shown. For lung and liver, the intravascular subsets numbers were shown; for spleen, lymph node and bone marrow, the extravascular subsets numbers were shown. n=4-8, one-way ANOVA. (manuscript in preparation).

4.6. Control of rhythmic leukocyte migration by the circadian clock

4.6.1. Circadian genes oscillate in leukocyte subsets

Clock genes control circadian oscillations. The core clock genes are *Bmal1* (also known as *Arntl*) and *Clock* which are negatively regulated by the clock genes *Per1*, *Per2*, *Cry1* and REV-ERB α (encoded by *Nr1d1*). We analyzed the mRNA levels of these important clock genes from isolated monocytes and neutrophils from bone marrow, and isolated B cells from spleen. We found some clock genes to oscillate at the mRNA level over 24 hours (Figure 4.34).

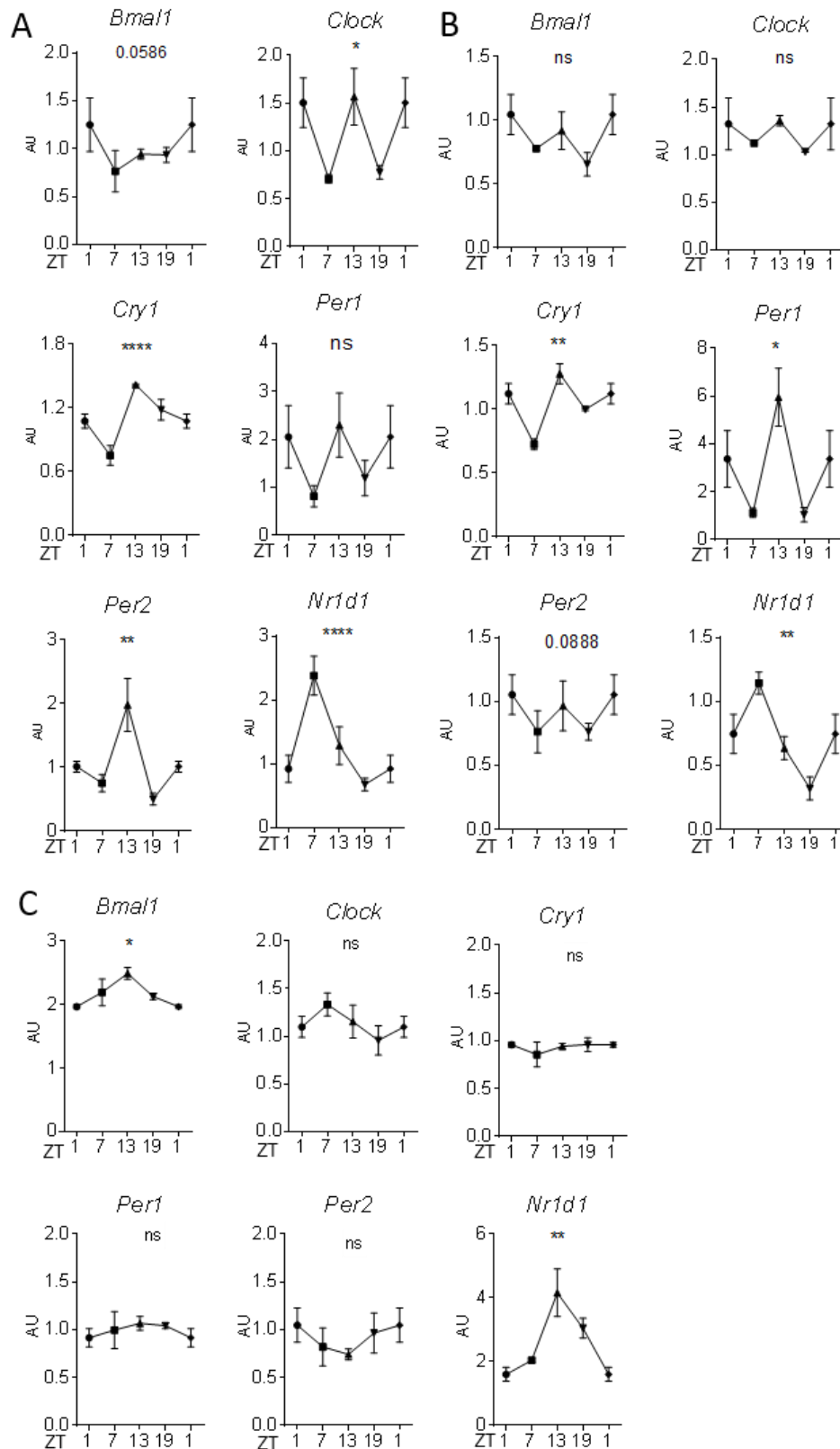


Figure 4.34 Q-PCR analysis of circadian genes in isolated cells

Relative mRNA expression levels of *Bmal1*, *Clock*, *Cry1*, *Per1*, *Per2*, and *Nr1d1* analyzed from isolated monocytes (A), neutrophils (B) and B cells (C) over 24 hours. n=3, one-way ANOVA. *p<0.05, **p<0.01, ****p<0.0001 (manuscript in preparation).

4.6.2. Leukocyte clocks and rhythmic migration

In the next step, we assessed whether the different recruitment capacity of donor cells at different times was controlled by the circadian clock. Therefore, we performed adoptive transfer experiments using donor cells with ablation of the circadian gene *Bmal1* (Figure 4.35 and Figure 4.36).



Figure 4.35 Adoptive transfer with *Bmal1* KO donor cells

Spleen and bone marrow cells were collected from mice at ZT1 and Zt13 time point as donor cells. After incubation in CFSE, donor cells were injected into ZT6 recipients. After 55 minutes, CD45 antibody was injected i.v. to recipient mice. Five minutes later, mice were perfused and spleen was harvested and analyzed by flow cytometry.

We performed experiments using *Lyz2-cre* and *CD19-cre Bmal1* knockout mice as donors. While *Lyz2-cre Bmal1* targets *Bmal1* expression in myeloid cells, such as neutrophils and monocytes, the *CD19-cre Bmal1* specifically targets B cell *Bmal1* expression. The difference of recruitment capacity between ZT1 and ZT13 donor cells in spleen was abolished in neutrophils and inflammatory monocytes when using *Lyz2-cre Bmal1^{flox/flox}* donor cells, and was lost in B cells when using *CD19-cre Bmal1^{flox/flox}* donor cells, indicating that the recruitment capacity of cells over the day was controlled by *Bmal1* and the circadian clock (Figure 4.36).

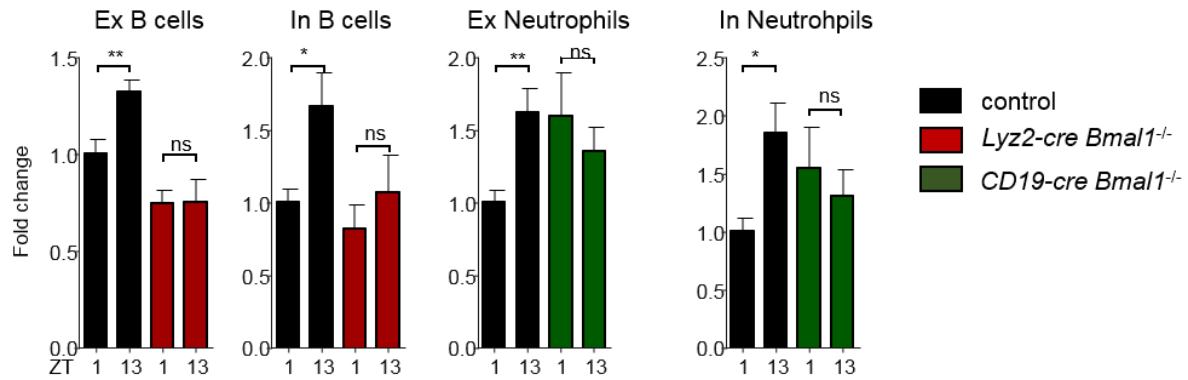


Figure 4.36 Donor cells in spleen with *Bmal1* KO or control mice as donors

Spleens were harvested from ZT6 recipients and analyzed by flow cytometry. Recruited donor cells were compared with control groups. 'Ex': cells outside the vasculature, 'In': cells inside the vasculature. n=5-6, t-test. *p<0.05, **p<0.01 (manuscript in preparation).

We performed flow cytometry analyses to compare the expression levels of adhesion molecules on the *CD19-cre Bmal1^{flx/flx}* blood cells or *Lyz-cre Bmal1^{flx/flx}* blood cells with cells from their littermate controls. *Bmal1* knockout B cells exhibited lower expression levels of CD11a, CD49d and CXCR5, all critical molecules for B cell migration (Figure 4.37 A). *Bmal1* knockout neutrophils exhibited lower expression level of PSGL-1 (Figure 4.37 B).

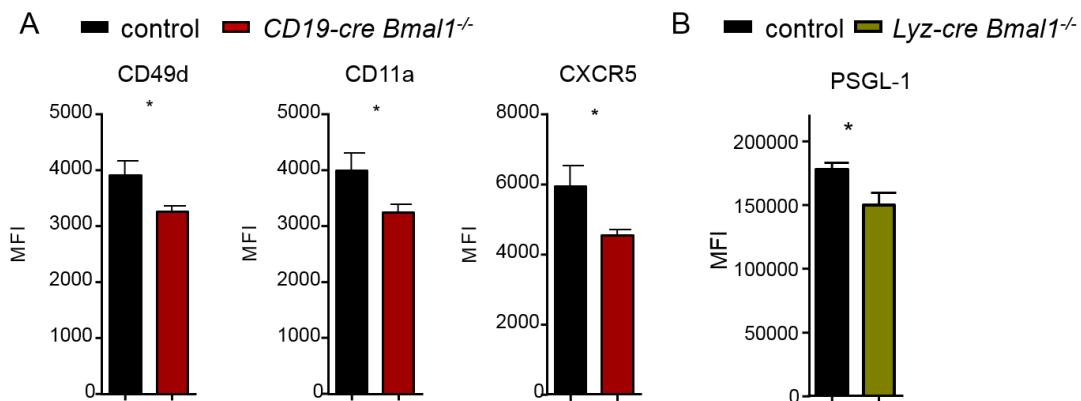


Figure 4.37 Expression levels of adhesion molecules and chemokine receptors on B cells

(A) Expression levels of CD11a, CD49d and CXCR5 were measured by flow cytometry on the surface of blood B cells of *CD19-cre Bmal1* knockout mice and their controls. n=8, unpaired Student's t-test. (B) Expression level of PSGL-1 on the surface of blood neutrophils of *Lyz-cre Bmal1* knockout mice and their controls. n=4-5, unpaired Student's t-test. *p<0.05 (manuscript in preparation).

4.6.3. Endothelial cell clocks and rhythmic migration

We investigated whether not only the leukocytes but also the microenvironment was directly controlled by circadian genes. We therefore performed adoptive transfer experiments using *Cdh5-cre/ERT2 Bmal1^{flox/flox}* and control mice as recipients (Figure 4.38), thus deleting *Bmal1* in endothelial cells. To induce *Cre* expression, mice were treated with tamoxifen i.p. for five consecutive days.

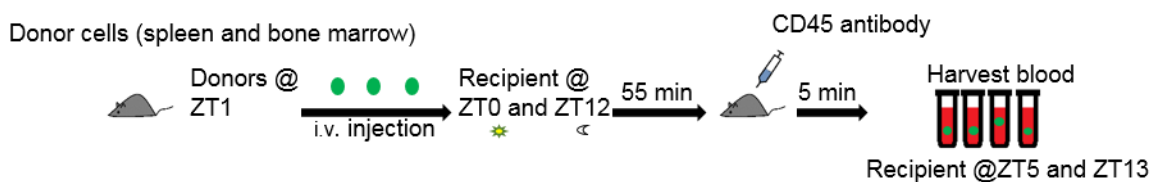


Figure 4.38 Adoptive transfer experiment with *Bmal1* KO recipients

Spleen and bone marrow cells were collected from mice at the ZT1 time point as donor cells. After incubation with CFSE, donor cells were injected into ZT1 and ZT13 recipients. One hour later, was blood harvested and analyzed by flow cytometry.

The results in control mice confirmed the previous results that ZT13 recipients had fewer total donor cells left in blood as well as specific leukocyte subsets (Figure 4.3). However, in *Cdh5-cre/ERT2 Bmal1* knockout recipients, this difference was abolished (Figure 4.39).

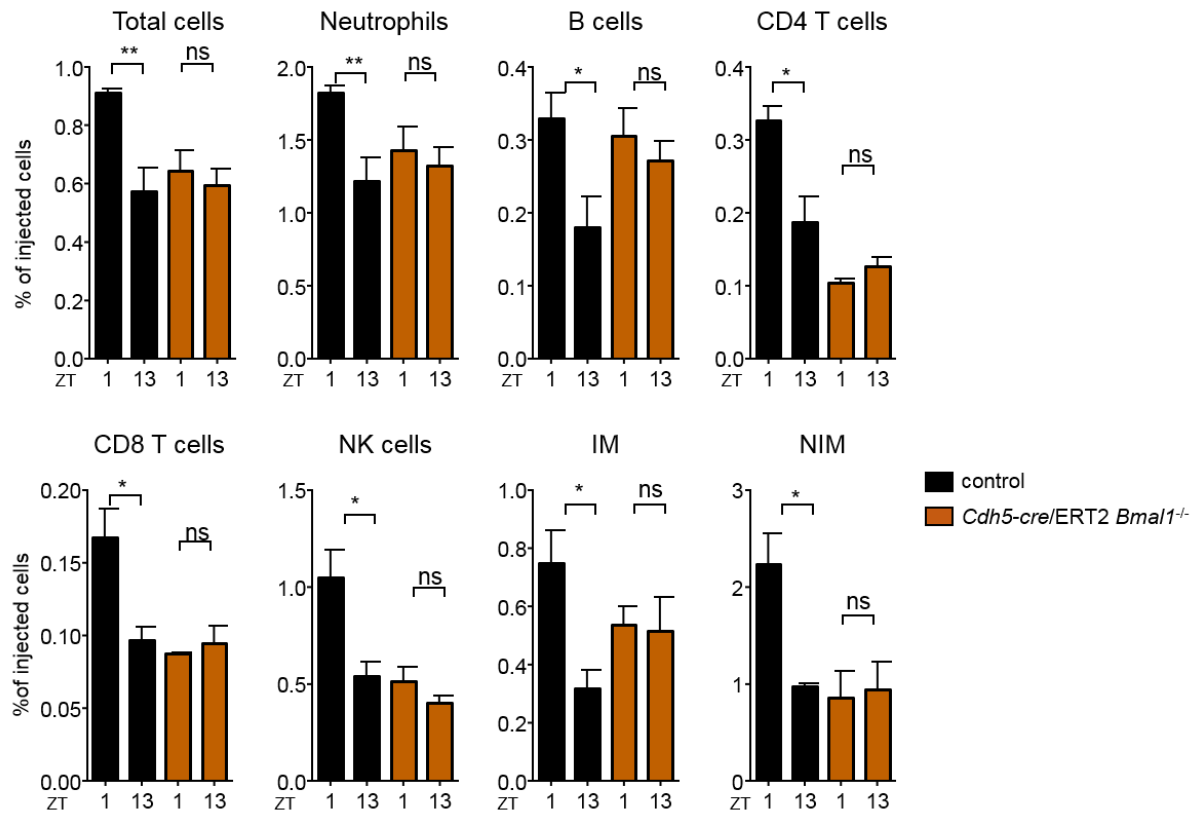


Figure 4.39 Adoptive transfer experiment with endothelial cell *Bmal1* KO
 Blood was harvested from ZT1 and ZT13 *Cdh5-cre/ERT2 Bmal1* knockout and control mice and analyzed by flow cytometry. Donor cells in blood were compared between ZT1 and ZT13 groups. n=3-5, unpaired Student's t-test. *p<0.05, **p<0.01 (manuscript in preparation).

4.7. Human blood oscillation

We further investigated the circadian rhythms in human capillary blood by finger puncture, and checked the leukocyte subsets number at several time points. Our data showed human blood leukocyte number peaked at night and troughed during the day (Figure 4.40), which is inverse to murine blood (Figure 4.1).

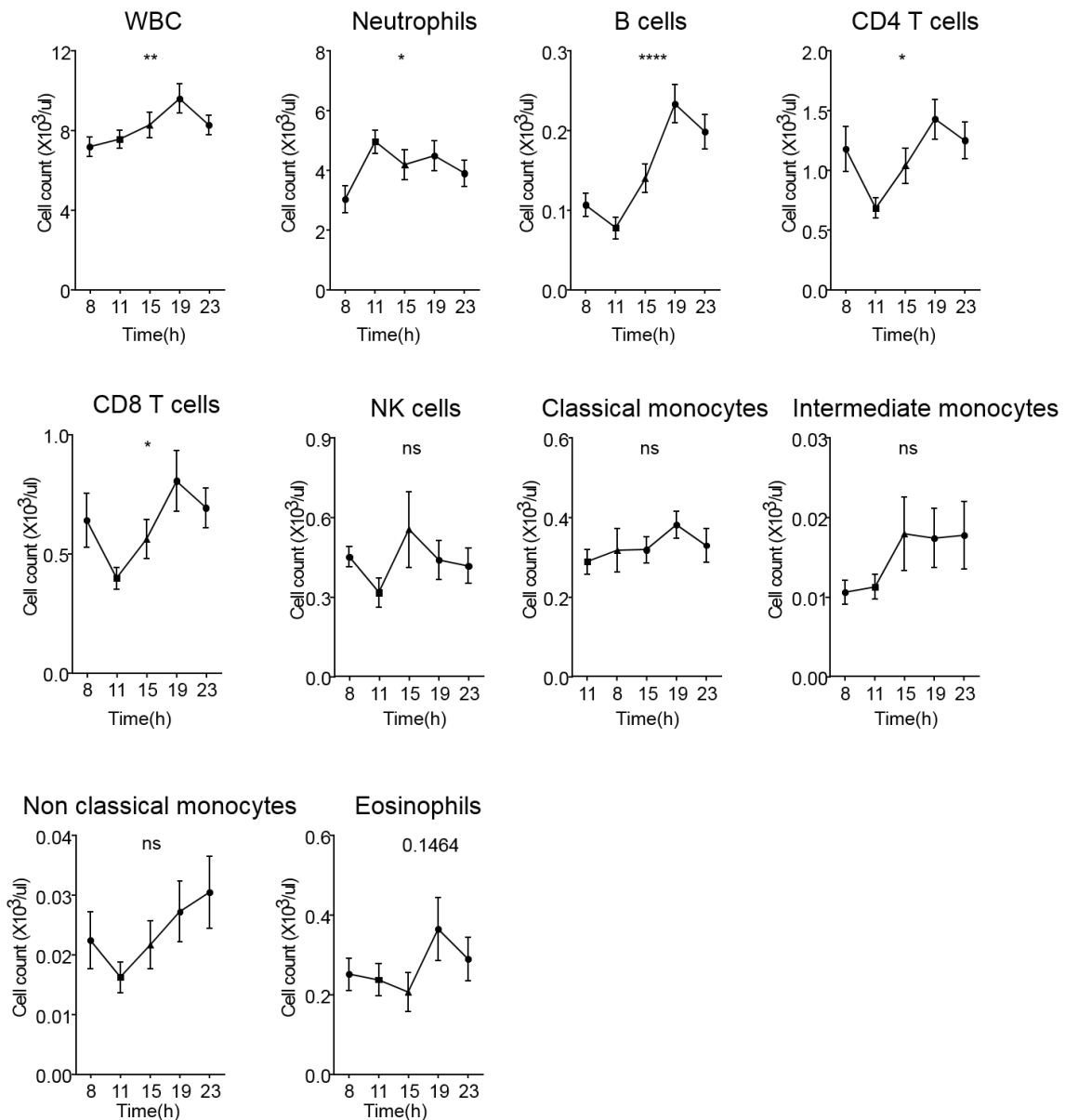


Figure 4.40 Human blood flow cytometry

Human capillary blood was measured at five human time points by flow cytometry. (A) Human blood leukocyte number. (B) CXCR4 expression on leukocyte subsets. $n=8$, repeated measures one-way ANOVA. * $p<0.05$, ** $p<0.01$, *** $p<0.001$, **** $p<0.0001$ (manuscript in preparation).

We measured the CXCR4 expression levels on the surface of human blood leukocyte subsets as well as murine blood leukocytes by flow cytometry. Almost all human blood leukocytes subsets showed oscillatory expression of CXCR4 with a peak during the day and a trough at night (Figure 4.41 A). CXCR4 expression also oscillated on murine blood cells, but at an inverse trend to humans (Figure 4.41 B).

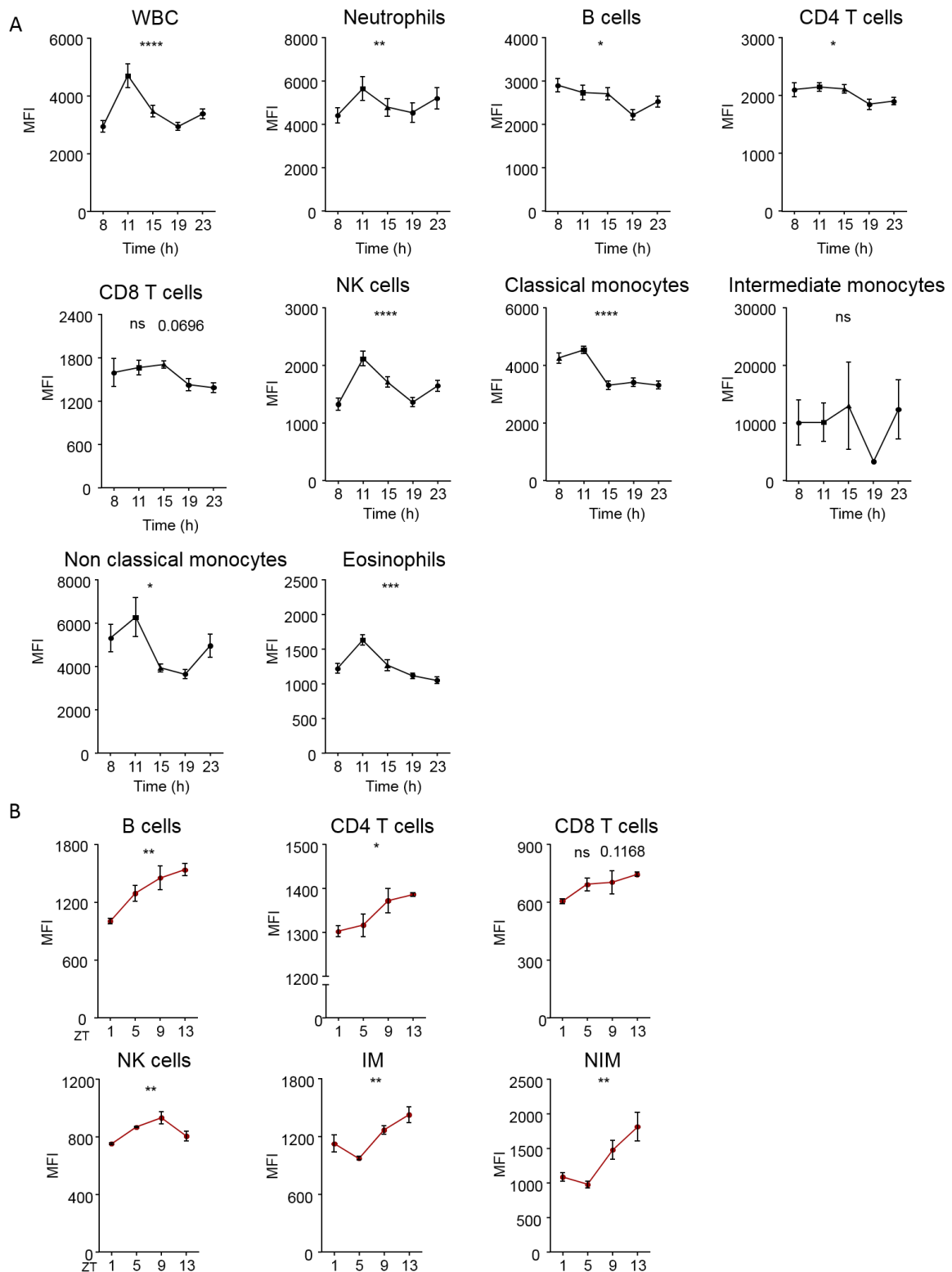


Figure 4.41 CXCR4 expression on human leukocytes and murine leukocytes
 (A) CXCR4 expression on human blood leukocyte subsets. n=8, repeated measures one-way ANOVA. (B) CXCR4 expression on murine blood leukocytes. n=3, one-way ANOVA. *p<0.05, **p<0.01, ***p<0.001, ****p<0.0001 (manuscript in preparation).

5. Discussion

5.1. Oscillation and recruitment process of murine blood leukocytes

We describe here a circadian rhythmicity in the trafficking behavior of leukocyte subsets in murine blood, including neutrophils, B cells, CD4 T cells, CD8 T cells, inflammatory monocytes, non-inflammatory monocytes, NK cells, NKT cells and eosinophils (Figure 4.1). Although distinct leukocyte subset serves specific immune functions, they all showed similar oscillation patterns exhibiting a peak in their number in blood during the day when mice are in the behavioral resting phase, and a trough at the onset of darkness. In contrast to nocturnal rodents, humans are diurnal and generally exhibit inverse circadian rhythms in peripheral blood numbers compared to mice (Born et al. 1997). This close relationship of circadian rhythms of blood cell numbers with the change in light suggests that leukocytes are synchronized by the central clock to optimize their immune function in accordance with environmental changes.

The recruitment of leukocytes out of the blood is one of the reasons for the dramatic leukocyte number change seen over 24 hours. Our data show that more donor cells leave the circulation at night than during the day (Figure 4.3). The leukocytes that have left the blood were shown to be either still attached to the inside of the vessel wall (as seen for the lung and the liver) or to have transmigrated across the endothelial barrier into the underlying tissue (as seen for spleen, bone marrow and lymph node) (Figure 4.22). Since the migration of leukocytes occurs in multiple steps governed by their interactions with endothelial cells, we wanted to investigate which of the cell types were essential for a rhythmic recruitment process. A recent study using a humanized mouse model found that human cells in mouse blood still keep human blood cell rhythmicity peaking at the night phase, which is inverse to mouse blood cells, suggesting that the leukocyte intrinsic clock is critical even in an out-of-phase environment (Zhao et al. 2017). However, in our assay, through performing adoptive transfer experiments by changing the donor cells and microenvironment, respectively, we could show that both

the leukocytes and the microenvironment were essential for the rhythmic recruitment process (Figure 4.3, Figure 4.5).

We further confirmed our results through reciprocal adoptive transfer experiments. We found that ZT13 donor cells injected into ZT13 recipients showed the highest emigration capacity (Figure 4.7). Since the migration of leukocytes occurs by the interactions of pro-migratory molecules on leukocytes and endothelium, this finding indicated that some pro-migratory molecules may have higher expression at ZT13.

5.2. A zip code for the circadian leukocyte recruitment process

We screened the expression levels of pro-migratory molecules including adhesion molecules and chemokine receptors at various time points. We found their expression levels were distinct across the day on the endothelium of organs and also on the surface of leukocyte subsets (Figure 4.8, Figure 4.13). Previous research in the lab had found that hematopoietic stem and progenitor cells were recruited to the bone marrow by rhythmic P-selectin, E-selectin and VCAM-1 expression, while monocytes and neutrophils to skeletal muscle depended on ICAM-1 expression, demonstrating that cells migrate to distinct places due to a different combination of molecules (Scheiermann et al. 2012).

Interestingly, the expression of pro-migratory molecules is not constant, instead they are oscillatory with a cell-type and organ-specific signature (Druzd et al. 2017). In humans, blood T cells have higher expression of L-selectin, CD49d, CX₃CR1, CXCR1 and CXCR4 in the morning (Dimitrov et al. 2009). These time-of-day differences of the expression of pro-migratory molecules drive leukocytes to leave blood and migrate into organs at different times, which could explain that more homing of leukocytes occurs at night in mice.

We investigated the role of pro-migratory molecules in rhythmic homing by functional blocking these molecules, including VCAM-1, ICAM-1, L-selectin, CD11a, CD49d and CXCR4, and compared the number of injected cells left in blood. In control

experiments, we noticed that donor cell numbers were lower at ZT13 compared to ZT1, indicating that a recruitment/clearing process from blood occurred more prominently at night (Figure 4.10). However, with the injection of functional blockers, this homing rhythmicity was abolished for VCAM-1, ICAM-1, CXCR4 and CD49d (Figure 4.10, Figure 4.15, Figure 4.17), suggesting that these molecules are essential for a rhythmic homing process. Interestingly, the blocking effects were not seen for every leukocyte subset, suggesting a leukocyte-specific blocking effect.

On the endothelium, VCAM-1 and ICAM-1 are two widely expressed adhesion molecules that have essential roles for leukocyte migration (Ley et al. 2007). Antibody treatment against VCAM-1 abolished the homing rhythmicity of all investigated leukocyte subsets, while blocking ICAM-1 mainly targeted lymphocytes, non-inflammatory monocytes, and eosinophils (Figure 4.10).

On the leukocyte side, L-selectin is a molecule important in the initiation of the adhesion cascade (Marelli-Berg et al. 2008). We found the expression of L-selectin to be oscillatory on the surface of many leukocyte subsets (Figure 4.13). Compared with the control group of the donor cells left in blood, blocking L-selectin inhibited the migration of neutrophils, B cells, CD4 T cells, CD8 T cells, non-inflammatory monocytes and eosinophils in the evening time point, but not NK cells, and inflammatory monocytes (Figure 4.15).

VLA-4 (CD49d) and LFA-1 (CD11a), two very important integrins in the adhesion cascade also have oscillatory expression levels on leukocyte subsets. Blocking VLA-4 affected the migration of neutrophils, B cells, CD4 T cells, CD8 T cells, NK cells, inflammatory monocytes. For NK cells and B cells, the blocking effects after VLA-4 blockade were found both in the day and evening time points, while more subsets such as neutrophils, CD4 T cells, CD8 T cells and inflammatory monocytes were inhibited in the evening time point. Blocking LFA-1 decreased the emigration process of neutrophils at night, based on the remaining donor cells numbers in blood (Figure 4.15).

Among the chemokine receptors, CXCR4 plays an important role in the homing process. Some studies demonstrated that an CXCR4 antagonist can inhibit the neutrophil recruitment process (Furze and Rankin 2008). We found that CXCR4 was not only important for neutrophils, but that it is also crucial for the recruitment process

of other leukocyte, including B cells, CD4 T cells, CD8 T cells, NK cells, non-inflammatory monocytes, and eosinophils, but interestingly not for inflammatory monocyte based on the cells left in blood (Figure 4.17).

Of importance, blocking ICAM-1, VCAM-1, CXCR4 and CD49d at night (ZT13) generated a much stronger effect than during the day (ZT1), indicating more leukocyte homing occurs at night than during the day, a process governed by these pro-migratory molecules.

In conclusion, the differences in the molecular signature of circadian expression of endothelial cell adhesion molecules and chemokines in tissues are responsible for the diurnal preference in the recruitment process.

5.3. Specific migration to organs

Leukocytes are transported by the blood across the body. By using spleen and bone marrow as donor cells, we found that specific donor cell subsets preferentially migrated to select organs. In the lymph nodes, most of the migrated donor cells were lymphocytes. In the spleen, the three major recruited populations were neutrophils, B cells, and CD8 T cells, while in bone marrow, they were neutrophils, B cells and inflammatory monocytes. Neutrophils were recruited at higher numbers than any other leukocyte subset to the lung, followed by B cells and inflammatory monocytes. In liver, it was inflammatory monocytes that made up the biggest population, followed by neutrophils and B cells (Figure 4.20).

Interestingly, the recruited cells were quite differently located in various organs. In lung and liver, more than 97% of donor cells were found in the vessel after perfusion, while in bone marrow, spleen and lymph node, more than 90% of donor cells had migrated into the tissues (Figure 4.22), suggesting that the unique morphology of each organ can determine the spatial localization of the donor cells.

Through the combination of blocking and homing experiments for each major organ (Figure 4.12) we found that blocking one molecule could cause distinctive effects for specific leukocyte subsets in specific organs. For example, CXCR4 is an important

chemokine receptor for leukocyte homing to the bone marrow (Casanova-Acebes et al. 2013). The CXCR4 antagonist AMD3100 blocked neutrophil, B cell, CD4 T cell and CD8 T cell homing to bone marrow (Figure 4.31). But AMD3100 did not block the same population in other organs. It blocked neutrophils and B cells homing to lymph nodes (Figure 4.27), and only affected CD4 T cells homing to spleen (Figure 4.29), suggesting CXCR4 to specifically target some leukocytes subsets in the recruitment process to specific organs.

Therefore, the discussion of the functional blocking effects of each molecule will be addressed in each organ. The lung contains a big marginated pool of neutrophils. Neutrophils are retained in the lung capillaries and temporarily sequestered from the circulating blood (Kuebler and Goetz 2002). In accordance with a previous study (Doyle et al. 1997), our data showed that blocking homing could not decrease the numbers of injected donor neutrophils in the lung, suggesting neutrophil margination in the lung is mainly due to the morphology of neutrophils, and that it is not an adhesion molecule dependent process, at least during steady state. However, other leukocyte subsets were influenced by blocking pro-migratory molecules. Consistent with a previous study (Lehmann et al. 2003), decreased number of lymphocytes were found in the lung after VLA-4/VCAM-1 blocking and LFA-1/ICAM-1 blocking. Our data showed inflammatory monocytes could also be inhibited by LFA-1/ICAM-1 blocking. And the CXCR4 antagonist affected B cells, CD4 T cells, and inflammatory monocytes. Consistent with previous studies (Doyle et al. 1997), none of these cells' migration to the lung was found to be L-selectin dependent (Figure 4.23, Figure 4.24).

The liver is another major site for neutrophil recruitment, this process was only affected by VCAM-1 of all the molecules we investigated (Figure 4.25), and may also be CD44 dependent (Lee and Kubes 2008), a molecule we did not test functionally. In line with a previous study (Lee and Kubes 2008), LFA-1 was not required for liver homing, because none of the cells we invested were blocked by an anti-LFA-1 antibody. However, ICAM-1 blockade inhibited homing of lymphocytes, which confirms a previous study (John and Crispe 2004), as well as inflammatory monocytes. Besides ICAM-1, CD4 T cells and inflammatory monocytes adhesion to liver endothelium and migration were mediated by VCAM-1. Although CXCR4 was essential for neutrophil homing to bone marrow, it didn't mediate neutrophil but CD4 T cells and inflammatory monocytes homing to liver (Figure 4.25, Figure 4.26). On the contrary, CD49d blocking

elevated the number of recruited B cells in the liver, as well as L-selectin blocking. We also observed an increase of neutrophils after L-selectin inhibition. The most likely explanation for this is that these cells were prevented from recruitment to their regular homing sites because of antibody blockade and therefore transported to the liver with the blood flow where they became adherent to liver sinusoidal endothelial cells.

The major population homing to lymph nodes are CD4 T cells, CD8 T cells and B cells. Very small numbers of donor neutrophils and monocytes were found in lymph nodes (Figure 4.22). The migration to lymph nodes was greatly dependent on L-selectin (Arbones et al. 1994), since anti-L-selectin antibody blocked recruitment of every leukocyte subset we investigated to lymph node, both into the tissue and attached to the endothelium. This indicated L-selectin to be an indispensable molecule to initiate interactions between leukocytes and HEV. For the firm adhesion steps, LFA-1/ICAM-1 is an essential pair of adhesion molecules for lymphocytes (Lehmann et al. 2003), and our data showed blocking LFA-1 or ICAM-1 decreased the homing of lymphocytes. CXCR4 is widely expressed on leukocytes, but blocking CXCR4 only decreased B cells but not T cells homing to lymph nodes (Figure 4.27, Figure 4.28), which is consistent with a previous study (Okada et al. 2002), possibly because T cell migration in lymph nodes are more CCR7 dependent (Druzd et al. 2017).

The homing process of leukocytes to the spleen is complex, since the spleen consists of white pulp and red pulp. The recruitment process to red pulp is supposed to be passive (Nolte et al. 2002), which means that if the donor cells are blocked from recruitment into other organs, the circulating donor cells increase (as we observed in blood), which would also increase the cells in the red pulp. Therefore, the blocking effect in the white pulp may be masked by the increased cell number in the red pulp which contain a lot of blood. If an effect of decreased leukocyte subsets in total spleen was found, we presume this effect to be due to decreased homing to white pulp. Similar to the finding in the lymph node, anti-L-selectin antibody could inhibit all leukocyte subsets we investigated from migrating into spleen, which is contradictory to a previous study which found L-selectin not to be required for entering the white pulp (Nolte et al. 2002), and another study found L-selectin^{-/-} lymphocytes numbers were not decreased in spleen compared with wild type donor cells after adoptive transfer (Tang et al. 1998). The possible explanation is that we used different donor cells and performed experiment in the evening. The previous experiments all used donor cells harvested

from secondary lymphoid organs, while we used a mixture of spleen and bone marrow cells. A previous study showed blocking VLA-4 had no effects of spleen lymphocytes homing to the spleen white pulp, because the contribution of VLA-4 is fully redundant to LFA-1, whereas LFA-1 is just partly redundant to VLA-4. However, the total transferred lymphocyte number in the spleen was not affected (Lo, Lu, and Cyster 2003). Our experiment did not distinguish the transferred cells in white pulp and red pulp, however, we could still see a blocking effect for B cells after CD11a blockade, for CD4 T cells after VLA-4 blockade in the evening time point. ICAM-1 is highly expressed at the marginal sinus where lymphocytes enter the white pulp (Nolte et al. 2002). B cell recruitment was LFA-1/ICAM-1 dependent. Inflammatory monocytes (Ly6C^{high}) migration was also blocked by an anti-ICAM-1 antibody, but not anti-LFA-1 antibody (Figure 4.29, Figure 4.30).

In the bone marrow, both ICAM-1 and VCAM-1 are expressed on the endothelium and are involved in the migration of leukocytes (Itkin et al. 2016). Anti-ICAM-1 antibody could target neutrophils, CD8 T cells and B cells, but this effect was not seen by blocking LFA-1. Blocking VLA-4 and VCAM-1 can affect B cells, CD4 T cells and CD8 T cells, suggesting B cells and T cells (Mazo et al. 2005) migrated to bone marrow by interaction of VLA-4/VCAM-1. Decreased neutrophil numbers after L-selectin blockade indicates that neutrophil migration to bone marrow was mediated by L-selectin, while more CD4 T cells accumulated in bone marrow after L-selectin blocking, probably due to the redistribution process of donor cells after L-selection blockade. CXCR4 contributes greatly to the homing process to the bone marrow. Blocking CXCR4 inhibited the homing of neutrophils, B cells and T cells. Interestingly, while the CXCR4 antagonist decreased the recruited donor cells in the tissue of bone marrow, the numbers of adherent donor cells actually increased, suggesting that CXCR4 antagonist specifically blocked the transmigration process (Figure 4.31, Figure 4.32).

5.4. Rhythmic homing is under the control of the circadian clock

Various studies have shown that circadian genes are expressed in leukocytes, including eosinophils (Baumann et al. 2013), mononuclear cells (Boivin et al. 2003), macrophages (Keller et al. 2009), NK cells (Logan, Arjona, and Sarkar 2011), neutrophils (Ella, Csepanyi-Komi, and Kaldi 2016) as well as T cells (Bollinger et al. 2011; Druzd et al. 2017) Our data demonstrated that the expression of some circadian genes was oscillatory in isolated neutrophils, monocytes and B cells (Figure 4.34). Some studies have revealed the rhythmic expression of pro-migratory molecules is driven by circadian genes (Scheiermann et al. 2012; Druzd et al. 2017; Nguyen et al. 2013). Our findings confirm that circadian genes can control the rhythmic expression of these molecules and drive the rhythmic recruitment process to specific places at specific times for many leukocyte subsets.

In our homing experiments, more ZT13 donor cells migrated to spleen than ZT1 donor cells for neutrophils and B cells. However, using donor cells from *Lyz2-cre Bmal1* knockout mice, where the most important circadian gene *Bmal1* (or *Arntl*) was deleted from neutrophils, monocytes and other myeloid cells, we found that the recruitment rhythmicity in spleen was abolished specifically in neutrophils (Figure 4.36). Using the *CD19-cre Bmal1^{flox/flox}* mice as donor mice, where the circadian gene *Bmal1* was knocked out specifically in B cells, *Bmal1* null donor B cells failed to show increased homing to the spleen (Figure 4.36). In addition, compared with wild type B cells, the *Bmal1* knockout B cells showed lower expression levels of VLA-4 and CXCR5 (Figure 4.37), both critical molecules for B cell homing, *Bmal1* knockout neutrophils showed lower expression of PSGL-1, suggesting that the expression of pro-migratory molecules are controlled by circadian genes, and thereby influence the rhythmic recruitment capacity.

On the other hand, by using *Cdh5-cre/ERT2 Bmal1^{flox/flox}* mice as recipients, where the circadian gene *Bmal1* was knocked out specifically in endothelial cells, the recruitment rhythmicity was abolished for all leukocyte subsets (Figure 4.39), suggesting that the endothelial cell circadian clock can control the rhythmic recruitment process.

5.5. The pathway from SCN to leukocytes

Together, we have described here that the circadian clock is crucial for the recruitment rhythmicity of leukocytes. As described in the introduction, circadian rhythms are controlled at multiple levels. Since similar circadian rhythms were found in all leukocyte subsets, therefore, they definitely need to be synchronized by the SCN.

One important pathway to transfer a synchronization signal from the SCN is via a humoral pathway. In humans, CD4 T cell numbers decline 40% during the early morning when cortisol levels rise (Dimitrov et al. 2009). This decline was hindered by the glucocorticoid receptor (GR) antagonist mifepristone, suggesting that glucocorticoids induced the T cell number drop in the morning. Endogenous cortisol activates GR and up-regulates CXCR4 expression in the morning, which will affect T cells homing to lymph node resulting in a redistribution of CD4 T cells (Dimitrov et al. 2009; Okutsu et al. 2005).

Another important hormone is epinephrine. Increased epinephrine levels in human plasma at the beginning of the activity phase can cause an increase in effector CD8+ T cells which have higher level of β -adrenergic receptors (β -AR), and therefore, are more sensitive to epinephrine signals (Dimitrov et al. 2009). Epinephrine can induce higher CX3CR1 expression, reduce the adhesive properties of effector CD8+ T cells and therefore recruit more cells from the marginal pool to the circulation and cause an increase in the morning of effector CD8+ T cells (Dimitrov et al. 2009).

In addition to hormones, another way to transfer the central synchronizing signal is by local neural innervation. Neural input from β 2-adrenergic receptors (β ₂-AR) can reduce the egress of lymphocytes from lymph nodes, and increase the lymphocytes number at night in this tissue in mice (Suzuki et al. 2016). Another study found that abolishing *Bmal1* could abolish rhythmic expression of *S1pr1* in T cells and thus inhibit the egress of leukocytes (Druzd et al. 2017). Together, the humoral pathways and local sympathetic tone likely collaborate with the intrinsic clock to control the timed expression of pro-migratory molecules, and therefore govern the rhythmicity of leukocyte migration.

5.6. Human blood oscillation

Human blood number was known to present inverse oscillation pattern to mice likely because humans are diurnal and not nocturnal as mice (Born et al. 1997). Our data expand the knowledge of human blood oscillation pattern by investigating multiple leukocyte subset at several time points in combination with the expression levels of the key pro-migratory molecule CXCR4. We showed that different human blood leukocyte subsets numbers displayed the same oscillation pattern with a trough at 11am and a peak at 7pm (Figure 4.40). In line with another study (Zhao et al. 2017), we found that CXCR4 expression levels oscillated in antiphase to leukocyte numbers both in humans and mice. For human blood leukocyte subsets, CXCR4 expression levels increased in the day time when lower leukocyte numbers occurred, and decreased during the night when leukocyte number began to increase (Figure 4.41), suggesting that time-dependent expression of pro-migratory molecule could drive the recruitment process of human blood cells.

5.7. Outlook

Oscillations in human and murine leukocytes have been known (Born et al. 1997; Ohkura et al. 2007), but no study has comprehensively investigated the migration properties of multiple leukocyte subsets over the course of the day. Our study clarified the circadian rhythms for major leukocyte subsets in blood for mice and humans and proved that the circadian rhythms of blood cells is at least in part due to rhythmic homing, which is governed by the interactions of pro-migratory molecules on endothelial cells and leukocytes.

With our big screening experiments, we found that the expression of many pro-migratory molecules is time-dependent. Most of these proved to be of importance in the rhythmic leukocyte recruitment process. Our study shows that the circadian gene *Bmal1* controls rhythmic leukocyte trafficking in a cell-autonomous and tissue-specific manner. Together, a different combination of pro-migratory molecules guides

leukocyte migration to distinct organs at specific times. This time-dependent expression feature gives us the opportunity to find the best time for treatment. Therefore, future research should focus on time-of-day to improve the efficacy of drugs, specifically targeting leukocytes and their migration behavior.

Besides circadian genes, the relaying signal from the central clock is also crucial for rhythmic migration. There is evidence that hormones could be the link between leukocytes and rhythmic expression of pro-migratory molecules (Gibbs et al. 2014; Dimitrov et al. 2009). Some key adhesion molecules, such as CXCR4, CD49d, CD11a, VCAM-1 and ICAM-1, were found to be rhythmically expressed in our study. The mechanisms of how their expression profiles are regulated by the central clock was largely unknown. This study provides the basis for future investigations into the shape of the signal transmission route from the central clock to peripheral tissues and leukocytes.

6. Reference

- Ala, A., A. P. Dhillon, and H. J. Hodgson. 2003. 'Role of cell adhesion molecules in leukocyte recruitment in the liver and gut', *Int J Exp Pathol*, 84: 1-16.
- Almon, R. R., E. Yang, W. Lai, I. P. Androulakis, S. Ghimbovschi, E. P. Hoffman, W. J. Jusko, and D. C. Dubois. 2008. 'Relationships between circadian rhythms and modulation of gene expression by glucocorticoids in skeletal muscle', *Am J Physiol Regul Integr Comp Physiol*, 295: R1031-47.
- Arbones, M. L., D. C. Ord, K. Ley, H. Ratech, C. Maynard-Curry, G. Otten, D. J. Capon, and T. F. Tedder. 1994. 'Lymphocyte homing and leukocyte rolling and migration are impaired in L-selectin-deficient mice', *Immunity*, 1: 247-60.
- Baekkevold, E. S., T. Yamanaka, R. T. Palframan, H. S. Carlsen, F. P. Reinholt, U. H. von Andrian, P. Brandtzaeg, and G. Haraldsen. 2001. 'The CCR7 ligand eic (CCL19) is transcytosed in high endothelial venules and mediates T cell recruitment', *J Exp Med*, 193: 1105-12.
- Bai, Z., H. Hayasaka, M. Kobayashi, W. Li, Z. Guo, M. H. Jang, A. Kondo, B. I. Choi, Y. Iwakura, and M. Miyasaka. 2009. 'CXC chemokine ligand 12 promotes CCR7-dependent naive T cell trafficking to lymph nodes and Peyer's patches', *J Immunol*, 182: 1287-95.
- Balsalobre, A., S. A. Brown, L. Marcacci, F. Tronche, C. Kellendonk, H. M. Reichardt, G. Schutz, and U. Schibler. 2000. 'Resetting of circadian time in peripheral tissues by glucocorticoid signaling', *Science*, 289: 2344-7.
- Baumann, A., S. Gonnenwein, S. C. Bischoff, H. Sherman, N. Chapnik, O. Froy, and A. Lorentz. 2013. 'The circadian clock is functional in eosinophils and mast cells', *Immunology*, 140: 465-74.
- Benarroch, E. E. 2008. 'Suprachiasmatic nucleus and melatonin: reciprocal interactions and clinical correlations', *Neurology*, 71: 594-8.
- Bhadra, U., N. Thakkar, P. Das, and M. Pal Bhadra. 2017. 'Evolution of circadian rhythms: from bacteria to human', *Sleep Med*, 35: 49-61.
- Boivin, D. B., F. O. James, A. Wu, P. F. Cho-Park, H. Xiong, and Z. S. Sun. 2003. 'Circadian clock genes oscillate in human peripheral blood mononuclear cells', *Blood*, 102: 4143-5.

- Bollinger, T., A. Leutz, A. Leliavski, L. Skrum, J. Kovac, L. Bonacina, C. Benedict, T. Lange, J. Westermann, H. Oster, and W. Solbach. 2011. 'Circadian clocks in mouse and human CD4+ T cells', *PLoS One*, 6: e29801.
- Born, J., T. Lange, K. Hansen, M. Molle, and H. L. Fehm. 1997. 'Effects of sleep and circadian rhythm on human circulating immune cells', *J Immunol*, 158: 4454-64.
- Cailotto, C., J. Lei, J. van der Vliet, C. van Heijningen, C. G. van Eden, A. Kalsbeek, P. Pevet, and R. M. Buijs. 2009. 'Effects of nocturnal light on (clock) gene expression in peripheral organs: a role for the autonomic innervation of the liver', *PLoS One*, 4: e5650.
- Campbell, I. D., and M. J. Humphries. 2011. 'Integrin structure, activation, and interactions', *Cold Spring Harb Perspect Biol*, 3.
- Carman, C. V., and T. A. Springer. 2004. 'A transmigratory cup in leukocyte diapedesis both through individual vascular endothelial cells and between them', *J Cell Biol*, 167: 377-88.
- Casanova-Acebes, M., C. Pitaval, L. A. Weiss, C. Nombela-Arrieta, R. Chevre, A. Gonzalez N, Y. Kunisaki, D. Zhang, N. van Rooijen, L. E. Silberstein, C. Weber, T. Nagasawa, P. S. Frenette, A. Castrillo, and A. Hidalgo. 2013. 'Rhythmic modulation of the hematopoietic niche through neutrophil clearance', *Cell*, 153: 1025-35.
- Chung, S., E. J. Lee, H. K. Cha, J. Kim, D. Kim, G. H. Son, and K. Kim. 2017. 'Cooperative roles of the suprachiasmatic nucleus central clock and the adrenal clock in controlling circadian glucocorticoid rhythm', *Sci Rep*, 7: 46404.
- Darlington, T. K., K. Wager-Smith, M. F. Ceriani, D. Staknis, N. Gekakis, T. D. Steeves, C. J. Weitz, J. S. Takahashi, and S. A. Kay. 1998. 'Closing the circadian loop: CLOCK-induced transcription of its own inhibitors *per* and *tim*', *Science*, 280: 1599-603.
- Dibner, C., U. Schibler, and U. Albrecht. 2010. 'The mammalian circadian timing system: organization and coordination of central and peripheral clocks', *Annu Rev Physiol*, 72: 517-49.
- Dickmeis, T. 2009. 'Glucocorticoids and the circadian clock', *J Endocrinol*, 200: 3-22.
- Dimitroff, C. J., J. Y. Lee, S. Rafii, R. C. Fuhlbrigge, and R. Sackstein. 2001. 'CD44 is a major E-selectin ligand on human hematopoietic progenitor cells', *J Cell Biol*, 153: 1277-86.

- Dimitrov, S., C. Benedict, D. Heutling, J. Westermann, J. Born, and T. Lange. 2009. 'Cortisol and epinephrine control opposing circadian rhythms in T cell subsets', *Blood*, 113: 5134-43.
- Doi, M., J. Hirayama, and P. Sassone-Corsi. 2006. 'Circadian regulator CLOCK is a histone acetyltransferase', *Cell*, 125: 497-508.
- Doyle, N. A., S. D. Bhagwan, B. B. Meek, G. J. Kutkoski, D. A. Steeber, T. F. Tedder, and C. M. Doerschuk. 1997. 'Neutrophil margination, sequestration, and emigration in the lungs of L-selectin-deficient mice', *J Clin Invest*, 99: 526-33.
- Druzd, D., O. Matveeva, L. Ince, U. Harrison, W. He, C. Schmal, H. Herzel, A. H. Tsang, N. Kawakami, A. Leliavski, O. Uhl, L. Yao, L. E. Sander, C. S. Chen, K. Kraus, A. de Juan, S. M. Hergenhan, M. Ehlers, B. Koletzko, R. Haas, W. Solbach, H. Oster, and C. Scheiermann. 2017. 'Lymphocyte Circadian Clocks Control Lymph Node Trafficking and Adaptive Immune Responses', *Immunity*, 46: 120-32.
- Eash, K. J., J. M. Means, D. W. White, and D. C. Link. 2009. 'CXCR4 is a key regulator of neutrophil release from the bone marrow under basal and stress granulopoiesis conditions', *Blood*, 113: 4711-9.
- Eide, E. J., E. L. Vielhaber, W. A. Hinz, and D. M. Virshup. 2002. 'The circadian regulatory proteins BMAL1 and cryptochromes are substrates of casein kinase Iepsilon', *J Biol Chem*, 277: 17248-54.
- Ella, K., R. Csepanyi-Komi, and K. Kaldi. 2016. 'Circadian regulation of human peripheral neutrophils', *Brain Behav Immun*, 57: 209-21.
- Engelhardt, B., and H. Wolburg. 2004. 'Mini-review: Transendothelial migration of leukocytes: through the front door or around the side of the house?', *Eur J Immunol*, 34: 2955-63.
- Etchegaray, J. P., K. K. Machida, E. Noton, C. M. Constance, R. Dallmann, M. N. Di Napoli, J. P. DeBruyne, C. M. Lambert, E. A. Yu, S. M. Reppert, and D. R. Weaver. 2009. 'Casein kinase 1 delta regulates the pace of the mammalian circadian clock', *Mol Cell Biol*, 29: 3853-66.
- Fleming, S. D., J. Anderson, F. Wilson, T. Shea-Donohue, and G. C. Tsokos. 2003. 'C5 is required for CD49d expression on neutrophils and VCAM expression on vascular endothelial cells following mesenteric ischemia/reperfusion', *Clin Immunol*, 106: 55-64.

- Furze, R. C., and S. M. Rankin. 2008. 'The role of the bone marrow in neutrophil clearance under homeostatic conditions in the mouse', *Faseb j*, 22: 3111-9.
- Gan, Y., R. Liu, W. Wu, R. Bomprezzi, and F. D. Shi. 2012. 'Antibody to alpha4 integrin suppresses natural killer cells infiltration in central nervous system in experimental autoimmune encephalomyelitis', *J Neuroimmunol*, 247: 9-15.
- Gekakis, N., D. Staknis, H. B. Nguyen, F. C. Davis, L. D. Wilsbacher, D. P. King, J. S. Takahashi, and C. J. Weitz. 1998. 'Role of the CLOCK protein in the mammalian circadian mechanism', *Science*, 280: 1564-9.
- Gibbs, J., L. Ince, L. Matthews, J. Mei, T. Bell, N. Yang, B. Saer, N. Begley, T. Poolman, M. Pariollaud, S. Farrow, F. DeMayo, T. Hussell, G. S. Worthen, D. Ray, and A. Loudon. 2014. 'An epithelial circadian clock controls pulmonary inflammation and glucocorticoid action', *Nat Med*, 20: 919-26.
- Girard, J. P., C. Moussion, and R. Forster. 2012. 'HEVs, lymphatics and homeostatic immune cell trafficking in lymph nodes', *Nat Rev Immunol*, 12: 762-73.
- Golden, S. S., M. Ishiura, C. H. Johnson, and T. Kondo. 1997. 'CYANOBACTERIAL CIRCADIAN RHYTHMS', *Annu Rev Plant Physiol Plant Mol Biol*, 48: 327-54.
- Golombek, D. A., and R. E. Rosenstein. 2010. 'Physiology of circadian entrainment', *Physiol Rev*, 90: 1063-102.
- Gordy, C., H. Pua, G. D. Sempowski, and Y. W. He. 2011. 'Regulation of steady-state neutrophil homeostasis by macrophages', *Blood*, 117: 618-29.
- Gorlino, C. V., R. P. Ranocchia, M. F. Harman, I. A. Garcia, M. I. Crespo, G. Moron, B. A. Maletto, and M. C. Pistoresi-Palencia. 2014. 'Neutrophils exhibit differential requirements for homing molecules in their lymphatic and blood trafficking into draining lymph nodes', *J Immunol*, 193: 1966-74.
- Griffin, E. A., Jr., D. Staknis, and C. J. Weitz. 1999. 'Light-independent role of CRY1 and CRY2 in the mammalian circadian clock', *Science*, 286: 768-71.
- Gunn, M. D., K. Tangemann, C. Tam, J. G. Cyster, S. D. Rosen, and L. T. Williams. 1998. 'A chemokine expressed in lymphoid high endothelial venules promotes the adhesion and chemotaxis of naive T lymphocytes', *Proc Natl Acad Sci U S A*, 95: 258-63.
- Hampton, H. R., and T. Chtanova. 2016. 'The lymph node neutrophil', *Semin Immunol*, 28: 129-36.

- Hardin, P. E. 2011. 'Molecular genetic analysis of circadian timekeeping in *Drosophila*', *Adv Genet*, 74: 141-73.
- Hardin, P. E., and S. Panda. 2013. 'Circadian timekeeping and output mechanisms in animals', *Curr Opin Neurobiol*, 23: 724-31.
- Henderson, R. B., L. H. Lim, P. A. Tessier, F. N. Gavins, M. Mathies, M. Perretti, and N. Hogg. 2001. 'The use of lymphocyte function-associated antigen (LFA)-1-deficient mice to determine the role of LFA-1, Mac-1, and alpha4 integrin in the inflammatory response of neutrophils', *J Exp Med*, 194: 219-26.
- Hidalgo, A., A. J. Peired, M. Wild, D. Vestweber, and P. S. Frenette. 2007. 'Complete identification of E-selectin ligands on neutrophils reveals distinct functions of PSGL-1, ESL-1, and CD44', *Immunity*, 26: 477-89.
- Hokeness, K. L., E. S. Deweerd, M. W. Munks, C. A. Lewis, R. P. Gladue, and T. P. Salazar-Mather. 2007. 'CXCR3-dependent recruitment of antigen-specific T lymphocytes to the liver during murine cytomegalovirus infection', *J Virol*, 81: 1241-50.
- Iigo, Y., M. Suematsu, T. Higashida, J. Oheda, K. Matsumoto, Y. Wakabayashi, Y. Ishimura, M. Miyasaka, and T. Takashi. 1997. 'Constitutive expression of ICAM-1 in rat microvascular systems analyzed by laser confocal microscopy', *Am J Physiol*, 273: H138-47.
- Itkin, T., S. Gur-Cohen, J. A. Spencer, A. Schajnovitz, S. K. Ramasamy, A. P. Kusumbe, G. Ledergor, Y. Jung, I. Milo, M. G. Poulos, A. Kalinkovich, A. Ludin, O. Kollet, G. Shakhar, J. M. Butler, S. Rafii, R. H. Adams, D. T. Scadden, C. P. Lin, and T. Lapidot. 2016. 'Distinct bone marrow blood vessels differentially regulate haematopoiesis', *Nature*, 532: 323-8.
- Jin, X., L. P. Shearman, D. R. Weaver, M. J. Zylka, G. J. de Vries, and S. M. Reppert. 1999. 'A molecular mechanism regulating rhythmic output from the suprachiasmatic circadian clock', *Cell*, 96: 57-68.
- John, B., and I. N. Crispe. 2004. 'Passive and active mechanisms trap activated CD8+ T cells in the liver', *J Immunol*, 172: 5222-9.
- Keller, M., J. Mazuch, U. Abraham, G. D. Eom, E. D. Herzog, H. D. Volk, A. Kramer, and B. Maier. 2009. 'A circadian clock in macrophages controls inflammatory immune responses', *Proc Natl Acad Sci U S A*, 106: 21407-12.

- Kim, C. H. 2005. 'The greater chemotactic network for lymphocyte trafficking: chemokines and beyond', *Curr Opin Hematol*, 12: 298-304.
- Kolaczkowska, E., and P. Kubes. 2013. 'Neutrophil recruitment and function in health and inflammation', *Nat Rev Immunol*, 13: 159-75.
- Kreisel, D., R. G. Nava, W. Li, B. H. Zinselmeyer, B. Wang, J. Lai, R. Pless, A. E. Gelman, A. S. Krupnick, and M. J. Miller. 2010. 'In vivo two-photon imaging reveals monocyte-dependent neutrophil extravasation during pulmonary inflammation', *Proc Natl Acad Sci U S A*, 107: 18073-8.
- Kuebler, W. M., and A. E. Goetz. 2002. 'The marginated pool', *Eur Surg Res*, 34: 92-100.
- Lahm, T., P. R. Crisostomo, T. A. Markel, M. Wang, K. D. Lillemoe, and D. R. Meldrum. 2007. 'The critical role of vascular endothelial growth factor in pulmonary vascular remodeling after lung injury', *Shock*, 28: 4-14.
- Lamia, K. A., K. F. Storch, and C. J. Weitz. 2008. 'Physiological significance of a peripheral tissue circadian clock', *Proc Natl Acad Sci U S A*, 105: 15172-7.
- Lee, W. Y., and P. Kubes. 2008. 'Leukocyte adhesion in the liver: distinct adhesion paradigm from other organs', *J Hepatol*, 48: 504-12.
- Lehman, M. N., R. Silver, W. R. Gladstone, R. M. Kahn, M. Gibson, and E. L. Bittman. 1987. 'Circadian rhythmicity restored by neural transplant. Immunocytochemical characterization of the graft and its integration with the host brain', *J Neurosci*, 7: 1626-38.
- Lehmann, J. C., D. Jablonski-Westrich, U. Haubold, J. C. Gutierrez-Ramos, T. Springer, and A. Hamann. 2003. 'Overlapping and selective roles of endothelial intercellular adhesion molecule-1 (ICAM-1) and ICAM-2 in lymphocyte trafficking', *J Immunol*, 171: 2588-93.
- Leick, M., V. Azcutia, G. Newton, and F. W. Luscinskas. 2014. 'Leukocyte recruitment in inflammation: basic concepts and new mechanistic insights based on new models and microscopic imaging technologies', *Cell Tissue Res*, 355: 647-56.
- Ley, K., C. Laudanna, M. I. Cybulsky, and S. Nourshargh. 2007. 'Getting to the site of inflammation: the leukocyte adhesion cascade updated', *Nat Rev Immunol*, 7: 678-89.
- Lim, L. H., R. J. Flower, M. Perretti, and A. M. Das. 2000. 'Glucocorticoid receptor activation reduces CD11b and CD49d levels on murine eosinophils:

- characterization and functional relevance', *Am J Respir Cell Mol Biol*, 22: 693-701.
- Lo, C. G., T. T. Lu, and J. G. Cyster. 2003. 'Integrin-dependence of lymphocyte entry into the splenic white pulp', *J Exp Med*, 197: 353-61.
- Logan, R. W., A. Arjona, and D. K. Sarkar. 2011. 'Role of sympathetic nervous system in the entrainment of circadian natural-killer cell function', *Brain Behav Immun*, 25: 101-9.
- Looney, M. R., and J. Bhattacharya. 2014. 'Live imaging of the lung', *Annu Rev Physiol*, 76: 431-45.
- Lucas, R. J., M. S. Freedman, M. Munoz, J. M. Garcia-Fernandez, and R. G. Foster. 1999. 'Regulation of the mammalian pineal by non-rod, non-cone, ocular photoreceptors', *Science*, 284: 505-7.
- Marchesi, V. T., and J. L. Gowans. 1964. 'THE MIGRATION OF LYMPHOCYTES THROUGH THE ENDOTHELIUM OF VENULES IN LYMPH NODES: AN ELECTRON MICROSCOPE STUDY', *Proc R Soc Lond B Biol Sci*, 159: 283-90.
- Marelli-Berg, F. M., L. Cannella, F. Dazzi, and V. Mirenda. 2008. 'The highway code of T cell trafficking', *J Pathol*, 214: 179-89.
- Maronde, E., and J. H. Stehle. 2007. 'The mammalian pineal gland: known facts, unknown facets', *Trends Endocrinol Metab*, 18: 142-9.
- Martin, C., P. C. Burdon, G. Bridger, J. C. Gutierrez-Ramos, T. J. Williams, and S. M. Rankin. 2003. 'Chemokines acting via CXCR2 and CXCR4 control the release of neutrophils from the bone marrow and their return following senescence', *Immunity*, 19: 583-93.
- Maury, E., K. M. Ramsey, and J. Bass. 2010. 'Circadian rhythms and metabolic syndrome: from experimental genetics to human disease', *Circ Res*, 106: 447-62.
- Maywood, E. S., J. E. Chesham, N. J. Smyllie, and M. H. Hastings. 2014. 'The Tau mutation of casein kinase 1epsilon sets the period of the mammalian pacemaker via regulation of Period1 or Period2 clock proteins', *J Biol Rhythms*, 29: 110-8.
- Mazo, I. B., M. Honczarenko, H. Leung, L. L. Cavanagh, R. Bonasio, W. Weninger, K. Engelke, L. Xia, R. P. McEver, P. A. Koni, L. E. Silberstein, and U. H. von

- Andrian. 2005. 'Bone marrow is a major reservoir and site of recruitment for central memory CD8+ T cells', *Immunity*, 22: 259-70.
- McDonald, B., and P. Kubes. 2015. 'Interactions between CD44 and Hyaluronan in Leukocyte Trafficking', *Front Immunol*, 6: 68.
- McDonald, B., E. F. McAvoy, F. Lam, V. Gill, C. de la Motte, R. C. Savani, and P. Kubes. 2008. 'Interaction of CD44 and hyaluronan is the dominant mechanism for neutrophil sequestration in inflamed liver sinusoids', *J Exp Med*, 205: 915-27.
- McDonald, B., K. Pittman, G. B. Menezes, S. A. Hirota, I. Slaba, C. C. Waterhouse, P. L. Beck, D. A. Muruve, and P. Kubes. 2010. 'Intravascular danger signals guide neutrophils to sites of sterile inflammation', *Science*, 330: 362-6.
- McNab, G., J. L. Reeves, M. Salmi, S. Hubscher, S. Jalkanen, and D. H. Adams. 1996. 'Vascular adhesion protein 1 mediates binding of T cells to human hepatic endothelium', *Gastroenterology*, 110: 522-8.
- Mebius, R. E., and G. Kraal. 2005. 'Structure and function of the spleen', *Nat Rev Immunol*, 5: 606-16.
- Mendez-Ferrer, S., D. Lucas, M. Battista, and P. S. Frenette. 2008. 'Haematopoietic stem cell release is regulated by circadian oscillations', *Nature*, 452: 442-7.
- Mionnet, C., S. L. Sanos, I. Mondor, A. Jorquera, J. P. Laugier, R. N. Germain, and M. Bajenoff. 2011. 'High endothelial venules as traffic control points maintaining lymphocyte population homeostasis in lymph nodes', *Blood*, 118: 6115-22.
- Moreland, J. G., R. M. Fuhrman, J. A. Pruessner, and D. A. Schwartz. 2002. 'CD11b and intercellular adhesion molecule-1 are involved in pulmonary neutrophil recruitment in lipopolysaccharide-induced airway disease', *Am J Respir Cell Mol Biol*, 27: 474-80.
- Nakajima, M., K. Imai, H. Ito, T. Nishiwaki, Y. Murayama, H. Iwasaki, T. Oyama, and T. Kondo. 2005. 'Reconstitution of circadian oscillation of cyanobacterial KaiC phosphorylation in vitro', *Science*, 308: 414-5.
- Nguyen, K. D., S. J. Fentress, Y. Qiu, K. Yun, J. S. Cox, and A. Chawla. 2013. 'Circadian gene Bmal1 regulates diurnal oscillations of Ly6C(hi) inflammatory monocytes', *Science*, 341: 1483-8.

- Nieminen, M., T. Henttinen, M. Merinen, F. Marttila-Ichihara, J. E. Eriksson, and S. Jalkanen. 2006. 'Vimentin function in lymphocyte adhesion and transcellular migration', *Nat Cell Biol*, 8: 156-62.
- Nolte, M. A., A. Hamann, G. Kraal, and R. E. Mebius. 2002. 'The strict regulation of lymphocyte migration to splenic white pulp does not involve common homing receptors', *Immunology*, 106: 299-307.
- O'Neill, J. S., and A. B. Reddy. 2011. 'Circadian clocks in human red blood cells', *Nature*, 469: 498-503.
- Ohkura, N., K. Oishi, Y. Sekine, G. Atsumi, N. Ishida, J. Matsuda, and S. Horie. 2007. 'Comparative study of circadian variation in numbers of peripheral blood cells among mouse strains: unique feature of C3H/HeN mice', *Biol Pharm Bull*, 30: 1177-80.
- Oishi, K., N. Ohkura, K. Kadota, M. Kasamatsu, K. Shibusawa, J. Matsuda, K. Machida, S. Horie, and N. Ishida. 2006. 'Clock mutation affects circadian regulation of circulating blood cells', *J Circadian Rhythms*, 4: 13.
- Okada, T., V. N. Ngo, E. H. Ekland, R. Forster, M. Lipp, D. R. Littman, and J. G. Cyster. 2002. 'Chemokine requirements for B cell entry to lymph nodes and Peyer's patches', *J Exp Med*, 196: 65-75.
- Okutsu, M., K. Ishii, K. J. Niu, and R. Nagatomi. 2005. 'Cortisol-induced CXCR4 augmentation mobilizes T lymphocytes after acute physical stress', *Am J Physiol Regul Integr Comp Physiol*, 288: R591-9.
- Panda, S., M. P. Antoch, B. H. Miller, A. I. Su, A. B. Schook, M. Straume, P. G. Schultz, S. A. Kay, J. S. Takahashi, and J. B. Hogenesch. 2002. 'Coordinated transcription of key pathways in the mouse by the circadian clock', *Cell*, 109: 307-20.
- Papazyan, R., Y. Zhang, and M. A. Lazar. 2016. 'Genetic and epigenomic mechanisms of mammalian circadian transcription', *Nat Struct Mol Biol*, 23: 1045-52.
- Preitner, N., F. Damiola, L. Lopez-Molina, J. Zakany, D. Duboule, U. Albrecht, and U. Schibler. 2002. 'The orphan nuclear receptor REV-ERB α controls circadian transcription within the positive limb of the mammalian circadian oscillator', *Cell*, 110: 251-60.

- Rivera-Nieves, J., T. L. Burcin, T. S. Olson, M. A. Morris, M. McDuffie, F. Cominelli, and K. Ley. 2006. 'Critical role of endothelial P-selectin glycoprotein ligand 1 in chronic murine ileitis', *J Exp Med*, 203: 907-17.
- Sato, T. K., S. Panda, L. J. Miraglia, T. M. Reyes, R. D. Rudic, P. McNamara, K. A. Naik, G. A. FitzGerald, S. A. Kay, and J. B. Hogenesch. 2004. 'A functional genomics strategy reveals Rora as a component of the mammalian circadian clock', *Neuron*, 43: 527-37.
- Scheiermann, C., P. S. Frenette, and A. Hidalgo. 2015. 'Regulation of leucocyte homeostasis in the circulation', *Cardiovasc Res*, 107: 340-51.
- Scheiermann, C., Y. Kunisaki, and P. S. Frenette. 2013. 'Circadian control of the immune system', *Nat Rev Immunol*, 13: 190-8.
- Scheiermann, C., Y. Kunisaki, D. Lucas, A. Chow, J. E. Jang, D. Zhang, D. Hashimoto, M. Merad, and P. S. Frenette. 2012. 'Adrenergic nerves govern circadian leukocyte recruitment to tissues', *Immunity*, 37: 290-301.
- Spencer, J. A., F. Ferraro, E. Roussakis, A. Klein, J. Wu, J. M. Runnels, W. Zaher, L. J. Mortensen, C. Alt, R. Turcotte, R. Yusuf, D. Cote, S. A. Vinogradov, D. T. Scadden, and C. P. Lin. 2014. 'Direct measurement of local oxygen concentration in the bone marrow of live animals', *Nature*, 508: 269-73.
- Storch, K. F., O. Lipan, I. Leykin, N. Viswanathan, F. C. Davis, W. H. Wong, and C. J. Weitz. 2002. 'Extensive and divergent circadian gene expression in liver and heart', *Nature*, 417: 78-83.
- Strydom, N., and S. M. Rankin. 2013. 'Regulation of circulating neutrophil numbers under homeostasis and in disease', *J Innate Immun*, 5: 304-14.
- Subramanian, V., P. A. Fields, and L. A. Boyer. 2015. 'H2A.Z: a molecular rheostat for transcriptional control', *F1000Prime Rep*, 7: 01.
- Sumova, A., Z. Bendova, M. Sladek, R. El-Hennamy, K. Laurinova, Z. Jindrakova, and H. Illnerova. 2006. 'Setting the biological time in central and peripheral clocks during ontogenesis', *FEBS Lett*, 580: 2836-42.
- Suratt, B. T., S. K. Young, J. Lieber, J. A. Nick, P. M. Henson, and G. S. Worthen. 2001. 'Neutrophil maturation and activation determine anatomic site of clearance from circulation', *Am J Physiol Lung Cell Mol Physiol*, 281: L913-21.

- Suzuki, K., Y. Hayano, A. Nakai, F. Furuta, and M. Noda. 2016. 'Adrenergic control of the adaptive immune response by diurnal lymphocyte recirculation through lymph nodes', *J Exp Med*, 213: 2567-74.
- Tahara, Y., H. Kuroda, K. Saito, Y. Nakajima, Y. Kubo, N. Ohnishi, Y. Seo, M. Otsuka, Y. Fuse, Y. Ohura, T. Komatsu, Y. Moriya, S. Okada, N. Furutani, A. Hirao, K. Horikawa, T. Kudo, and S. Shibata. 2012. 'In vivo monitoring of peripheral circadian clocks in the mouse', *Curr Biol*, 22: 1029-34.
- Takahashi, J. S., H. K. Hong, C. H. Ko, and E. L. McDearmon. 2008. 'The genetics of mammalian circadian order and disorder: implications for physiology and disease', *Nat Rev Genet*, 9: 764-75.
- Tang, M. L., D. A. Steeber, X. Q. Zhang, and T. F. Tedder. 1998. 'Intrinsic differences in L-selectin expression levels affect T and B lymphocyte subset-specific recirculation pathways', *J Immunol*, 160: 5113-21.
- Tosini, G., S. Owino, J. L. Guillaume, and R. Jockers. 2014. 'Understanding melatonin receptor pharmacology: latest insights from mouse models, and their relevance to human disease', *Bioessays*, 36: 778-87.
- van Ewijk, W., and P. Nieuwenhuis. 1985. 'Compartments, domains and migration pathways of lymphoid cells in the splenic pulp', *Experientia*, 41: 199-208.
- Vestweber, D. 2015. 'How leukocytes cross the vascular endothelium', *Nat Rev Immunol*, 15: 692-704.
- Vielhaber, E., E. Eide, A. Rivers, Z. H. Gao, and D. M. Virshup. 2000. 'Nuclear entry of the circadian regulator mPER1 is controlled by mammalian casein kinase I epsilon', *Mol Cell Biol*, 20: 4888-99.
- Volpes, R., J. J. Van Den Oord, and V. J. Desmet. 1992. 'Vascular adhesion molecules in acute and chronic liver inflammation', *Hepatology*, 15: 269-75.
- Wagner, J. G., and R. A. Roth. 2000. 'Neutrophil migration mechanisms, with an emphasis on the pulmonary vasculature', *Pharmacol Rev*, 52: 349-74.
- Wang, Q., C. M. Doerschuk, and J. P. Mizgerd. 2004. 'Neutrophils in innate immunity', *Semin Respir Crit Care Med*, 25: 33-41.
- Wong, J., B. Johnston, S. S. Lee, D. C. Bullard, C. W. Smith, A. L. Beaudet, and P. Kubes. 1997. 'A minimal role for selectins in the recruitment of leukocytes into the inflamed liver microvasculature', *J Clin Invest*, 99: 2782-90.

- Yamazaki, S., R. Numano, M. Abe, A. Hida, R. Takahashi, M. Ueda, G. D. Block, Y. Sakaki, M. Menaker, and H. Tei. 2000. 'Resetting central and peripheral circadian oscillators in transgenic rats', *Science*, 288: 682-5.
- Zhao, Y., M. Liu, X. Y. Chan, S. Y. Tan, S. Subramaniam, Y. Fan, E. Loh, K. T. E. Chang, T. C. Tan, and Q. Chen. 2017. 'Uncovering the mystery of opposite circadian rhythms between mouse and human leukocytes in humanized mice', *Blood*.

7. Appendix

7.1. Curriculum Vitae

Education

09/2014-	Ph.D. in medical research Ludwig-Maximilians-Universität München, Germany
09/2012-06/2014	Master degree of clinical medicine Chongqing Medical University, China
09/2007-07/2012	Medical degree Chongqing Medical University, China

Awards

09/2014-06/2015	Scholarship of IRTG 914
04/2016	Trainee Travel Award of ASIP

Scientific presentations

04/2017	Poster and oral presentation in EB conference, USA
07/2016	Poster in IRTG retreat at Kloster Schöntal, Germany
04/2016	Poster and oral presentation in EB conference, USA
01/2016	Oral presentation at Walter-Brendel-Centrum, Germany

Membership of scientific society

Since 03/2016	American society of investigated medicine (ASIP)
---------------	--